Author:
Wang, Rui

Title:
Resource Allocation and Optimisation of Elastic Optical Networks in Nonlinear Regime

Resource Allocation and Optimisation of Elastic Optical Networks in Nonlinear Regime

Rui Wang

Department of Electrical and Electronic Engineering

University of Bristol

This dissertation is submitted for the degree of

Doctor of Philosophy

June 2019

I would like to dedicate this thesis to my loving parents . . .

Declaration

I hereby declare that except where specific reference is made to the work of others, the contents of this dissertation are original and have not been submitted in whole or in part for consideration for any other degree or qualification in this, or any other university. This dissertation is my own work and contains nothing which is the outcome of work done in collaboration with others, except as specified in the text and Acknowledgements.

Rui Wang

June 2019

Acknowledgements

First and foremost, I would like to express my thanks and appreciation to my supervisor Professor Reza Nejabati for providing me with the opportunity to pursue a Doctor degree in High Performance Network Group. His wide knowledge of optical networks and his spirit towards the research activities have deeply inspired me. I would thank him for giving me the opportunity with funding for the completion of this PhD thesis. Without his priceless guidance, help and suggestion, it is impossible for me to complete the PhD study.

I would like to thank my co-supervisor, Professor Dimitra Simeonidou, for her continuous guidance and support during my PhD period.

Special thanks to Dr. Sarvesh Bidkar for detailed technical debate and discussion during the first two years of PhD study. His encouragement, support and suggestions have helped me improve the quality of work. I would also like to thank my current and former colleagues, all my friends made in Bristol. PhD life becomes rich and colourful with the presence of them.

Finally, I offer my special thanks and appreciation to my loving family. My dad, Yiquan Wang and my mother Qinghua Tang are always supporting me. Words cannot convey how grateful I am to their encouragement and commitment during my whole life. To my love, Yanru Yao, who is always firmest standing beside me, bringing me pleasure, joy and happiness.

Abstract

Elastic optical networks have emerged as a promising technology for the backbone networks to support increasing popular applications and service such as ultra high-definition video and inter data centre communication. These applications require to accommodate high-capacity and dynamic bandwidth, which pose a significant challenge to the backbone networks. This thesis aims at making the efficient use of the elastic optical networks and increasing the network utilisation subject to the transmission impairments constraints which degrade the quality of the optical signal.

This thesis begins with the quality of transmission model considering the nonlinear impairments and the amplified spontaneous emission noise as the dominant impairments in the elastic optical networks. Based on widely adopted Gaussian noise nonlinear impairments model, a novel load-aware nonlinear impairments estimation method is proposed. The accuracy of the proposed nonlinear model is evaluated, which effectively approximates the real performance when the link occupation exceeds 100 GHz for different signal power spectral densities and fibre span lengths.

Then, various novel resource allocation algorithms based on the proposed load-aware nonlinear impairments estimation strategy are proposed for the case where the traffic requests are sequentially loaded into the network. The proposed optimisation algorithm and its corresponding service reconfiguration functions achieve higher spectral efficiency and higher network throughput compared to the benchmark solutions.

This thesis also investigates the dynamical resource allocation problem in elastic optical networks with service provisioned and expired, utilising the proposed nonlinear impairments model. The proposed solution significantly improves the dynamical service acceptance ratio and yields higher network utilisation. Further, a novel traffic grooming scheme is presented to explore the potential capability of both bandwidth-variable transponders and the network spectrum resources. The proposed traffic grooming scheme shows tremendous transponders saving over the non-traffic grooming benchmark method and better service acceptance ratio over the traffic grooming benchmark.

Finally, a coordinated fibre span power optimisation and ROADM input power management scheme is introduced based on the proposed nonlinear impairments model. The experimental results show that the proposed coordinated power management scheme leads to 50% bit error rate reduction. The benefit of BER reduction is verified in the elastic optical network through extensive simulation, which depicts 15% higher network capacity compared to an ordinary power optimisation method.

Table of contents

List of figures

List of tables

Acronyms

Acronyms / Abbreviations

4G 4th generation

ADC Analogue to Digital Converter

AoD Architecture on Demand

ASE Amplified Spontaneous Emission

AWG Arrayed Waveguide Gratings

AWGN Additive White Noise Gaussian Noise

BER Bit Error Rate

BVT Bandwidth Variable Transceiver

CDC Colorless, Directionless and Contentionless

CD Chromatic Dispersion

DAC Digital to Analogue Converter

DCF Dispersion Compensation Fibres

DEMUX Demultiplexer

DP Dual Polarization

DSP Digital signal processing

DWDM Dense Wavelength Division Multiplexing

EB ExtraByte

EDFA Erbium Doped Fibre Amplifier

EDFA Erbium-Doped Fibre Amplifier

EON Elastic Optical Network

FC Filter concatenation

FEC Forward Error Correction

FWM Four Wave Mixing

Gbps Gigabit per second

GN Gaussian Noise

GVD Group Velocity Dispersion

ILP Integer Linear Programming

ITU International Telecommunication Union

LARA Load and nonlinearity Aware Resources Allocation

LOGON Local Optimum Global Optimum with Nyquist shape

MCF Multi-Core Fibre

MCI Multi-Channel Interference

MILP Mixed Integer Linear Programming

MMF Multi-Mode Fibre

MPLS Multi-Protocol Label Switching

MUX Multiplexer

NDFIS National Dark Fibre Infrastructure Service

NF Noise Figure

NLI Non-Linear Impairments

NP Non-deterministic Polynomial-time

NSF National Science Foundation

O-OFDM Optical Orthogonal Frequency-Division Multiplexing

O-E-O Optical-Electronic-Optical

OFDM Orthogonal Frequency-Division Multiplexing

OSA Optical Spectrum Analyser

OSNR Optical Signal-to-Noise Ratio

PDL Polarization Dispersion Loss

PMD Polarization mode Dispersion

PM Polarization Multiplexing

PSD Power Spectral Density

QAM Quadrature Amplitude Modulation

QoT Quality of Transmission

ROADM Reconfigurable Optical Add-Drop Multiplexer

RMSA Routing, Modulation format and Spectrum Assignment

RSA Routing and Spectrum Allocation

RWA Routing and Wavelength Assignment

Rx Receiver

SBS Stimulated Brillouin Scattering

SDH Synchronous Digital Hierarchy

SLA Service-Level Agreement

SMF Single-Mode Fibre

SNR Signal-to-Noise Ratio

SONET Synchronous Optical Networking

SPM Self Phase Modulation

SRS Stimulated Raman Scattering

SSE Source Spontaneous Emission

SSMF Standard Single-Mode Fibres

SSS Spectrum Selective Switch

Tx Transmitter

WDM Wavelength Division Multiplexing

Wi-Fi Wireless Fidelity

WSS Wavelength Selective Switch

XPM Cross Phase Modulation

XT Crosstalk

Chapter 1

Introduction

1.1 Role of Optical Transport Networks and Network Planning

The optical communication system was first invented and introduced to the world in the late 1970s and then served as the fundamental part of the whole society for information transmission and exchange. The research and development activity was carried out since then for the optical devices and technologies. In the meantime, network infrastructure providers and operators experienced immensely increased bandwidth requirements, being driven by the insight that future networks should provide high capacity, high flexibility, and high reliability. Besides, to achieve these features, such optical networks should provide the multiplexing/demultiplexing and switching functionalities, which was viewed as an economically efficient pathway to reduce the overall network investment and operation expense. As a result, the wavelength division multiplexed optical system has been world-wide deployed now to support high-bandwidth, long-distance transmission. The optical transport networks are built upon the development of WDM technique. It forms the foundation of the nowadays Internet and globally interconnected networks. The development of optical

communication system was the evolution of the low power loss fibre and its high capacity nature that made it an ideal candidate to provide high bandwidth, low latency and long-distance connections to users around the world.

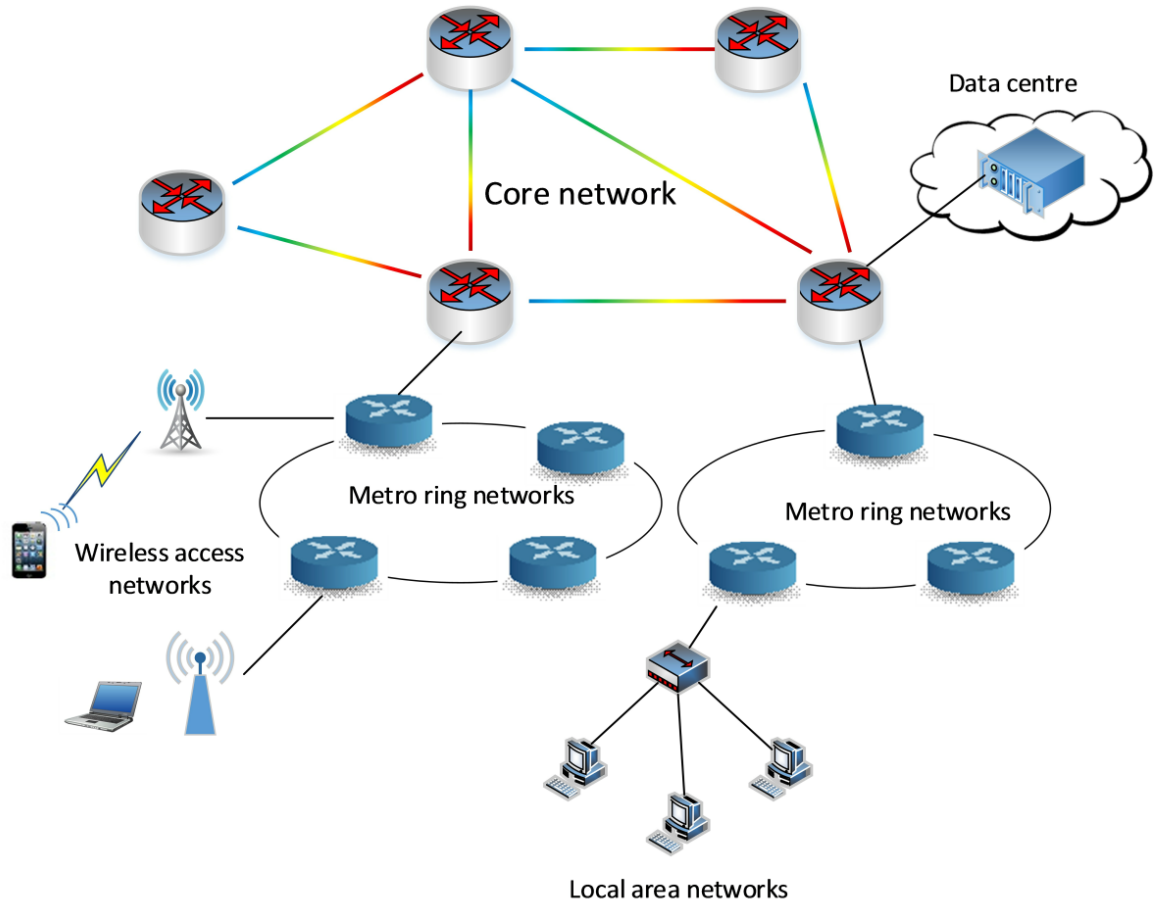

Fig. 1.1 The hierarchy architecture of current Internet infrastructure

Today's Internet infrastructure can be viewed as a mesh network, globally interconnecting different network domains with their own individual networking protocols [1–3], as shown in figure 1.1. In each network domain, the network nodes are connected with certain types of medium for the corresponding transport technique. The information is coded, encrypted, modulated and transmitted into this big mesh network and being routed and switched to the desired destination. The traffic from end users such as mobile phones, laptops and desktops are supported by access networks such as local area networks, passive optical networks,

cellular networks or Wi-Fi networks. The traffic from local access networks is aggregated and fed to the metropolitan ring networks, which allow connection between a large number of user subscribers and the core optical networks. Similarly, electronic edge routers of the core optical networks aggregate the traffic flows from metropolitan networks. The core optical transport networks, connected by fibre links and optical switching elements, can support huge amount of traffic to enable nationwide, international or even intercontinental data transmission and information exchange and serve millions of users.

The requirements of the network application have driven the development and evolvement of configurable/automatic optical networks. Apart from the evolution of software-defined networking on the control plane and centralised management plane, the automatically configurable optical networks need a smart algorithm to inform control plane how the networks should be configured to achieve certain goals, such as load balancing, green networking, capacity maximisation. This is also describing as the long-term network planning phase, focusing on determining the optimum strategies from infrastructure deployment to network resources allocation. In addition to the long-term planning, the short-term planning is more reliable on the configuration ability of the optical networks, as one traffic demand is usually processed each time with a little amount of time permitted between the planning stage and the deployment stage. It considers the constraints of physical infrastructure, the physical layer impairments while may provide a sub-optimum resource or path due to the algorithm or certain policy. In this thesis, we mainly focus on the short-term optical network planning, which includes routing algorithms, wavelength assignment, regeneration-based optical network, traffic grooming technique and optical lightpath protection.

1.2 Motivation

According to Cisco, it is estimated that by 2021, the global Internet users will reach 4.6 billion with 27.1 billion devices connected with each other [4]. New services and applications

such as ultra high-definition video, inter data centre communication, low latency online video game and self-driving vehicles will appear, requiring the increased need of network bandwidth, which poses a great challenge to current networks.

Figure 1.2a shows that the global number of network devices are expected to increase from 17.1 billion in 2016 to 27.1 billion by 2021. Among all these network devices, around 43% of them will be mobile connected. In figure 1.2b, the global Internet traffic per month will grow from 70.3 EB in 2016 to 227.6 EB in 2021. The growing number of network devices to support the increasing need for these bandwidth-consuming service and application requires a significant revolution of the networks.

For optical transport network with the capability to support long-distance transmission, adaptive modulation format assignment and wavelength division multiplexing have been proposed to improve the optical capacity. However, the fibre Kerr effect poses the limitation of maximum launch power allowed in the fibre, which set the upper limit to the channel capacity [5]. The core optical transport network will have to face the capacity crunch problem in the near future without introducing new technology to allow more degrees of freedom operated in the networks.

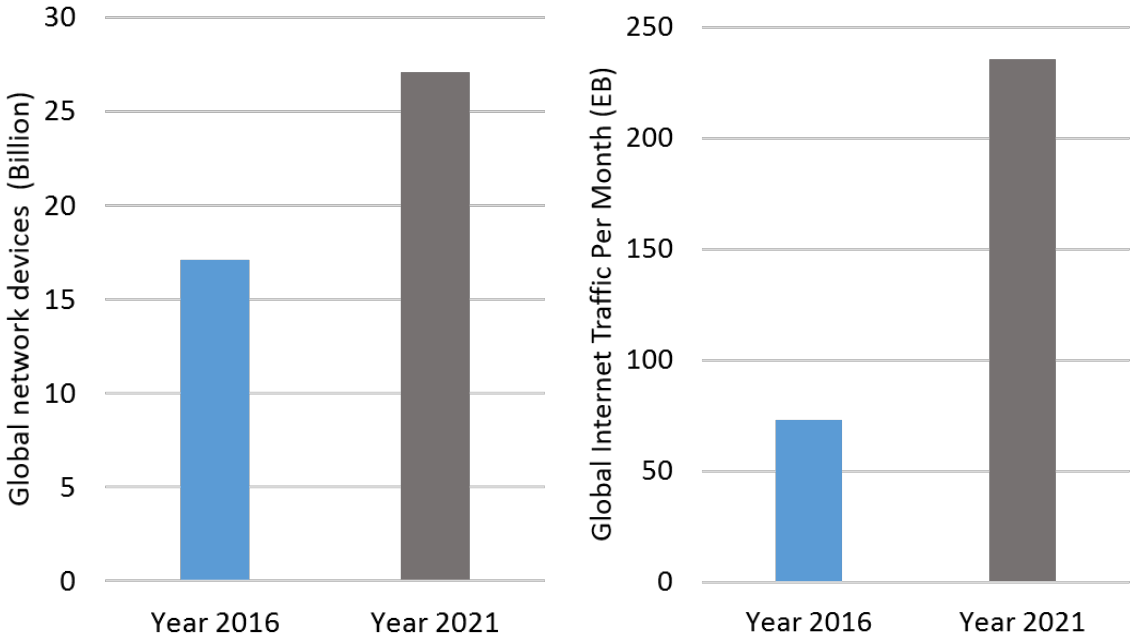

(a) Global number of network devices (b) Global Internet traffic per month

Fig. 1.2 Cisco visual networking index forecast, (a): Number of global network devices and (b): Internet traffic per month in 2016 and 2021 [4].

1.3 Problem Statement and Research Objectives

In this work, we focus on the transparent elastic optical networks with flexible modulation and spectrum assignment. The modern optical network paradigm is considered of using coherent transmission and detection, the dispersion uncompensated fibre links and dual polarisation multiplexing. Considering such future networks deploying these techniques, the question becomes how to improve and maximize the network capacity under the installed network resource in the infrastructure to overcome or postpone the capacity crunch problem.

To improve resource utilization in large optical transport networks, knowledge of physical impairments is essential. Physical layer impairments result in signal shape distortion which decreases the transmission data rate and the spectrum efficiency. In the era of coherent transmission and detection in core optical networks, the amplitude and phase of the optical signal can be precisely captured at the coherent receiver. The powerful and efficient compensation

of the physical layer linear impairments such as chromatic dispersion and polarisation mode dispersion can be carried out using digital signal processing techniques in the electrical domain. Coherent transmission system combined with digital signal processing is able to provide a powerful tool for the next generation of optical core networks. However, the non-linear impairments like self-phase modulation, cross-phase modulation and four-wave mixing are difficult to mitigate in real time. Therefore, we consider the fibre non-linear impairments and the stochastic noise as the dominant impairments in the coherent optical networks of this work.

Traditionally, the distortion of the signal quality due to non-linear impairments is allocated a certain signal-to-noise margin to model their worst impact [6] [7]. Using the SNR margin to model the impact of non-linear impairments is simple and does not require complex non-linear impairments calculation. However, the SNR margin is usually calculated assuming the worst-case interference to guarantee the network service at any condition, leading to overestimation of the interference. In this case, some lightpaths may adopt a conservative modulation format or using lower forward error correction coding rate with high FEC overhead, which reduces the overall network spectral efficiency and underutilises the optical network resources.

In the optical networks operating in the non-linear regime, a simple and efficient non-linear impairments validation tool is essential. Such a tool should provide the feasibility to predict the quality of transmission of lightpaths travelling various routing paths in the optical networks, which cause a variety of non-linear impairments interplay among those signals. The non-linear impairments validation tool should also capture these various features to provide end-to-end signal quality estimation and prediction.

To improve the network capacity in this new era of deploying coherent transmission, the limited network resource needs to be utilised efficiently. But what are the resources and constraints in optical network and how can we utilise these resources within the constraints

effectively to improve the network capacity considering stochastic noise and the nonlinear impairments?

In the optical fibre link, spectrum and optical amplifiers are the resources. Clearly, the spectrum is a kind of resource and it needs to be managed and carefully coordinated with other resources such as reconfigurable optical add-drop multiplexer and the transponders. As the spectrum needs to be assigned in a continuous and contiguous way along the routing path in the transparent optical networks, spectrum should be allocated in the way of reducing the impact due to spectrum fragmentation problem. The optical amplifiers is also a resource which should be managed carefully. This is because the channel power within fibre spans relies on the optical amplifier. The optical network operates in the non-linear regime with sufficiently high power in the fibre spans or links, leading to decreasing of SNR and causing data rate declining. On the other hand, the SNR will also decrease with a relatively small amount of signal power launched into the fibre since the stochastic noise like ASE noise dominates the end-to-end performance. Apart from signal power, the noise figure of the amplifiers is not a constant value with various input power and gains. This may further affect the SNR and the optimum launch power in the optical links.

The transponders and the reconfigurable optical add-drop multiplexers are also the resources in the optical networks. The parameters of the transponders or bandwidth variable transponders such as the modulation level, the launch power, the FEC overhead, the signal central frequency, occupied bandwidth and its baud rate affect the performance and the reach distance of the lightpath, thus those can be regarded as the type of resources in the network. For ROADM, the resources are the switching granularity, the colourless, directionless and contentionless constraints, the degrees and its associated impairments like insertion loss, chromatic dispersion, polarisation mode dispersion and polarisation dependent loss. These constraints form resources. As a result, ROADM needs to be configured carefully according to its resources and the traffic in the network to improve the overall network capacity.

To achieve higher optical network throughput considering these resources and constraints, the global optimisation strategy is required to increase the overall network throughput and reduce hardware cost. Therefore, the focus of this work is to push the optical network optimisation further into physical layer impairments aware network resource allocation. This work is to address the routing, spectrum and modulation assignment for elastic optical networks in the non-linear regime. The target is to first propose an accurate nonlinear impairment model, and then to improve the network efficiency using the proposed model by allowing more requests to be established in the network with various proposed optimisation schemes.

1.4 Thesis Organisation and Contribution Outline

The contribution of the thesis to the research area of optical networking mainly focuses on the resource analysis, allocation and optimisation of the optical network in the nonlinear regime. The detailed contributions and the related publication are listed in this section.

In chapter 2, the physical layer linear impairments and nonlinear impairments in the optical fibre and their impact to the signal quality are classified, discussed and reviewed. Then, the latest work and application of Gaussian noise nonlinear impairments model are briefly discussed. Further, the state-of-art research output regarding the EDFA power control and the impact of impairments due to ROADM are detailed reviewed and analysed. Finally, the optical signal quality assessment model is formulated for the uncompensated dual-polarisation optical networks with coherent transmission technique and the relationship between the quality assessment model and the forward error correction coding rate is studied.

In chapter 3, the basic knowledge and the state-of-art work in the optical networks are reviewed and studied. This chapter begins with the wavelength division multiplexing technique in the optical network. Then, the elastic optical networks and its relevant techniques: bandwidth-variable transponders and flex-grid reconfigurable optical add-drop multiplexer

are introduced. Latest work of routing, spectrum and modulation format assignment to increase elastic optical network capacity, utilisation is also discussed. To further improve the network capacity, traffic grooming technique and spectrum defragmentation are studied in elastic optical networks. Finally, the recent publication of physical impairments-aware resource allocation in elastic optical networks are presented.

In chapter 4, the detailed quality of transmission model is derived based on the ASE noise and the nonlinear impairments due to the Kerr effect. We then demonstrate the drawbacks of using the exact nonlinear impairments and the worst-case nonlinear impairments. Based on the analysis, the first target aims at providing a hybrid non-linear impairments validation tool to enable fast and more importantly, accurate nonlinearity prediction in flexible and dynamic elastic optical networks. The proposed hybrid nonlinearity model is first shown in [C4] and then being extended in [J1]. The chapter then discusses and analyses the accuracy of the proposed nonlinearity framework with point-to-point transmission and a simple resource allocation scheme. The proposed nonlinear impairments model proves to be a simple and accurate model for quality of transmission validation in optical networks. This work has been published in [C4], shown in the publication list below.

In chapter 5, we focus on efficient resource allocation schemes for the traffic sequentially loaded elastic optical networks using the proposed non-linear impairments model to improve overall network capacity. The proposed resource allocation algorithm consists of three service reconfiguration strategies in case that the non-linear impairments accumulated with the increasing number of provisioned lightpaths are beyond the acceptable value. The proposed service reconfiguration algorithms provide the capability of traffic balancing, decreasing the nonlinear impairments estimation error, and maximizing the available network capacity. The overall performance is verified through extensive simulation studies. The efficient resource optimisation in elastic optical networks has been published in [J1], shown in the publication list below.

In chapter 6, a routing, modulation format and spectrum assignment scheme are proposed to provision dynamic traffic requests considering the nonlinear impairments. The proposed strategy is studied against different intervals of requests arrival time and different requests holding time. The dynamic resource allocation based on the proposed hybrid nonlinearity model is published in [C3]. A traffic grooming technique is proposed with the capability of bandwidth-variable transponder to utilise the excess SNR margin to groom multiple requests into a large bit-rate lightpath. The proposed solution is compared with multiple benchmark solution and is proved to increase network efficiency and reduce the number of transponders. The proposed traffic grooming scheme to improve the capacity of elastic optical networks is published in [C2].

The power management is essential in optical networks to guarantee the signal quality of transmission. In chapter 7, the coordinated optical power optimisation and management strategy over optical spans and the ROADMs are introduced. The proposed power management solution is experimentally explored and demonstrated to reduce the bit error rate of the lightpaths. It is also studied with various simulation work using BT topology and network capacity improvement is verified by applying corresponding power optimisation scheme. The power optimisation and management method in elastic optical networks have been published in [C1].

Publication List

The works listed below are the publication directly related to this thesis.

J1 **R. Wang**, S. Bidkar, F. Meng, R. Nejabati, D. Simeonidou, "Load-Aware Nonlinearity Estimation for Elastic Optical Network Resource Optimization and Management," Journal of Optical Communication and Networking. 11, 164-178 (2019)

C1 **R. Wang**, Y. Bi, Y. Ou, E. Hugues-Salas, F. Meng, S. Yan, R. Nejabati D. Simeonidou, "Coordinated Fibre Span Power Optimisation and ROADM Input Power Management

Strategy for Optical Networks", 44th EUROPEAN CONFERENCE ON OPTICAL COMMUNICATION (ECOC), 2018.

C2 **R. Wang**, F. Meng, R. Nejabati D. Simeonidou, "A Novel Traffic Grooming Scheme for Nonlinear Elastic Optical Network." 2017 European Conference on Optical Communication (ECOC). IEEE, 2017.

C3 **R. Wang**, S. Bidkar, R. Nejabati, D. Simeonidou, "Load-aware nonlinearity estimation for efficient resource allocation in elastic optical networks." Optical Network Design and Modeling (ONDM), 2017 International Conference on. IEEE. 2017.

C4 **R. Wang**, S. Bidkar, R. Nejabati, D. Simeonidou, "Load and nonlinearity aware resource allocation in elastic optical networks." Optical Fiber Communication Conference. Optical Society of America, 2017.

The publication listed below are linked with the thesis as a co-author (C-A), however, not the key part of this work.

C-A1 R. Nejabati, **R. Wang**, A. Bravalheri, A. Muqaddas, N. Uniyal, T. Diallo, R. Tessinari, R. S. Guimaraes, S. Moazzeni, E. Hugues-Salas, G. T. Kanellos, and D. Simeonidou, "First Demonstration of Quantum-Secured, Inter-Domain 5G Service Orchestration and On-Demand NFV Chaining over Flexi-WDM Optical Networks," in Optical Fiber Communication Conference Postdeadline Papers 2019, (Optical Society of America, 2019), paper Th4C.6.

C-A2 D. J. Ives, S. Yan, L. Galdino, D. J. Elson, F. J. Vaquero-Caballero, G. Saavedra, **R. Wang**, D. Lavery, R. Nejabati, P. Bayvel, D. Simeonidou, and S. J. Savory, "A Comparison of Impairment Abstractions by Multiple Users of an Installed Fiber Infrastructure," in Optical Fiber Communication Conference (OFC) 2019, OSA Technical Digest (Optical Society of America, 2019), paper M4J.4.

C-A3 E. Hugues-Salas, **R. Wang**, G. T. Kanellos, R. Nejabati, and D. Simeonidou, "Co-existence of 9.6 Tb/s classical channels and a quantum key distribution (QKD) channel over a 7-core multicore optical fibre," in2018 IEEE British and Irish Conference on Optics and Photonics (BICOP). IEEE, 2018, pp. 1–4.

C-A4 B. Yu, M. Carlos, **R. Wang**, F. Meng, R. Nejabati, and D. Simeonidou, 2019, "Resource Allocation for Ultra-low Latency Virtual Network Services in Hierarchical 5G Network". in: IEEE International Conference on Communications.

[C-A5] F. Meng, A. Mavromatis, Y. Bi, **R. Wang**, S. Yan, R. Nejabati, and D. Simeonidou, "Self-Learning Monitoring On-Demand Strategy for Optical Networks," J. Opt. Commun. Netw. 11, A144-A154 (2019)

C-A6 Y. Ou, E. Hugues-Salas, F. Ntavou, **R. Wang**, Y. Bi, S. Yan, G. Kanellos, R. Nejabati, and D. Simeonidou, "Field-Trial of Machine Learning-Assisted Quantum Key Distribution (QKD) Networking with SDN." 2018 European Conference on Optical Communication (ECOC). IEEE, 2018.

C-A7 F. Meng, S. Yan, K. Nikolovgenis, Y. Ou, **R. Wang**, Y. Bi, E. Hugues-Salas, R. Nejabati, and D. Simeonidou "Field Trial of Gaussian Process Learning of Function-Agnostic Channel Performance Under Uncertainty." Optical Fiber Communication Conference. Optical Society of America, 2018.

C-A8 F. Meng, A. Mavromatis, Y. Bi, S. Yan, **R. Wang**, Y. Ou, K. Nikolovgenis, R. Nejabati, and D. Simeonidou, "Field Trial of Monitoring On-Demand at Intermediate-Nodes Through Bayesian Optimization." Optical Fiber Communication Conference. Optical Society of America, 2018.

C-A10 F. Meng, S. Yan, **R. Wang**, Y. Ou, Y. Bi, R. Nejabati, D. Simeonidou, "Robust Self-Learning Physical Layer Abstraction Utilizing Optical Performance Monitoring and

Markov Chain Monte Carlo", 2017 European Conference on Optical Communication (ECOC). IEEE, 2017.

C-A11 S. Yan, A. Aguado, Y. Ou, **R. Wang**, R. Nejabati, D. Simeonidou, "Multilayer network analytics with SDN-based monitoring framework." IEEE/OSA Journal of Optical Communications and Networking 9.2 (2017): A271-A279

Chapter 2

Physical Layer Transmission Impairments Modelling

2.1 Introduction

The rapid growth of demand for the bandwidth across the global networks and the new services/applications have put a significant challenge to the current network. The optical networks with the capability to support high bandwidth demand have been deployed in the metro networks and the core networks to support high bandwidth transmission [8]. The bit error rate of the optical signal and the reach distance of the system are determined by the physical layer impairments. These impairments generate from various network components such as DSP, ADC/DAC, lasers, amplifiers, ROADMs and the fibre. The impairments due to the electrical devices, lasers and the ROADMs are relatively constant since day one when they are deployed. In contrast, the physical layer impairments caused by launching an optical signal into the fibre medium affects the performance of signal dynamically. Therefore, it is necessary to understand and efficiently manage the impairments in the optical network to increase the network capacity.

In this work, we mainly review and study the physical layer technology and their related state-of-art research output. We first review the general linear and nonlinear impairments originated during transmission. Then Gaussian noise nonlinear impairments model is reviewed and related research work is discussed. We further study the work regarding the erbium-doped fibre amplifier control and the physical layer impairments from ROADMs. Followed by that, the physical layer quality of transmission model is reviewed and the corresponding forward error coding scheme is introduced with the quality of transmission model.

2.2 Optical Fibre

In the late 1970s, low loss optical fibre with 0.2 dB/km was manufacturing for 1550 nm transmission window and it was then widely deployed as the transmission medium for the long-haul and short distance transmission. In today's optical networks, different optical fibres are deployed for different network scenarios. Single-mode fibre typically has 8 - 10.5 μm core diameter, allowing only one transverse guided mode for the given spectrum and polarisation [9]. Multi-mode fibre has a core diameter of 62.5 μm, which allows multiple modes for transmission. Therefore, the transmission distance of using MMF is significantly shorter compared to using SMF. Despite different core diameters, both SMF and MMF have only one core wrapped with the cladding outside. To improve the bandwidth capacity within a single fibre, multi-core fibre is invented by providing multiple cores within a fibre in 1979 [10]. Each core, designed by allowing light transmitted in single transverse guided mode, can carry the same amount of information as the single-mode fibre. Unlike MMF or SMF, MCF faces a significant challenge and obstacle, known as inter-core crosstalk. The optical signal power leaks from one core through cladding into other cores, interfering the signal quality occupying the same frequency in neighbour cores. There is a lot of work studying the effect of inter-core crosstalk on the quality of the signal and inter-core crosstalk aware

core allocation [11] [12]. In this work, we mainly consider the SMF as the transmission medium. The fibre parameters used for simulation work in this thesis are shown in table 2.1. The absolute dispersion value of the fibre is calculated based on the value of chromatic dispersion coefficient value and is written as:

$$\beta_2 = |D| \cdot \lambda^2/(2\pi \cdot c) \tag{2.1}$$

where D is the chromatic dispersion coefficient, λ being the wavelength of the optical signal and c being the speed of light. According to the fibre span length, the effective fibre span length is calculated as:

$$L_{eff} = [1 - exp(- \cdot \alpha \cdot L_s)]/\alpha \tag{2.2}$$

where α is the linear fibre power loss coefficient and the L_s being the fibre span length. The effective fibre span length provides to be an effective and sufficient tool to simplify the calculation of the non-linear impairment by assuming the constant transmission power within the fibre span over the effective fibre span length.

2.3 A Brief Review of Physical Layer Impairments

The quality of the optical signal degrades as it travels along the optical network, due to a non-idea transmission medium. This leads to the signal received at the receiver side non-identical to the originally transmitted signal, which causes the received information to be incorrect. The quality of signal degradation is due to the stochastic noise, such as amplified spontaneous emission noise from erbium-doped fibre amplifiers or Raman amplifiers to compensate the signal power loss and due to the transmission impairments because of the non-ideal fibre medium fabrication technique. These impairments can be further classified as the linear

Table 2.1 Sing-mode fibre parameters used in this work

Parameters	Symbol	Value	Unit
Fibre power loss coefficient	α	0.22	dB/km
Chromatic dispersion coefficient	D	16.7	$ps/nm/km$
Absolute dispersion value	β_2	21	$ps^2 \cdot km^{-1}$
Fibre non-linearity Coefficient	γ	1.3	$W^{-1} \cdot km^{-1}$
Fibre span length	L_s	80	km
Effective Fibre span length	L_{eff}	19.4	km
Signal operating wavelength	λ	1550	nm

impairments and non-linear impairments, where linear impairments are either proportional to or not related to the signal power value while non-linear impairments scale nonlinearly against the increasing optical signal power [9, 13, 14].

The linear impairments include signal power attenuation, amplified spontaneous emission (ASE), chromatic dispersion (CD), polarization mode dispersion (PMD), polarization dispersion loss (PDL), filter concatenation (FC), amplifier tilt effects and inter-channel crosstalk (XT) [14–17]. Optical signal power loss is normally due to signal attenuation, photon absorption, light refraction from the core to cladding, reflection and connection insertion loss. To ensure long-haul transmission, the signal is re-amplified at certain transmission distance using the optical amplifiers. The amplification process introduces ASE noise to the optical signal, making the signal distorted and increasing the signal BER at the receiver. ASE is the main stochastic noise in the optical network. Apart from it, the electronic noise during digital-to-analogue conversion, the laser relative intensity noise also affects the quality of the signal at the transmitter [9, 18]. Similar to the stochastic noise at the transmitter, there is shot

noise, electronic and thermal noise, non-ideal analogue-to-digital converter and digital signal processor at the receiver side.

2.3.1 Chromatic Dispersion

In the optical fibre, the phenomenon that various spectrum components transmit at a different speed is called chromatic dispersion. Chromatic dispersion causes: 1) the optical spectrum shape broadening in the frequency domain, which leads to inter-channel interference (ICI) and 2) symbol waveform deformation in the time domain, known as inter-symbol interference (ISI) [19]. CD is independent of signal power but related to the signal modulation format, the baud rate and the fibre type. The CD accumulates incoherently along different fibre spans and links. The common strategy to mitigate the impact of CD is to deploy dispersion compensation fibres (DCF), which generates 'negative' CD compared to using normal single mode fibre. As a result, the overall CD at the end of each fibre link is approximate to zero, despite some spectrum components over-compensated while others are under-compensated. Recent research work proposes the dispersion uncompensated system which removes the DCF unit from the optical links. In dispersion uncompensated system, the effect of chromatic dispersion can be compensated by digital signal processing technique at the receivers.

2.3.2 Polarization Mode Dispersion and Polarization Dependent Loss

Besides the CD, there exists another type of dispersion in the optical communication system, known as polarization mode dispersion. Due to the imperfect fabrication, the fibre might not be ideal circular or may contain impurities. These defectives result in different polarization modes travelling at different group velocities, causing the spectrum shape expanding[20] [21]. Polarization dependent loss (PDL) is known as the two orthogonal polarization modes in polarization multiplexing (PM) or dual polarization (DP) WDM system suffering different power attenuation due to defects of the fibre. The interplay of PMD and PDL can further

decrease the quality of the signal. Usually, PDL occurs in passive devices such as splitters, MUX, DEMUX and isolators.

2.3.3 Erbium Doped Fibre Amplifiers and Amplified Spontaneous Emission Noise

The ASE noise generated by the optical amplifiers is the major additive noise in the optical networks where its spectrum shape follows the amplifiers' spectrum gain curve. Optical amplifiers, especially EDFA are extensively deployed in current optical networks to compensate for the signal power loss because of the propagation and insertion loss. In this work, we only consider the EDFA as the amplifiers in the optical system. During the process of the amplification, the incoming light triggers the stimulated emission as the electrons in the erbium atoms jump to lower energy level, where the energy is released in the form of photons following the same direction and phase of the incoming photons. As a result, the weak signal is amplified with extra photons following the exact same state [22]. Apart from simulated emission, there also exits spontaneous emission as a small portion of electrons recombines at a random energy level. When the spontaneous emission occurs, electrons release the energy as photons in an uncontrolled and random manner. Those photons are then mixed with signal and are amplified. The ASE noise is completely random in amplitude and phase thus it looks 'white' in the frequency domain. To quantify the performance of the EDFA, the noise factor F is denoted as the ratio of the signal SNR performance before amplification to the SNR after the amplification [23] which is presented as:

$$F = \frac{SNR_{in}}{SNR_{out}} \tag{2.3}$$

where the SNR_{in} is the SNR at the input of the optical amplifiers and the SNR_{out} is the SNR at the output of the amplifier. The noise factor of the amplifiers or the EDFAs are used

to quantify their accumulated ASE noise contribution to the signal [24]. To simplify the presentation, the noise figure F is expressed as the decibel of the noise factor:

$$NF = 10 \cdot \log_{10}(F) \tag{2.4}$$

According to the noise factor of EDFA, the single-sided ASE noise power spectral density (PSD) at the output of an EDFA in a dual-polarization system can be expressed as [25] [26]:

$$G_{ASE} = h\nu \cdot (G-1) \cdot F \tag{2.5}$$

where the G is the linear gain of EDFA, h being the Planck's constant(6.63×10^{-34} J$\cdot$ s) and ν being the optical signal carrier frequency. The ASE noise PSD can be rewritten using the noise figure as:

$$G_{ASE} = h\nu \cdot (G-1) \cdot 10^{\frac{NF}{10}} \tag{2.6}$$

The noise figure of EDFA is not a constant value, which relies on the input power, the optical signal spectrum location and the pump power of EDFA [27]. The most common way for the EDFA noise figure measurement is to subtracting the source spontaneous emission (SSE) noise of the laser. This technique is described in the equation 2.7 below [24].

$$F = \frac{2\rho_{total}}{Gh\nu} + \frac{1}{G} - \frac{2\rho_{SSE}}{h\nu} \tag{2.7}$$

where ρ_{total} is the total ASE noise power spectral density and the ρ_{SSE} being the power spectral density of source spontaneous emission noise of the laser.

With the help of optical spectrum analyser (OSA), the SSE subtraction technique is able to address the problem of separate the SSE noise from ASE noise by directly connect OSA to the laser. In this work, there is the requirement that various EDFA gains will be provided.

In this case, the pump power of the amplifiers will change, causing the fluctuation of the EDFA noise figure. Therefore, we assume the EDFA noise figure is a constant value in this work for the simulation setup unless otherwise specified.

2.3.4 Amplifier Gain Tilt and Filter Concatenation

The gain curve of the EDFA is not uniform in the frequency domain. As a result, the amplifiers provide a different amount of gains to the optical signal with different wavelengths or spectrum. This is a serious problem when the signal travels along a cascade of EDFAs. The non-flatness gain issue leads to the performance degradation of the optical system [28] [29]. To ensure the gain flatness, gain flatness filter can be placed at the output of the EDFA for power equalization. Some intermediate ROADM nodes also can adjust the attenuation of each wavelength to realize the power equalization. Due to the non-ideal optical filter, the signal spectral bandwidth is narrowing when it travels along with a series of filters (usually the ROADM, MUX and DEMUX) along its path. This phenomenon is called filter concatenation. FC causes the distortion of signal spectral shape and reduce the transmission reach distance to ensure certain signal quality of transmission (QoT) [30] [31]. The effect of FC reduces with the certain guard band between neighbour WDM channels or flexible guard band in elastic optical networks [32].

2.3.5 Inter-Channel Crosstalk

The linear inter-channel crosstalk is the effect that the power of optical signal leaks to other channels. This occurs because the equipment in the optical network such as: ROADMs, MUX and DEMUX cannot completely isolate different channels. The linear inter-channel crosstalk can be further classified as: out-of-band crosstalk and in-band crosstalk. Out-of-band crosstalk, as its name suggests, is the crosstalk interference from the channels outside the interfered channels. It mostly depends on the power of two neighbour channels. The

in-band crosstalk is due to incomplete isolation of the channels with the same wavelength but from/to different ports. The power of channels of the same wavelength mixed together, causing signal spectral shape distortion.

2.3.6 Self-Phase Modulation

The non-linear impairments, as known as Kerr effects, occurs during the transmission as the optical signal travelling in the fibre, causing its refractive index varying. The temporal changing of the refractive index results in the frequency shifting higher with increasing refractive index and frequency shifting lower with decreasing refractive index. This frequency chirping is named as SPM. The SPM depends on its signal power spectral density. The effect of SPM is higher when the signal power density is higher. The mitigation of SPM can be achieved by digital backpropagation technique [33–35].

2.3.7 Cross-Phase Modulation

Apart from the non-linear refractive index alternation due to the signal itself, the co-propagation signal of other channels also contributes to the refractive index changing. The phase of the signal also varies due to the impact of other channels. This is called cross-phase modulation. The effect of XPM can be asymmetric spectrum expanding. Similar to SPM, the XPM depends on the power spectral density of other channels, the number of neighbouring channels and the spacing between the target channel and the interfered channels [13]. XPM might be the most significant non-linear impairments in optical telecommunication systems where multiple wavelengths are multiplexed into a single fibre. Compared to 100 GHz spacing DWDM system, 50 GHz spacing signal or Nyquist WDM signal suffers much higher pulse distortion due to XPM [36].

2.3.8 Four Wave Mixing

Unlike SPM and XPM where the signal phase shifts due to the power of the signal itself or co-propagation signal, FWM originates from the interplay of co-propagation of three optical signal with wavelengths of ω_1 ω_2 and ω_3 respectively and a new wavelength ω_4 will be generated as:

$$\omega_4 = \omega_1 \pm \omega_2 \pm \omega_3 \tag{2.8}$$

The frequency of newly generated waveforms takes the various combinations of co-propagation frequency. In other words, SPM can be viewed as the FWM of different spectral components within the signal frequency bandwidth while XPM is the result of FWM between two interfered channels. Similar to XPM, FWM largely depends on the co-propagation signal power spectral density and the frequency spacing between three interacted spectral components. In the future optical network where the flex-grid network, the Nyquist signal and coherent detection are deployed, the FWM can be regarded as the effect of the interplay of all the spectral components in the optical fibre link. In this case, the FWM creates interference across the whole C-band which degrade all the co-propagation optical signal quality.

2.3.9 Stimulated Brillouin Scattering and Stimulated Raman Scattering

Besides the non-linear impairments between the optical field and the fibre medium material refractive index, there are interactions between the optical signal and the density variation within the fibre medium [13] [15], known as Brillouin scattering and Raman scattering. Stimulated Brillouin scattering sets an upper bound on the power level launched into the fibre. SBS poses a great challenge to the narrow bandwidth signal. However, the amount of power permitted in the fibre without significant effect increases with raising optical signal

bandwidth. In optical telecommunication system where multiple channels are multiplexed into a single fibre, the effect of SBS is reduced. Raman scattering effect transfers the power of high-frequency components to the low-frequency spectral components. It leads to the reduced SNR of the channel with higher frequency and interference of the channels with lower frequency. This mechanism is used as power amplification where the power of low-frequency pump carrier tones is delivered to the desired spectrum. It is reported that the effect of SRS is significantly less severe with signal bandwidth less than 100 nm width compared to the wide bandwidth transmission system of occupying over 100 nm [37]. Thus, SRS may lead to slight power tilt problem but not introduce serious interference in the WDM system operating in C-band.

2.4 Nonlinear Propagation Model

The electric field $\boldsymbol{E}$ propagating in the dielectric medium, such as optical fibre, leads to the segmentation of the bound charges and thus creates the electric polarisation field in the material. The combination of the electric field $\boldsymbol{E}$ and the polarisation field $\boldsymbol{P}$ is defined as electric displacement $\boldsymbol{D}$, which is expressed as [38]:

$$\boldsymbol{D} = \varepsilon_0 \cdot \boldsymbol{E} + \boldsymbol{P} \tag{2.9}$$

where ε_0 is the permittivity in the free space. As the polarisation field $\boldsymbol{P}$ can be further expressed as $\boldsymbol{P} = \varepsilon_0 \chi \boldsymbol{E}$, the equation 2.9 can be written as:

$$\boldsymbol{D} = \varepsilon_0 \cdot (1 + \chi)\boldsymbol{E} = \varepsilon_0 \varepsilon_r \boldsymbol{E} \tag{2.10}$$

where $\varepsilon_r = 1 + \chi$ is the relative permittivity of the propagation medium.

The polarisation field density $\boldsymbol{P}$ depends on the electric field density $\boldsymbol{E}$, calculated as [39]:

$$\boldsymbol{D} = \varepsilon_0 \cdot \left(\chi^{(1)} \boldsymbol{E} + \chi^{(2)} \boldsymbol{E}^2 + \chi^{(3)} \boldsymbol{E}^3 + ... \right) \tag{2.11}$$

where $\chi^{(1)}$ represents the linear response of the transmission medium, $\chi^{(2)}$ and $\chi^{(3)}$ stand for the 2nd and the 3rd order of susceptibilities, reflecting the nonlinear effects. Solving the Maxwell equation in 2.11 results in the nonlinear refraction index of the transmission material, where the Kerr effect occurs.

To know the effect of non-linear impairments, solving Maxwell's equation is necessary. After certain simplification of the original model, the model shown below is derived, known as nonlinear Schrodinger equation [36] [40]:

$$-\frac{\partial E}{\partial z} + \frac{\alpha}{2} E + \frac{i\beta_2}{2} \frac{\partial^2 E}{\partial t^2} - \frac{i\beta_3}{6} \frac{\partial^3 E}{\partial t^3} - i\gamma |E|^2 E = 0 \tag{2.12}$$

where α is the power loss coefficient, β_n stands for the n-th order of dispersion and the γ represents the nonlinear parameter, defined as $\gamma = \frac{\omega_0 n_2(\omega_0)}{c A_{eff}}$. A_{eff} is the effective mode area. The above equation contains the effect of SPM, XPM, FWM.

2.5 The Gaussian Noise Non-linear Impairments Model

In this work, we consider the dual polarisation optical networks operating in a dispersion uncompensated non-linear propagation regime, deployed with coherent detection technique, as shown in figure 2.1. Dual polarisation is adopted as it can double the transmission data rate in the modern telecom industry. The robust digital signal processor placing at the coherent receiver is able to recover the signal from dispersions, leading to no requirement of dispersion compensation fibre deployed in the optical links. It is reported that the non-linear interference

due to Kerr effect appearing in high dispersion regime can be regarded as Gaussian and additive local white noise [41–43]. This is the non-linear impairments Gaussian noise model.

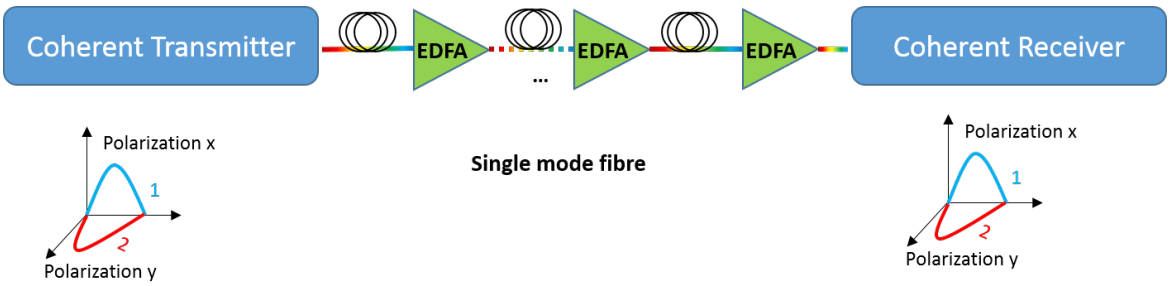

Fig. 2.1 A generic dual polarization dispersion uncompensated optical system

The Gaussian Noise (GN) non-linear impairments model proposed in [42] [43] has been proven to be an accurate tool to model the non-linear impairments in dispersion uncompensated optical system deployed with coherent detection technique. GN model views the optical signal as the combination of a series of spectral components and resorts the non-linear impairments generated in the fibre links as the frequency components interaction in means of FWM approach. The GN model is proposed assuming the NLI is the perturbation compared to the signal such that the non-linear impairments can be regarded as an additive noise following Gaussian distribution. These non-linear impairments are the summation results of interplay between all the spectral components within the existing optical signal. Compared to conventional non-linear Schroedinger equation, GN model provides simplified calculation using the double integration across the available spectrum bandwidth. In this section, we will only discuss the original GN model and its simple application, while the recent research output regarding the nonlinearity-aware resource allocation using GN model is shown in the next chapter. The original non-linear GN model equation in [42] can be expressed as:

$$G_{NLI}(f) = \frac{16}{27}\gamma^2 L_{eff}^2 \cdot \int_{-\infty}^{\infty}\int_{-\infty}^{\infty} G(f_1)G(f_2)G(f_1+f_2-f)\cdot\rho(f_1,f_2,f)\cdot\chi(f_1,f_2,f)df_1df_2 \tag{2.13}$$

where the $G_{NLI}(f)$ is the power spectral density (W/Hz) of the non-linear impairments of frequency component f, the G(f) being the power spectral density of the co-propagation channels in the fibre at frequency f. γ is the fibre non-linear coefficient ($W^{-1} \cdot km^{-1}$) and L_{eff} being the effective fibre span length (km), described in table 2.1. As the Gaussian noise reference formula can be described as the beating each tiny spectral components of the signal with co-propagation signal in a 'four wave mixing' way, the factor $\rho(f_1, f_2, f)$ in equation 2.13 presents the FWM process, written as:

$$\rho(f_1, f_2, f) = |\frac{1 - e^{-\alpha \cdot L_s} e^{j4\pi^2 \beta_2 L_s (f_1 - f)(f_2 - f)}}{\alpha - j4\pi^2 \beta_2 L_s (f_1 - f)(f_2 - f)}|^2 \cdot L_{eff}^{-2} \tag{2.14}$$

where the L_s is the fibre span length (km), α being the fibre power loss coefficient and the β_2 being the absolute chromatic dispersion value ($ps^2 \cdot km^{-1}$). The L_{eff}^{-2} is to normalize the 'FWM' factor ρ. The new generated non-linear impairment spectral component $G_{NLI}(f)$ is the result of beating of three spectral slice f_1, f_2 and $f_3 = f_1 + f_2 - f$ with the four wave mixing factor $\rho(f_1, f_2, f)$. The factor $\chi(f_1, f_2, f)$ is the phase factor, representing how the nonlinear impairments accumulates along the multiple fibre spans. The integrated factor $G(f_1)G(f_2)G(f_1 + f_2 - f)$ represents the strength/power of each of the non-linear impairments 'pumping' spectral slice. The factor $\chi(f_1, f_2, f)$ can be expressed as:

$$\chi(f_1, f_2, f) = \frac{sin^2[2\pi^2 (f_1 - f)(f_2 - f)\beta_2 L_s N_s]}{sin^2[2\pi^2 (f_1 - f)(f_2 - f)\beta_2 L_s]} \tag{2.15}$$

where N_s is the number of fibre span in the optical link. $\chi(f_1, f_2, f)$ is the phase factor accounting for the summation of the non-linear impairments across multiple fibre spans coherently. The phase of the NLI noise is important as it describes how the non-linear impairment noise can be accumulated for multiple fibre span optical system.

From the non-linear impairments Gaussian Noise reference formulation, it is observed that the non-linear impairments do not depend on the modulation format of the signal. This

simplification allows decoupling the validation of the signal quality of transmission from the selection of multiple modulation formats, which can largely reduce the complexity of the optical network optimisation strategy.

2.6 Brief review of non-linear impairments Gaussian noise model and its application

The non-linear interference Gaussian noise model regards the optical signal as a series of spectral slices and resorts the non-linear impairments produced in the fibre links as the frequency components interaction in means of four-wave mixing approach. According to the GN model, the non-linear interference noise can be categorised as three classes according to their origins and where the new interfered frequency components are generated: 1) self-channel interference, 2) cross-channel interference and 3) multi-channel interference. An example of 3 types of non-linear interference is shown in figure 2.2. The red arrows are the interplay frequency components of the original optical signal while the blue arrows are newly generated frequency components of the non-linear interference noise.

The self-channel interference is shown in figure 2.2 (a), where all relevant frequency components: f_1, f_2 and f_3 are within the same optical signal bandwidth, while the new beating frequency slice is within the same channel. The effect of cross-channel interference is shown in figure 2.2 (b), where the new beating up frequency components are due to the original optical channel and one another channel. Figure 2.2 (c) shows one example of the multi-channel interference whose relevant frequency slices f_1, f_2 and f_3 are the combination such that generated non-linear slice is due to at least two components coming different from the influenced channel. Multi-channel interference can also be generated at the fourth channel where the three 'pump' frequency slices are of three different channels.

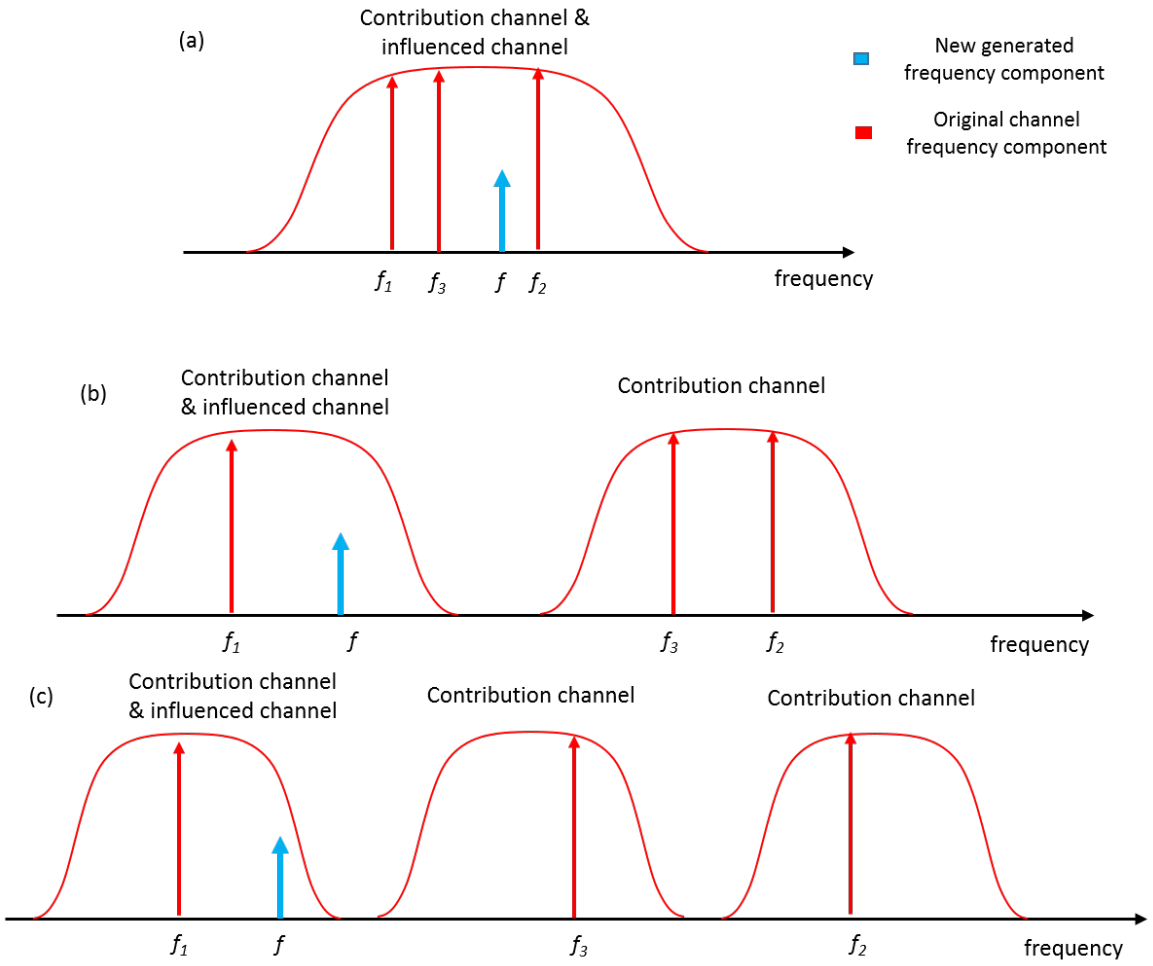

Fig. 2.2 An example view of three types of non-linear interference noise. Red tall arrows: . Blue short arrows: new generated non-linear interference spectral components. (a): self-channel interference; (b): cross-channel interference; (c): multi-channel interference

.

The self-channel interference is the nonlinear impairments caused and generated by its own frequency channel while the cross-channel interference and multi-channel interference are the results of interplay of multiple channels. The main difference between cross-channel interference and multi-channel interference is that cross-channel interference is the results of two channels while the interference on both channels are identical if the PSD of two channels is the same. The multi-channel interference is the result of three channels where the interference can be generated in any of three channels or the fourth channel.

2.6.1 GN Model Approximation and Simplification

Unlike the dispersion impairments which can be mitigated by placing robust digital signal processor at the receivers, the non-linear distortions introduce new frequencies among the transmission bandwidth. The new frequency slices interfere with the existing optical channel in a way of additive Gaussian noise, which degrades the quality of transmission of copropagating optical channels. Hence, it is essential to acquire the knowledge of non-linear impairments to evaluate the QoT performance of the lightpath before establishment. It can be observed from equation 2.13 that the calculation of non-linear interference power over the propagating channel using original GN model requires the triple integral calculation. This again results in a tremendous amount of computation complexity.

To overcome the computational complexity issue, approximate solutions have been proposed in [44] [45] [46] [47]. Rectangular spectrum shape of the bandwidth variable signal is assumed in [44] [45] to reduce the dependency of the signal spectrum shape. As the self-channel interference and cross-channel interference are the main contributors to the overall non-linear interference noise, authors in [44] [46] [47] ignore the multi-channel interference which can provide enough accuracy when channel spacing is more than 28 GHz. Integral area of calculating self-channel interference is approximated to square and circular respectively to derive a closed-form analytical mathematical expression of self-

channel interference. Neglecting the multi-channel interference results in model inaccuracy for channel spacing less than 28 GHz. This makes them inefficient tools for nonlinearity validation in elastic optical networks. Authors in [48] proposed an accurate one-dimensional integral formulation of the non-linear impairments computation for both Nyquist rectangular spectra and non-Nyquist rectangular spectra. Similar to other models, the formulation can only be applied for self-channel interference and the cross-channel interference estimation. A rapid analytical formulation of the non-linear impairments is developed for mesh networks based on GN model in [49]. The proposed solution is able to provide enough accuracy to model the non-linear impairments in WDM network with wavelengths add and drop in different locations. Their models are based on incoherent GN model.

2.6.2 Launch Power Optimization and Resource Allocation With GN Model

The strength of the non-linear interference of the propagating channels in the network increases non-linearly with the growing signal launch power. The optical system operates in the linear regime with the small launch power where the ASE noise is the dominant impairments of the lightpath. With the increasing launch power, the system moves to the non-linear regime while the non-linear interference noise becomes one of the dominant factors. A closed-form expression of optimal launch power of the worst NLI-interfered channel in the WDM system is shown in [42]. The same author also reported in [50] that the launch power of each fibre span can be optimized individually to achieve the global optimization assuming fully loaded links, signal spectra of Nyquist rectangular and non-linear interference accumulate incoherently along multiple spans, which is known as local optimum global optimum with Nyquist shape (LOGON).

However, LOGON strategy only considers the optimization of the worst interfered channel and assuming fully occupied C-band of the DWDM system, which results in the launch

power of non-central channels unoptimized. Individual channel launch power allocation to optimize the overall network performance is reported in [47, 51–55]. Individual channel power optimization of a single link, a three-node network and the entire network is presented in [47] [52] to achieve the maximum information capacity or Shannon capacity. In [53] and [55], the multi-objective optimisation linear integer programming is proposed to minimise the total transmit power thus to minimize the nonlinear impairments.

2.7 EDFA Power Control and Impairments from ROADM

Despite the non-linear impairments posing a great challenge to the optical networks, the ASE noise generated from the optical amplifiers is the dominant impairment. Distributed power amplification is widely adopted, especially using EDFA for long distance transmission in modern optical networks due to its great reliability [56]. Therefore, the EDFA power control is essential to impairments management in the optical networks. The EDFA spectrum gain and noise figure tilt problem of using a cascade of EDFAs have been analysed and addressed in [57]. [58] propose an analytical black box formulation to model the EDFA gain tilt and noise figure unflattering phenomenon and experimentally demonstrate the accuracy of the proposed analytical model. The EDFA power gain control and the noise figure under the multiple channels amplification case is investigated in [59]. It is reported that the gain and noise features of the EDFA largely depends on population inversion level of the erbium-doped fibre. [60] shows similar results that the optimal EDFA gain and noise figure can be achieved with different gain and noise figure combination. Noise figure is the factor to measure the SNR degradation due to the amplification. However, its value relates to the input power and pump power, making it hard to complete the characterisation without a large number of testing points. In [61], a neural networks based regression approach is proposed with a limited number of testing points as the training sample to obtain the whole characterisation performance of the gain flatness curve and the noise figure curve. The regression method

can achieve estimated errors of less than 0.1 dB compared to the test values for the noise figure over the entire propagation spectrum. The power and gain adjustment of the EDFA is essential to the overall performance of the optical networks. In [62], authors present a machine learning based solution to adaptively adjust a cascade of EDFAs to minimize the entire noise figure and the gain spectrum ripple of the end-to-end optical system. The proposed iterative method indicates that the optical link can be optimized while remains the pre-set input and output power level.

ROADM, as the optical switching element, adds extra loss apart from the optical link loss. The signal power loss due to the ROADM insertion loss needs to be compensated by EDFA to allow enough signal power within the sensitivity of the receivers as well allow enough power into the following optical link. Therefore, the additional power amplifiers to recover the signal power due to ROADM insertion loss will add more ASE noise to the original signal. The ROADM insertion loss depends on its architecture design, its size in terms of degrees and types of the components used [63]. The ROADM architectures and the common components for the ROADM are presented in [64]. Both couplers/splitters and wavelength selective switch can be served as MUX or DEMUX in the ROADM. According to the number of channels adding or dropping, the insertion loss using couplers or WSS are different. WSS with 16 ports served as the MUX or DEMUX adds 5 dB - 6 dB insertion loss to the ROADM while the 1×16 coupler can suffer 12 dB - 13 dB loss. Therefore, the ASE noise due to the ROADM varies with different ROADM architecture. Architecture on demand (AoD) is proposed in [65] [66] to provide programmable functions to the optical hardware and adapt the hardware architecture according to the requirement. Due to the concept of AoD, the ASE impairments of the AoD nodes vary with the flexible configuration demand. The number of spans the signal can reach with lower loss ROADMs or AoD nodes is more compared to high loss ROADM. Apart from the ASE noise due to the ROADM or AoD nodes insertion loss, polarization dependent loss of the ROADM also affects the signal QoT. It is reported

in [63] that the maximum number of spans reduces from 23 to 18 when the PDL increases from 0.5 dB to 1 dB. As it is hard to estimate the exact impact of the PDL, the statistical worst-case PDL due to ROADM is applied to the network design. The signal suffers spectra narrowing effect as it travels through multiple ROADMs due to the filter concatenation effect. The paper [30] suggests certain margin needs to be allocated due to the filtering effect.

2.8 Optical Signal Quality Assessment Model

In this work, we consider the modern polarization multiplexing optical network deployed with the latest coherent transceivers in the dispersion uncompensated paradigm. The signal transmits in the fibre generating high chromatic dispersion and polarization mode dispersion without any dispersion compensation fibre. The polarization multiplexing techniques which doubles the optical network throughput, are assumed to be deployed and PM signals are of the equal power in both orthogonal polarization modes.

We also assume the ideal transceivers with digital signal processors, thus there is no impairments or penalty from the transceivers. The amplified spontaneous emission noise due to the signal power amplification in optical links is the main source of stochastic noise. It is further assumed that the ideal digital processors can recover the signal from linear transmission impairments like chromatic dispersion and polarization mode dispersion (except ASE noise), that the wavelength selective switch or the demultiplexer in the ROADM can completely isolate the different channels without causing the filter concatenation effect. The gain curve of EDFA is assumed to be flat which gives the equal gain of different spectral components thus its noise figure is also a constant value. We consider the self-phase modulation, cross-phase modulation and four-wave mixing as the main the non-linear impairments while neglects the stimulated Brillouin scattering due to broadband communication as well as the stimulated Raman scattering. In this case, the electronic

signal-to-noise ratio at the receiver depends on the amplified spontaneous emission noise during amplification and non-linear impairments during transmission.

In this work, we choose the non-linear impairments Gaussian noise model to quantify the impact of third order electric susceptibility Kerr effect. The Gaussian shape of the non-linear impairments is the basis of the GN model in the dispersion uncompensated optical network. The unmanaged dispersion introduces inter-symbol interference in the time domain to the original optical signal, which causes the signal shape appearing to be Gaussian distribution in the time domain. Also, the phase noise or the spectrum broadening due to Kerr effect is regarded as a circular Gaussian distributed noise. At the receiver, the powerful digital processor recovers the signal to its undistorted form due to the dispersion. However, the non-linear impairments accumulated along the fibre spans cannot be restored correctly, leading to a circular Gaussian noise for both polarization modes and both IQ planes [41–43].

2.8.1 SNR and OSNR

The stochastic ASE noise is white additive Gaussian distributed interference across the operation bandwidth of EDFA. Under the assumption that the non-linear impairments being Gaussian distribution, the electronic signal-to-noise ratio can be expressed as:

$$SNR = \frac{P_{sig}}{P_{ASE} + P_{NLI}} \tag{2.16}$$

where P_{sig} is the received optical signal power, P_{NLI} being the received non-linear impairments power within the signal bandwidth and P_{ASE} being the received amplified spontaneous emission noise power within signal bandwidth. From equation 2.6, we can derive the ASE noise power at the receivers as:

$$P_{ASE} = h\nu B \cdot \sum_{k} (10^{\frac{G_k}{10}} - 1) \cdot 10^{\frac{NF}{10}} \tag{2.17}$$

where the B is the bandwidth of signal and G_k being the EDFA gain of k_{th} fibre span in dB. Similarly, the power of non-linear interference according to equation (2.13) are assumed to accumulate incoherently thus the 'phase array' factor $\chi(f_1, f_2, f)$ is set to 1 in our work. Therefore, the power of non-linear interference noise can be written as:

$$P_{NLI} = \frac{16}{27} \cdot N_k \cdot \gamma^2 \cdot L_{eff}^2 \cdot \int_{-\frac{B}{2}}^{\frac{B}{2}} \int_{-\infty}^{\infty} \int_{-\infty}^{\infty} G(f_1) \cdot G(f_2) \cdot G(f_1 + f_2 - f) \cdot \rho(f_1, f_2, f) \cdot df_1 df_2 \tag{2.18}$$

where $\frac{B}{2}$ is half of the signal bandwidth and the N_k being the number of fibre spans. By combining equation (2.16), (2.17) and (2.18), we can derive the optical signal quality of transmission assessment model considering the ASE noise and the non-linear impairments under the regime of coherent detection.

The optical signal-to-noise ratio is measured as the ratio of signal power to the noise power in the optical domain. The bandwidth of operating noise power measurement is usually specified as 0.1 nm, which is roughly around 12.5 GHz for 1550 nm C-band signal. The relationship between the electronic symbol SNR and OSNR in the optical domain can be described as:

$$OSNR = SNR \cdot \frac{B}{B_{ref}} \tag{2.19}$$

where the B_{ref} is the 0.1 nm reference bandwidth for the ASE noise measurement and SNR and $OSNR$ both being linear ratio. Considering 50 GHz channel spacing Nyquist WDM signal, the $OSNR$ can be further expressed as:

$$OSNR_{dB} = SNR_{dB} + 6dB \tag{2.20}$$

where the SNR_{dB} and $OSNR_{dB}$ is the electrical signal-to-noise ratio and optical signal-to-noise ratio in decibel unit respectively.

2.8.2 BER and SNR

At the receiver, the received signal is demodulated into an analogue electrical signal and then converted into digital bits. Hence, the recovered bits version might not be exactly the same as the original bits, which introduce errors to the original information stream. As described in the previous section, the quality of transmission of the signal is dependent on the SNR at the receiver. As a result, the bit error rate is the direct reflection of the noise effect over the signal. In this work, we consider the hard decision decoding [67] over the symbols. The BER of Additive White Noise Gaussian Noise (AWGN) channel from [68] [69] is calculated as:

$$BER = \frac{2(1-\frac{1}{L})}{log_2 L} Q\left[\sqrt{\left[\frac{3log_2 L}{L^2-1}\right]\frac{2E_b}{N_0}}\right] \tag{2.21}$$

where the L is the number of levels within I-Q plane for the M-ary modulation format, E_b being the energy per bit and the $N_0/2$ being the PSD of the additive white Gaussian noise. The function Q is similar to $erfc$ function, which is given by [70]:

$$Q(x) = \int_x^\infty \frac{1}{\sqrt{2\pi}} e^{-\frac{y^2}{2}} dy \tag{2.22}$$

The equation (2.21) can be further simplified and approximated as [71]:

$$BER \simeq A \cdot erfc(\sqrt{B \cdot SNR}) \tag{2.23}$$

The value of A and B alter for different M-ary square modulation schemes, which is expressed as [71]:

$$A = \frac{\sqrt{M}-1}{\sqrt{M}log_2(\sqrt{M})} \tag{2.24}$$

$$B = \sqrt{\frac{3log_2 M}{2(M-1)}} \tag{2.25}$$

2.9 Dependence of FEC coding rate on SNR

Forward error correction (FEC) is widely adopted in the current optical network system by giving redundancy to the coded information. The extra redundancy gives the receiver the capability to detect or even recover the errors occurring due to the dispersion, ASE noise and the non-linear interference. By correcting the error bits, the bit error rate maintains at an extremely low level, which can be regarded as error-free transmission. Therefore, by adding the FEC overhead to the original information, retransmission can be avoided, leading to a significant amount of bandwidth saving [72].

To analyse the impact of deploying forward error correction code rate over the bit error rate using polarization multiplexed quadrature amplitude modulation constellations, we choose using the model in the presence of AWGN channel. The maximum FEC coding rate of using hard decision decoding can be calculated as [73]:

$$CR_{FEC} = 1 + BER \cdot log_2(BER) + (1-BER)log_2(1-BER) \tag{2.26}$$

From equation (2.23), the pre-FEC bit error rate can be derived given the modulation format and the electrical SNR at the receiver. Certain pre-FEC bit error rate threshold is set according to its coding rate to deliver error-free transmission. The SNR difference between

Table 2.2 The required electrical SNR to achieve pre-FEC bit error rate

Modulation Format	Required Electrical SNR for pre-FEC BER 3.8×10^{-3}
PM-BPSK	5.5 dB
PM-QPSK	8.5 dB
PM-8QAM	12.5 dB
PM-16QAM	15.1 dB
PM-32QAM	18.1 dB
PM-64QAM	21.1 dB
PM-128QAM	23.9 dB
PM-256QAM	26.8 dB
PM-512QAM	29.6 dB
PM-1024QAM	32.6 dB

the uncoded transmission system and coded system to achieve the same BER level is often specified as the net coding gain. The net coding gain determines the performance of FEC, expressed as [74]:

$$NCG(dB) = 20log_{10}\left[erfc^{-1}(2 \cdot BER_{pre})\right] - 20log_{10}\left[erfc^{-1}(2 \cdot BER_{post})\right] + 10log_{10}CR \tag{2.27}$$

where BER_{pre} and BER_{post} are the bit error rate of the signal input to forward error correction decoder and reference bit error rate after FEC decoding respectively. CR is the FEC coding rate, representing the penalty because of adding redundancy to the original information bits in form of overhead, written as:

$$CR = \frac{k}{k+r} \tag{2.28}$$

where k is the number of bits for FEC overhead and r being the number of bits of the original information stream. The reference post-FEC bit error rate is often referred to achieve 10^{-15} as the error-free transmission [75]. Combining equation above, 9.35 dB and 10.5 dB FEC net coding gain can be achieved when deploying 7% and 20% FEC overhead respectively. Pre-FEC bit error rate of 3.8×10^{-3} and 1.5×10^{-2} is permitted with the benefit of the net coding gains deploying 7% and 20% FEC overhead respectively. In table 2.2, we list the required electrical SNR to achieve the pre-FEC bit error rate threshold with 7% FEC overhead for different modulation schemes.

2.10 Summary

In this chapter, the basic knowledge of optical fibre and the relevant parameters/information are first presented. As launching optical signal into the optical fibre would introduce the impairments and degrade the optical signal quality, the physical layer impairments are classified

and their impact on the signal quality are discussed. Then, the nonlinear impairment Gaussian noise model is introduced and current related state-of-art research works are detailed review. The main contribution of these works is targeting the approximation and simplification of the GN model. However, they either underestimate the nonlinear impairments or may fail the requirement of elastic optical networks with flex-grid spectrum allocation of 12.5 GHz or even 6.25 GHz grid. This motivates the work described in chapter 4 for a computationally simple and accurate nonlinear impairments tool. Finally, the signal quality assessment model is formed and used in the later chapters.

Chapter 3

Optical Networking and Resource Allocation

3.1 Introduction

Resource allocation and optimisation are regarded as one of the most important features in the optical networks. The network resource allocation and optimisation assign proper power, routing, modulation and spectrum resources to the traffic requests. It enables to reduce the optical network blocking probability, to increase optical network efficiency, to achieve energy efficiency, etc. In this chapter, we will start by reviewing the basic concepts and technologies in the optical backbone networks. Then we describe techniques to be deployed in the advanced elastic optical networks. Followed by that, the related work of routing modulation format and spectrum assignment problem is discussed and reviewed. At last, the resource allocation and optimisation problem based on GN nonlinear impairments model are introduced.

3.2 Wavelength Division-Multiplexing Optical System

Due to the increasing Internet traffic, the desire for high bandwidth service and to reduce the expenditure of deploying new MPLS or SONET/SDH networks, the WDM optical networks are introduced by network infrastructure providers during mid-1990s [76]. WDM is a multiplexing technique which allows a large number of optical signal with different wavelengths multiplexed into the same optical fibre [6] [77] [78] , as shown in figure 3.1. Therefore, less amount of fibre is needed due to multiplexing multiple channels into a single fibre. This technique can significantly improve communication throughput and efficiency. Optical fibre links and optical switching elements form the basis of the WDM optical networks. The optical signal is launched into optical fibre through the transmitters and then routed to the receivers at desired destinations through optical switching elements.

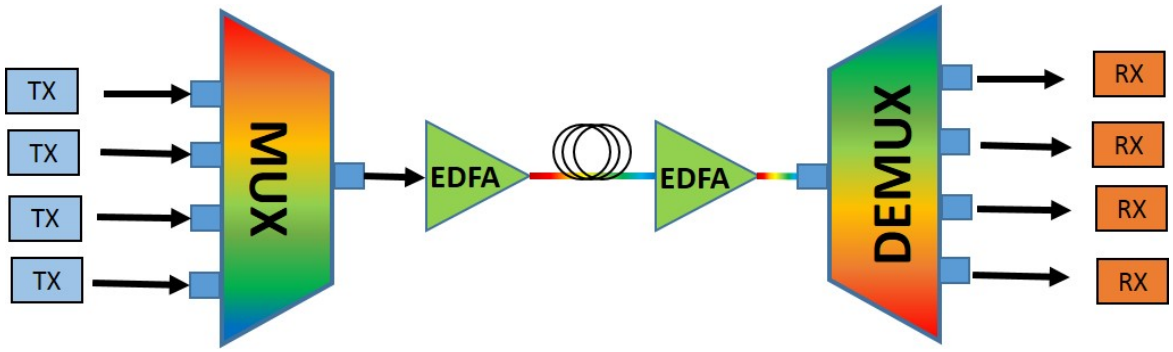

Fig. 3.1 Basic WDM system diagram

ROADMs are the main switching elements in WDM networks, which usually consist of wavelength selective switches, multiplexers, demultiplexers and couplers [64]. Apart from switching functionality, it also supports add/drop function which routes the locally added optical signal to other ROADMs or routes the optical signal from other optical nodes to the local receivers. Optical nodes or ROADMs are connected by optical fibre links. Each fibre link consists of a pair of fibre to enable bi-direction transmission and contains multiple fibre spans with optical amplifiers in between to compensate any signal power loss during the transmission.

DWDM system refers to the multiplexing technique within C-band (1530 nm - 1565 nm) and L-band (1565 nm - 1625 nm) defined as per ITU-T G.694.1 v2.0 [79]. Currently, it mainly operates within C-band transmitting and switching the optical signal wavelength at 100 GHz spacing for 40 channels or with 80 channels at 50 GHz spacing according to ITU-T G.694.1 standard. Traditionally, there are three types of DWDM networks, known as the transparent optical network where all the signal are routed optically, opaque optical network wherein the signal experiences O-E-O in the all the switching nodes and translucent optical network which contains the mixture of fully optical nodes and O-E-O nodes [80] [81]. In both opaque and translucent optical network, the signal in all or some intermediate nodes is received and converted into electronic domain first and then is modulated into the optical domain. Those O-E-O enabled nodes are named as repeater or regenerator, with the capability of wavelength conversion, modulation format adaptation or re-amplification, reshaping and re-timing as the functions of 3R regenerator [82] [83]. We consider the transparent optical network in this work without O-E-O conversion at the intermediate switching elements.

DWDM system operates and switches the optical signal according to their allocated channel. Due to fixed channel spacing, each channel tends to unlikely support traffic over 100 Gbps or 400 Gbps within fixed 50 GHz ITU grid [32]. Apart from this, the signal in the traditional DWDM system does not occupy the whole channel bandwidth, which in turn leaves unused spectrum [84]. This not only leads to spectrum waste but also limit the maximum capacity of each wavelength. Driven by the exponential growth of new applications and services such as cloud computing, high-definition video streaming, inter data centre communication, the conventional WDM or DWDM system currently deployed in the operator networks are unable to accommodate these high-bandwidth dynamic demands over the existing infrastructures. Also, the conventional DWDM system lacks adequate scalability to meet to highly increasing network traffic demand and the capability to adjust

rapid changing traffic profile. Therefore, we focus on the elastic optical networks in this work which can provide better efficiency, scalability and the flexibility [32] [85] [86].

3.3 Elastic Optical Networks

To overcome the problem of DWDM optical networks, elastic optical networks is proposed to support high-bandwidth, dynamic traffic requests and facilitate better network resources utilisation by employing flexible bandwidth allocation [32] [85] [87]. Compared to conventional WDM optical networks, EON can achieve flexible optical spectrum assignment. In EON, a certain amount of continuous and contiguous small bandwidth grids form the optical channels, which provide the possibility of carrying low bit rate data stream or offer the capability of transmitting over 400 Gbps per channel. In this case, the spectrum resources can be utilized efficiently and dynamically according to the corresponding service traffic request rate. It is reported in [32] that 5% - 150% spectrum efficiency improvement can be achieved in EON using flexible spectrum assignment compared to using fixed 50 GHz grid WDM channels with 10 GHz bandwidth as the guard band.

3.3.1 Bandwidth Variable Transceivers

The benefit of EON that delivers better spectrum efficiency compared to the DWDM system relies on the bandwidth variable transponders and bandwidth variable spectrum selective switches based ROADM deployed in the elastic optical networks [85]. BVT is a class of transponders which can dynamically tune certain attributes, such as: optical spectrum central frequency, the spectrum bandwidth, spectral shape, the signal launch power, the modulation format and its forward error correction coding rate [88], where its diagram is shown in figure 3.2. Recent research work focuses on sliceable BVT with the capability of allocating subcarriers to different connection requests [88–91]. It allows the data streams from the same

client interface to be mapped into several optical data paths, each with different modulation formats, FEC coding schemes and coding rates, or several data streams are aggregated to a large single optical super-channel according to traffic requests and network applications.

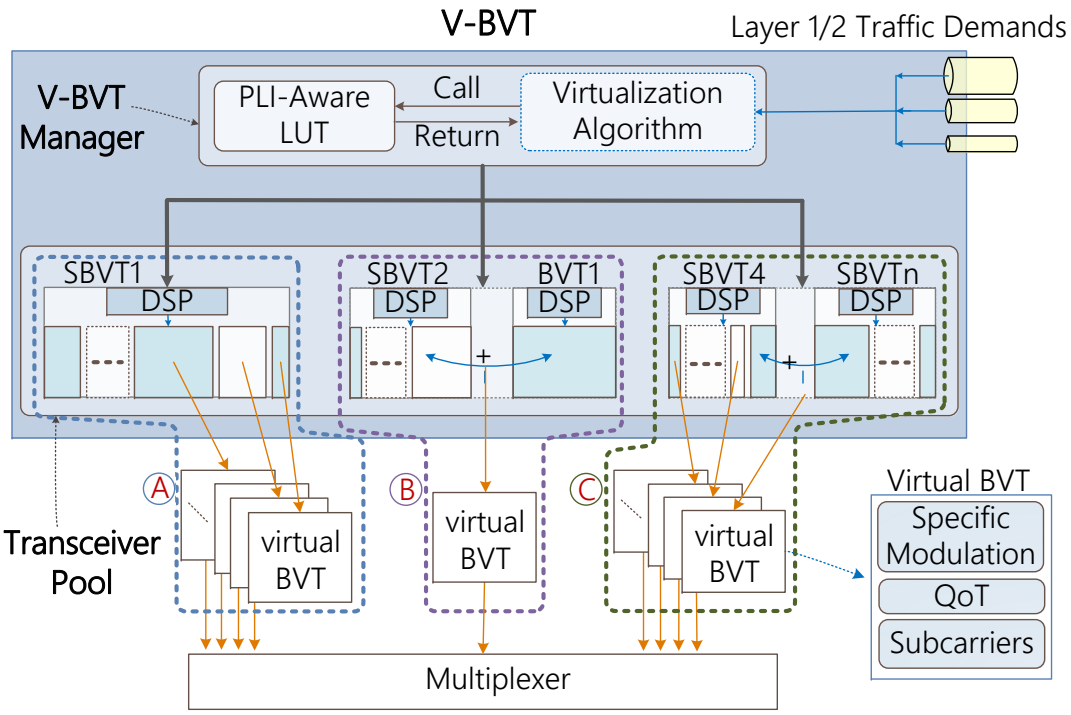

Fig. 3.2 The building diagram of the S-BVT architecture supporting O-OFDM [90].

3.3.2 Flex-Grid Reconfigurable Optical Add-Drop Multiplexer

To support the switching functionality in EON, ROADM supporting flex-grid signal routing/switching is needed. Traditionally, several wavelength selective switches are interconnected to form the ROADM in DWDM system. With the development of techniques of manufacturing flexible WSS or SSS, the new WSS/SSS allows near arbitrary spectrum switching of 6.25 GHz filtering bandwidth and 1 GHz incremental resolution step [92] [93]. A typical 2 degrees ROADM architecture is illustrated in figure 3.3.

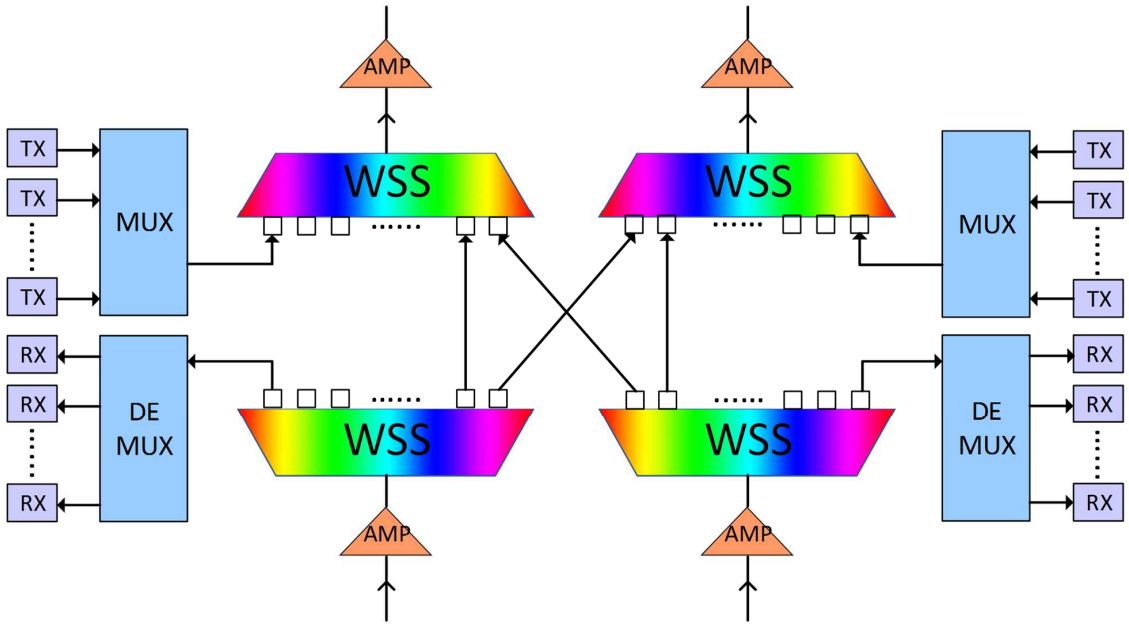

Fig. 3.3 Classic ROADM architecture design

The MUX and DEMUX are connected to WSS to add local lightpaths to the optical network or drop the lightpaths to the local IP edge router. In some cases, the MUX can be simple couplers to reduce the overall cost of ROADM. However, coupler suffers a high loss when too many lightpaths or sub-carriers are supported locally, which leads to a great challenge to the optical system design. In this case, the coupler can be replaced by a low loss reconfigurable arrayed waveguide grating or a flexible WSS to allow sufficient signal power launching into the network. The DEMUX can be an active device like WSS or a passive device as AWG, which can separate the wavelengths or channel spectrum bandwidths. WSS or SSS inside the flexible ROADM architecture can provide the colourless switching, which is able to support arbitrary spectrum routing into the specific port. The ROADM is classified as colourless in this case [64]. The amplifiers in the southbound compensate the signal power loss of the fibre span connected to the ROADM while the amplifiers in the northbound recover the signal power due to the ROADM insertion loss, such as coupler loss, fibre connector loss, WSS insertion loss and power equalization loss.

Apart from colorless ROADM, the ROADM can be classified according to their functions and constraints such as colorless, directionless ROADM and colorless, directionless and contentionless (known as CDC) ROADM [64, 94–96]. The directionless ROADM is able to provide the freedom to switch the optical spectrum to any output ports. The contentionless ROADM further removes the wavelength or spectrum constraint where any spectrum bandwidth resource can be allocated to any ports as long as spectrum non-overlapping restriction is satisfied at the output port. The CDC bandwidth flexible ROADM not only reduces the operational cost of the ROADMs as well as the overall network but also simplifies network resource management and eases the operational constraint.

3.4 Brief review of resource allocation in optical networks

The resource allocation problem in elastic optical networks often refers to the routing and spectrum allocation (RSA) problem. Similarly, it is equivalent to the routing and wavelength allocation (RWA) in DWDM optical networks. The difference is that elastic optical networks offer the flexible spectrum slots allocation to meet the various demands of bandwidth compared to assigning single wavelength in DWDM optical system. The allocated spectrum resources need to be assigned to be near each other as a whole spectrum block. This is known as the spectrum contiguity constraint in the optical networks [85] [97] [98]. In transparent elastic optical networks, where optical-electronic-optical conversion is not permitted, the same spectrum slots must be allocated to all the optical links along the selected end-to-end lightpath. Similar to spectrum contiguity constraint, this is called the spectrum continuity constraint in transparent optical networks.

Figure 3.4 shows an example of spectrum slots allocation in elastic optical network. We assume a connection request from node 1 to node 5 requires 4 spectrum slots. The path is calculated of utilizing the link 1 between node 1 and node 2, link 2 between node 2 and node 4 and link 3 between node 4 and node 5 and spectrum slot 1 - 4 is assigned in the example.

The route of node 1 - 3 - 4 - 5 is not selected as it does not meet the requirement to provide both continuous and contiguous slots. However, the requirement of two constraints can be met when the lightpath travels the node 1-2-4-5 and spectrum is assigned as index 1 - 4 slot.

RWA problem in conventional DWDM system has proven to be an NP-hard problem, which has been studied for years [97, 99–101]. The RSA problem in the elastic optical network can be regarded as the RWA problem when the number of spectrum slots is equivalent to the number of wavelengths. Therefore, the routing and spectrum allocation problem is also an NP-hard problem [98] [102]. Many generic heuristic algorithms have been proposed to solve the RSA problem. These generic RSA algorithms usually treat the problem by splitting it into two independent small topics: 1) the routing problem and 2) spectrum assignment problem.

3.4.1 Routing and Spectrum Assignment

There are several routing techniques in optical networks: 1) fixed path routing, 2) fixed alternative path routing, 3) least congested path routing and 4) dynamic adaptive path routing [97] [103] [104]. These routing techniques rely on the output of graph theory: Dijkstra's algorithm [105] [106]. In fixed path routing, usually, the physically shortest path is pre-calculated for each pair of the source node and destination node in the network. This technique maintains a single routing table for each pair of source and destination and the spectrum allocation scheme searches the available spectrum resources to establish the connection. In case that no spectrum is available to host the connection requirement, the connection request is rejected and regarded as blocked. The fixed alternative path routing is a direct extension of the fixed path routing algorithm. For each pair of source and destination, the routing table contains a list of routing paths. In case one path cannot provide enough spectrum resources, the algorithm continues searches the spectrum resource of the next candidate path in the routing table. Unlike fixed path routing and the fixed alternative path routing usually

calculate the physically shortest path or the physically K-shortest paths, least congested path routing [103] [107] determines the routing path according to the link congestion condition by the time the connection request arrives. Dynamic adaptive path routing calculates the path based on real-time link state information or certain policy [108].

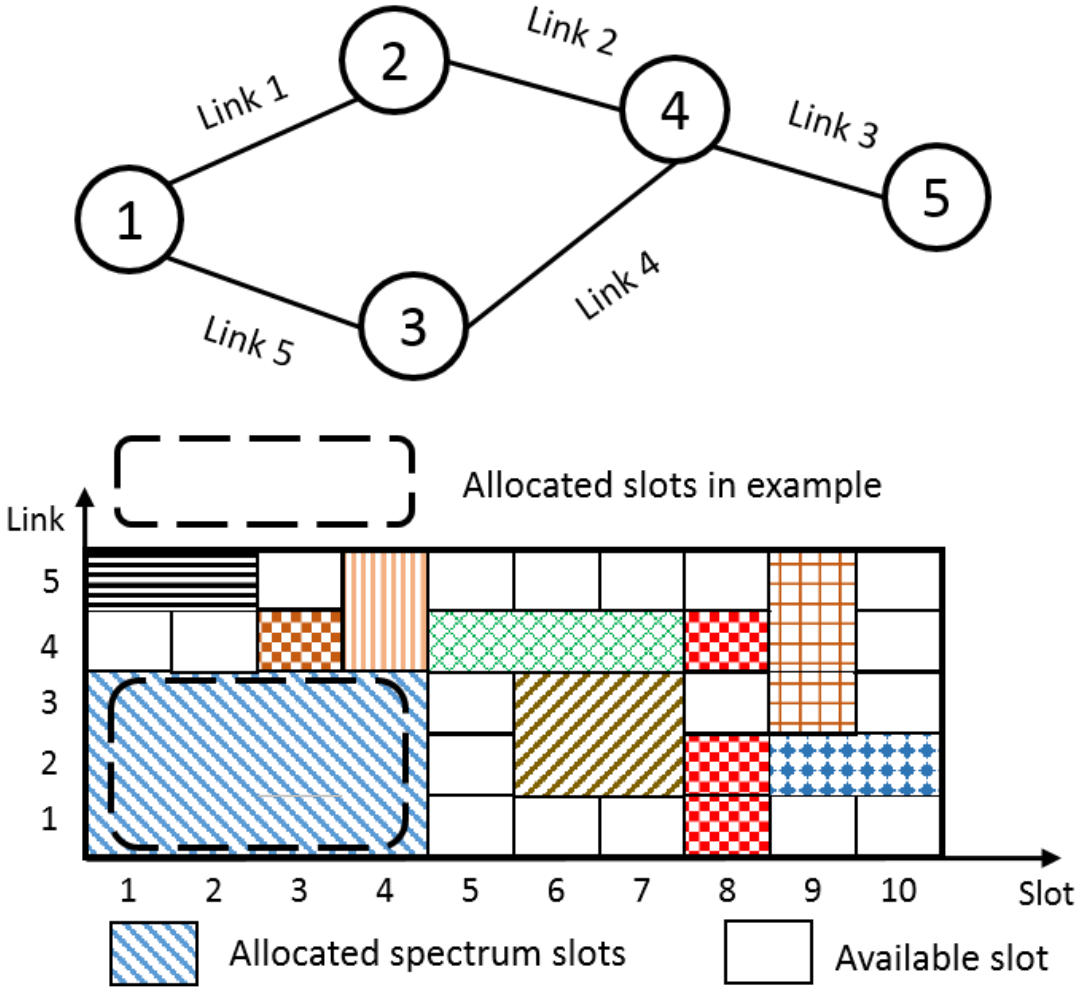

Fig. 3.4 An example of spectrum slots allocation in elastic optical networks

In elastic optical networks, the number of spectrum slots can be adapted flexibly according to the bandwidth requirement of the connection requests, thus to achieve higher spectral efficiency. The spectrum allocation can be performed either jointly with the routing process or independent of the routing path. First-fit spectrum slot allocation [109] [110] assigns the

first available spectrum slots block to the connection, which meets the spectrum continuity and contiguity constraint requirement for the selected path. Random-fit policy randomly chooses the available slots, to avoid multiple connection requests selecting the same slot [97] [109]. In contrast to the first-fit spectrum allocation, last-fit allocation allocates the highest possible index spectrum slots from the available slots pool. First-last fit spectrum assignment combines the feature of both first-fit and last-fit. The connection requests are divided into odd and even subset. When the odd indexed number of request arrives, the algorithm attempts to assign the spectrum slots in a first-fit way. The last-fit spectrum assignment is performed for the even indexed number of connection requests [110]. Exact-fit spectrum allocation searches the slots block from the lowest index and allocates the block to the connection if the available spectrum block exactly matches the bandwidth requirement of the request. Exact-fit spectrum allocation can improve network efficiency by reducing the spectrum fragmentation issue [111].

3.4.2 Routing, Modulation Format and Spectrum Assignment

RSA problem often refers to spectrum slots assignment with the connection requests being the number of spectrum slots. However, the generic traffic requests are the bandwidth requirement in the form of providing a certain bit rate lightpaths. This relates to assigning certain modulation format to the connection in addition to routing and spectrum allocation. This type of problem is called routing, modulation format and spectrum assignment (RMSA) problem. Similar to RSA, RMSA is also an NP-hard problem which jointly considers the three-dimensional resource allocation (path, modulation and spectrum).

In [98], an integer linear programming (ILP) has been proposed to minimize the network spectrum usage in elastic optical networks given the traffic matrix in advanced. It also presents the decomposition of the RMSA ILP formulation into two sub-problems: 1) routing and spectrum level ILP problem and 2) ILP based spectrum assignment problem. Considering the

computational complexity of solving the ILP and two sub-ILP problems, complete heuristic algorithms are introduced in [98] which serve a list of traffic requests one after the other, in a sequential manner. Further, several traffic requests reordering policies have been proposed to improve network remaining capacity. However, this method assumes a particular modulation format is permitted for certain transmission distance while does not consider other impact factors. Therefore, it may underutilise the network resources. In [112], detail analysis of ILP formulation to solve the RMSA problem in WDM based optical networks and elastic optical networks has been proposed. Similar to [98] and [112], ILP formulations and heuristic algorithms have been presented in [113–115] to allocate optical path, spectrum resource and modulation level resource to the connection requests. In these work, the traffic matrix is static while the corresponding ILP based formulation and heuristic algorithms can be regarded as the off-line algorithm. In this case, their algorithm is designed for the off-line requests which may fail to meet the demand of dynamic requests in future elastic optical networks.

In contrast to the off-line algorithm for the static traffic request scenarios, there are many works studying the RMSA problem for the dynamic traffic request [116–121]. These works aim at optimizing different targets during the resource allocation process. In [116], the open capacity of elastic optical networks is maximized with the proposed RMSA ILP formulation and the heuristic algorithm. Traffic lightpath restoration/re-routing is considered in [117, 119, 121] taking energy efficiency and spectrum fragmentation into account, to improve the number of provisioned service requests and service acceptance ratio.

3.4.3 Traffic Grooming and Spectrum Defragmentation in Elastic Optical Networks

To make the efficient use of the optical bandwidth-variable transponders, traffic grooming is adopted in the optical networks. Although the spectrum resource can be allocated in a just-enough manner in elastic optical networks, the bandwidth variable transponder is

designed for the maximum line-rate with tunable modulation format. Spectrum slots or O-OFDM sub-carriers variable with slicing capability is not maturely supported nowadays [122]. Traffic grooming is able to combine several low-speed traffic streams to form a large-bandwidth flow and modulate the information into high capacity lightpath through the optical bandwidth-variable transponders. In [123–125], RMSA problem is solved considering traffic grooming technique to improve spectral efficiency in elastic optical networks are proposed. Optical traffic grooming in O-OFDM based elastic optical networks exploring the capability of bandwidth variable transponders is studied in[123, 124]. The results show the significant network spectrum and bandwidth variable transponders saving with the proposed optical layer traffic grooming techniques compared with the non-traffic grooming scenario. Non-linear impairments aware multi-path traffic grooming is presented in [125] to improve the network spectral efficiency using the Gaussian noise non-linear impairments model. They presented a mixed integer linear programming formulation, a generic heuristic algorithm and show an improved network capacity with the proposed strategies. However, they assume single request can be divided into two halves if a single lightpath cannot support the its bit rate request. This requires significantly higher complexity at a higher network layer to reconstruct the information frames.

The spectrum slots are assigned in continuity and contiguity manner in transparent elastic optical networks. As the traffic demands and assigned modulation level vary, dynamically setting up and tearing down lightpath causes the spectrum fragmentation problem in the EON [98] [126]. In this case, there are some slots isolated from others in the spectrum domain and space domain (optical link). For example, it is difficult to utilize the slot 3 of link 5 as shown in figure 3.4 unless there is a traffic demand for 1 slot bandwidth between node 1 and node 3 and the spectrum allocation algorithm happens to assign slot 3 to the request. This is known as the spectrum fragmentation problem. If no available slots can satisfy the traffic demand, the request is regarded as rejected and network blocking occurs

because of the fragmented spectrum slots. To reduce the service request blocking probability due to the spectrum fragmentation, spectrum-aware RMSA has been studied in [127–129]. The service reconfiguration will be operated to tear down and re-establish the lightpaths to eliminate the impact of the spectrum fragmentation issue to the network acceptance probability in [127] [128], once the algorithms detect serious spectrum fragmentation in the optical networks. Although lightpaths tearing-down and re-establishment behaviour can improve the network capacity, this requires the disruption of existing service and additional network resources, such as spare transponders and spectrum slots resource. In [129], an entropy-based fragmentation metric calculation is performed during the RMSA process. The minimum entropy spectrum assignment algorithm expects to reduce the number of lightpath tearing down and re-establishment because of the spectrum defragmentation. At the reconfiguration level, pull and push defragmentation technique has been introduced in [130] to dynamically retune the frequency of allocated spectrum without disrupting the embedded service. In this case, the spectrum can be quickly tuned together with the spectrum switching elements along the lightpath to avoid the service disruption shown in [127] [128].

3.4.4 Impairments-Aware Resource Allocation in Optical Networks

For the modulation level assignment in the optical networks, the choice of the modulation format requires the optical signal satisfying the corresponding quality of transmission. In the work of solving the RMSA problem described earlier, the transmission distance or the number of fibre spans is the single factor affecting the signal quality. The highest modulation format is selected given the transmission distance of the routing decision, as shown in figure 3.5. This is also known as the distance adaptive routing, modulation format and spectrum allocation [86].

However, the maximum permitted transmission distance for each modulation format depends on a number of factors, such as: signal launch power, fibre span length, the number

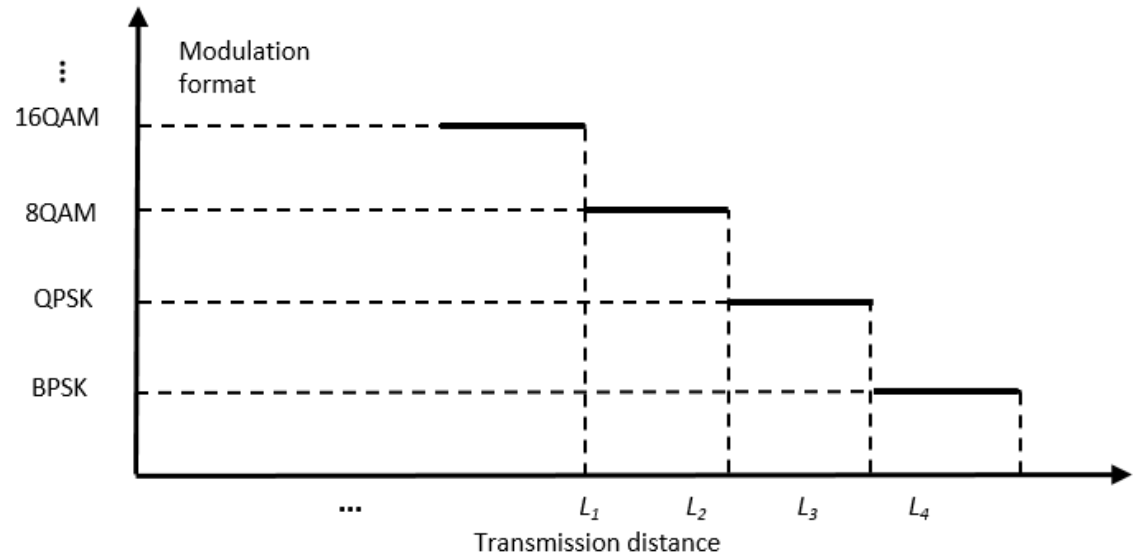

Fig. 3.5 Modulation format against maximum transmission distance

of ROADMs on the lightpath, fibre ageing condition, the noise figure of EDFA, linear impairments, non-linear impairments, the sensitivity of transponders and etc. Given a single transmission distance as the signal QoT factor while regarding these factors mentioned above cannot make the efficient use of the optical network resources.

The reality that the actual performance of the lightpaths is not solely dependent on the transmission distance may also lead to unacceptable QoT of some lightpaths in the optical network. The knowledge of physical layer impairments such as chromatic dispersion, polarisation dependent dispersion, self-phase modulation, cross-phase modulation and four-wave mixing is essential for the optical signal quality of transmission validation when establishing the new lightpath.

Routing, modulation format and spectrum assignment considering these real physical layer impairments have been studied in a variety of works. In [131], linear impairments ASE noise, non-linear interference cross-phase modulation and four-wave mixing are considered as the main physical layer impairments. The quality of transmission in terms of Q-factor is calculated of each request according to channel allocation and routing decision for both

single line rate requests and mixed line rate requests. The physical layer impairments are included in the proposed resource allocation mechanisms. Similarly, the ASE noise, fibre non-linear impairments and the impairments from the bandwidth variable ROADMs in elastic optical networks are mathematically modelled and have been applied to QoT-aware modulation format allocation with the computed routing path in [132]. The path with the best signal-to-noise metric is selected and the spectrum assignment considering distributing the traffic evenly is deployed. The network kriging technique [133] and Euclidean norm minimization is used in [134] [135] to model and account for the impairments of newly established lightpaths and the QoT degradation of existing lightpaths in the network due to new lightpath establishment. The proposed impairments estimation framework shows that 4×10^{-2} lower pre-FEC bit error rate can be achieved compared with the case of assuming the fully loaded links with the worst non-linear interference.

As coherent optical communication has drawn significant attention to support robust and high capacity long distance transmission [136] [137], impairments-aware RMSA problems proposed in recent years assume the quality of transmission is dominated by the ASE noise and non-linear impairments while other impairments can be compensated by the digital signal processors at the receivers. With the development of new non-linear impairments modelling tool, Gaussian noise model [41–43], the modelling of non-linear interference becomes accurate and faster than previous models or using nonlinear Schrödinger equation. GN model based non-linear impairments aware resource allocation has also been studied. Quality of transmission aware adaptive elastic optical networks has been proposed in [138] using the GN model for modelling the nonlinear impairments. Authors mainly focus on the network survivability and perform the network reconfiguration when the requirement of quality of the transmission of the existing lightpaths is no longer meet. Three strategies have been proposed to overcome the QoT degradation problem due to nonlinear impairments introduced by the newly established lightpaths: 1) adaptive modulation format, 2) shifting

spectrum by adding guardband and 3) adaptive FEC overhead. The proposed strategies can affect the existing service as none of them promises hit-less service re-planing. Non-linear impairments and congestion-aware routing are proposed and analysed in [107] to examine the 3 types of routing algorithms in the non-linear regime. The network blocking probability is evaluated with the 50 GHz, 25 GHz, 12.5 GHz and 6.25 GHz grid elastic optical network. The proposed weighted congestion-aware routing achieves the lowest blocking ratio compared to other routing algorithms.

Mixed integer linear programming based routing, modulation format and spectrum allocation is performed in [139] [140] by taking actual non-linear impairments into account. The actual non-linear impairments model in [140] refers to the work [44], which requires the channel spacing between connections more than 28 GHz. The proposed MILP minimizes the maximum allocated spectrum slot index in the network with different signal power spectral density. Their model requires the requests bandwidth over 300 Gbps, which is not feasible for all the lightpath demand.

Similarly, joint power. routing, modulation format and spectrum allocation is presented to achieve the maximum network capacity in [51] to collaborative minimize the number of allocated bandwidth variable transponders and the total physical layer impairments for static elastic optical networks in [54] [55] and to minimize maximum bandwidth usage, to minimize total launch power and maximize the SNR margins in [53].

To reduce the transmission errors due to the noisy optical links, the forward error coding is applied to the original information stream. The optical transmission system with the FEC encoder and decoder is shown in figure 3.6. The FEC encoder placed before the modulator adds redundancy to the original information stream. At the receiver, the message is decoded after the demodulation process. The impact of FEC overhead on the optical network in the non-linear regime is shown in [141]. In [141], authors present an ILP model to select the optimal combination of the routing path, modulation format and FEC overhead assuming the

self-channel interference can be fully compensated by the digital backpropagation technique [142]. The paper shows the soft decision-FEC is able to achieve 12%, 15% and 20% more network capacity compared to adopting hard decision-FEC for a national, continental and global network respectively.

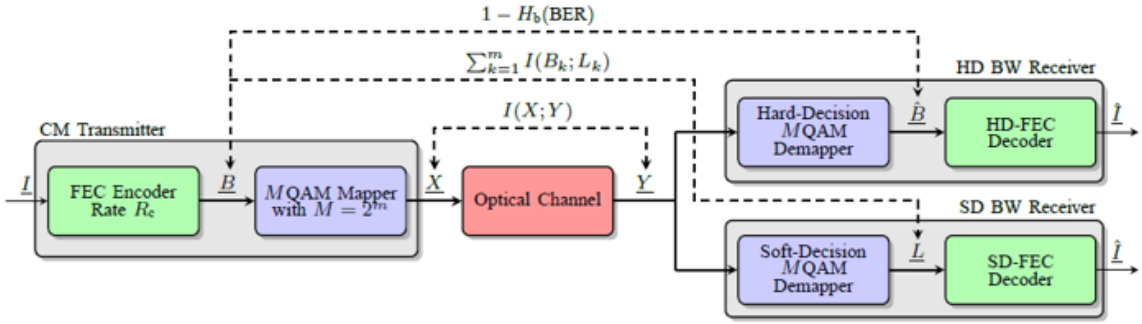

Fig. 3.6 The optical transmission system with with FEC encoder and HD/SD-FEC decoder [141].

Apart from the resource allocation strategy for the static traffic scenario, optical regenerator placement algorithms considering the effect of growing non-linear interference noise due to increasing link loading condition have been proposed in [143–145]. A load-aware maximum reach distance approach has been proposed based on Gaussian noise model in [143] and the O-E-O regenerators placement has been deployed when the QoT of certain lightpaths can no longer support the selected modulation level. Similarly, the regenerators allocation algorithms have been studied in [144] [145] with dynamic traffic in the elastic optical networks. An ILP based algorithm in [145] aims at allocating the minimum number of regenerators and demonstrates around 30% more traffic demands can be accepted. A heuristic algorithm is raised in [144] for non-linear flex-grid optical networks with the traffic demand of variable line rates requirements. The proposed optimisation framework is verified with the Monte-Carlo method to achieve lower network blocking probability and fewer number of regenerators required.

3.5 Summary

In this chapter, we describe the fundamental background of the optical networks. The concept WDM optical network and the elastic optical network are introduced. The flex-grid ROADM and bandwidth variable transponders in EON is discussed in detail as relating to the proposed network optimisation strategy and corresponding simulation work in the next few chapters. The state-of-art research work regarding the resource allocation and optimisation in DWDM or elastic optical networks have been studied. However, these works do not consider the actual physical layer impairments along the lightpath, causing the network resources underutilised. Finally, the nonlinear impairments-aware routing, modulation format and spectrum assignment problem are also reviewed and discussed. They either do not consider the dynamic traffic cases or require high bit rate requests, which violates the purpose of the elastic optical network. Therefore, in the next few chapters, the novel physical layer impairments aware resource allocation algorithms and optimisation schemes are proposed to overcome the above problems.

Chapter 4

Load-Aware Nonlinear Impairments Model

4.1 Introduction

To improve the optical network resource utilisation and to increase the optical network capacity, the knowledge of the physical layer impairments is essential. These impairments generated during the transmission affect the SNR of the lightpaths, the reach distance of the system and the overall network capacity. In the era of using coherent transmission and detection techniques, chromatic dispersion and polarisation mode dispersion can be mitigated by placing digital signal processor at the coherent receivers. In this sense, the stochastic noise like ASE noise and non-linear impairments become the major impairments. While ASE noise has a simple mathematical model, the model of non-linear impairments is often associated with solving complex equations. The traditional way of modelling and solving the nonlinear Schrodinger equation is computationally complex, making it impossible as the physical layer impairments evaluation tool for optical network optimisation. The recent proposed non-linear GN model is a sufficient tool with relatively low complexity. However, to solve the GN model in real-time for the optical networks with dynamic traffic is still challenging. Therefore,

this chapter presents a low complex non-linear impairments model for accurate non-linear impairments. The accuracy of the proposed model is verified compared to the original GN model and a LARA resource allocation using the proposed non-linear impairments model is evaluated. The idea of this chapter is presented in 2017, The Optical Networking and Communication Conference and Exhibition in Los Angelas [146].

4.2 Physical Layer Quality of Transmission Model

In this section, we explain the physical layer impairments model for the signal quality of transmission evaluation and various assumptions made for this work. The assumptions made are listed as:

- A transparent dual-polarization (DP) optical system using coherent detection without in-line compensation.
- Polarisation dependent loss is not considered.
- Polarisation mode dispersion and chromatic dispersion are fully compensated using digital signal processing technique at the receivers.
- All-optical routing nodes consist of bandwidth-variable spectrum selective switches with the colourless directionless and contentionless capability and they can isolate channels without creating crosstalk.
- Signal spectrum close to rectangular, without guard band between different channels.
- Nonlinearity accumulates incoherently along multiple spans.
- Equal signal transmission power spectral density among channels within the same fibre span.

- Power loss is completely compensated by the erbium doped fibre amplifiers placed at the end of each fibre span.
- The optical system is deployed with completely tunable, bandwidth variable and modulation level adaptable transponders.
- The bandwidth request includes the capacity for forward error correction (FEC) overhead.

Due to assuming polarization mode dispersion and chromatic dispersion being fully compensated by DSP, polarization dependent loss not considered, the bandwidth-variable spectrum selective switches can completely isolate different channels without crosstalk, the dominant impairments in such dual-polarization uncompensated optical network are the amplified spontaneous emission noise and the non-linear impairments. Therefore, the SNR at the receiver is calculated as:

$$SNR_{Rx} = (\sum_{l} \frac{1}{SNR_l})^{-1} \tag{4.1}$$

where the $\frac{1}{SNR_l}$ is the linear SNR degradation of link l. The end-to-end linear SNR_{Rx} depends on the linear SNR degradation of each link along the path. The linear SNR degradation of a link is calculated as:

$$\frac{1}{SNR_l} = \frac{G^l_{ASE} + G^l_{NLI}}{G^l_{sig}} \tag{4.2}$$

where G^l_{ASE}, G^l_{NLI} and G^l_{sig} are the PSD for the ASE noise, the non-linear impairments and the optical signal of link l within the channel bandwidth respectively. Since we assume the signal power loss can be fully compensated by EDFA placed between fibre spans, the single

sided PSD of ASE noise of link l is expressed as [25] [26]:

$$G_{ASE}^{l} = \sum_{e} 10^{\frac{NF_e}{10}} \cdot h\nu(10^{\frac{A_e}{10}} - 1) \tag{4.3}$$

where NF_e is the noise noise figure of EDFA e of link l, h is Planck's constant, ν is signal carrier frequency and A_e stands for signal power loss over fibre span e of link l in dB.

While the ASE noise has a simple mathematical model, the non-linear impairments are difficult to fast and accurate formulate as a tool for impairments-aware resource allocation in the optical network. In the next section, the state-of-art NLI modelling and their impact on resource allocation will be discussed.

4.3 Exact Nonlinear Impairments and Worst-Case Nonlinear Impairments for Resource Allocation in Elastic Optical Networks

The original GN model [42] [41] is described in equation 2.13 in chapter 2 to derive the power spectral density of the non-linear interference. This model has been proven to effectively approximate the real NLI during the transmission via multiple work [147] [148] [149] [150] [151]. However, forming the non-linear impairments power within channel bandwidth requires the triple integration of the equation 2.13. For the optical network with already established connections, the QoT or SNR of newly embedded lightpath needs to be evaluated using the original GN model. Furthermore, the QoT or SNR of existing lightpaths utilizing the common optical links as the new lightpaths requires re-evaluation due to the changing signal power spectral density in the view of the GN model. Those multiple QoT calculations cannot be performed in real time as they require a significant amount for computation.

A simplified version of GN model has been proposed in [44] to model the NLI power of the channels with various spectrum bandwidth. In [47], the NLI model is applied to the signal of 50 GHz bandwidth spacing. These simplified versions of GN model enable the fast NLI calculation. However, only self-channel interference and cross-channel interference are considered while multi-channel interference (MCI) shown in figure 2.2 (c) are ignored in these works. As a result, they require the channel spacing more than 28 GHz to obtain the accurate NLI information. For the channel spacing less than 28 GHz, they lead to considerable NLI underestimation. Therefore, these models cannot provide accurate NLI estimation for flex-grid optical networks with 12.5 GHz per incremental spectrum grid.

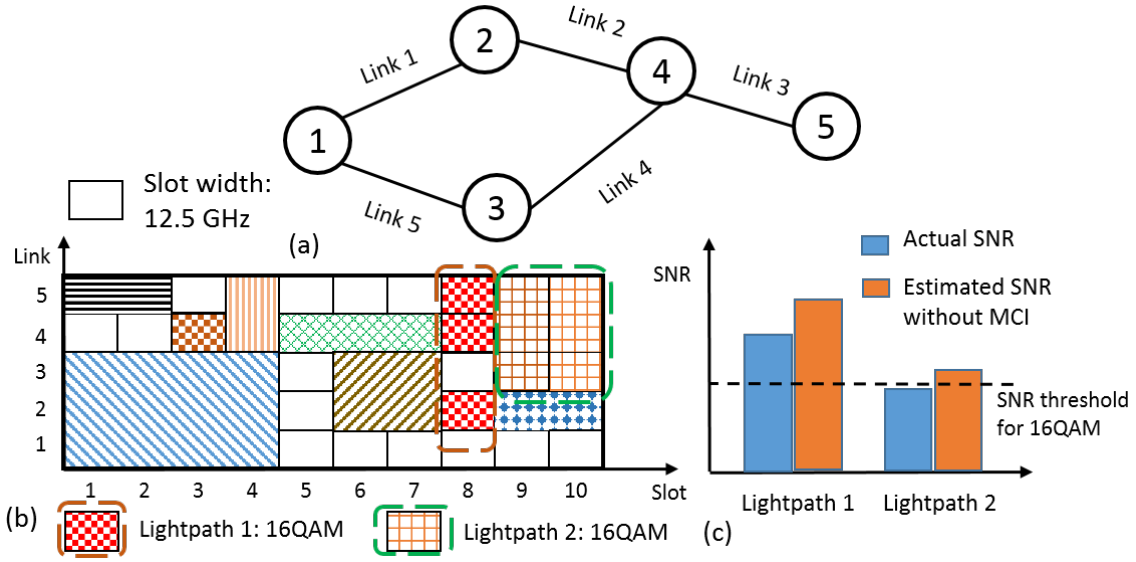

Fig. 4.1 An example of network with NLI underestimation using model in [44] and [47]. (a): Simple network topology; (b): Spectrum slot assignment in the network; (c): Actual SNR versus estimated SNR without MCI using model [44] and [47]

.

An example is shown in figure 4.1 to demonstrate the negative impact due to NLI underestimation. The channel spacing between lightpath 1 and lightpath 2 is less than 28 GHz as per slot width is 12.5 GHz according to ITU-T standard [79]. When adopting the NLI model not considering MCI, both lightpath 1 and 2 are regarded with the capability to utilize 16QAM as modulation format for transmission through calculation. However, NLI

overestimation due to neglecting multi-channel interference causes the actual SNR smaller than the estimated value. Therefore, the actual SNR of lightpath 2 does not permit it using 16QAM. As a result, the connection is blocked at the initial lightpath provisioning stage as error-free transmission cannot be guaranteed.

Apart from the inaccuracy of the simplified GN model or the huge amount of computation complexity using original GN model, deriving the accurate SNR for resource allocation in the optical network is not always a good option. For a dynamic network with lightpaths setting up and tearing down, the accurate SNR always changes with the varying real-time network status. Therefore, some previous lightpaths setting up with 'old' NLI information may no longer support the assigned modulation format due to additional NLI from new lightpaths established in the optical network. As a result, serious service blocking may occur when allocating routing, spectrum and modulation format to the connections with greedy accurate NLI. This phenomenon is shown in [152] [153] as the inter-channel interference. The capacity of such optical network operating only according to current status but neglecting future requests is significantly reduced. The virtual optical network embedding blocking ratio is shown in figure 4.2 for using the accurate NLI and the worst-case NLI. It is observed that the blocking ratio for allocating network resource using accurate NLI is approximate 60 % while it is 24% for using worst-case NLI. The higher network blocking ratio of using accurate NLI is due to the aforementioned inter-channel blocking problem.

Compared to using the exact NLI for routing, modulation format and spectrum assignment in optical networks, current network operators assign certain margins to model the impact of non-linear impairments [6] [7]. From [6], 0.5 dB margin is assigned to SPM, XPM, FWM and SBS/SRS respectively. Hence, the SNR is reduced by 2dB - 2.5 dB by combining all types the NLI. Similarly, it is reported in [7] that 1.5 dB - 3 dB margin should be assigned to NLI. These margins are usually calculated according to the worst-case impact of NLI, which guarantee optical network surviving at any NLI conditions. However, NLI margins

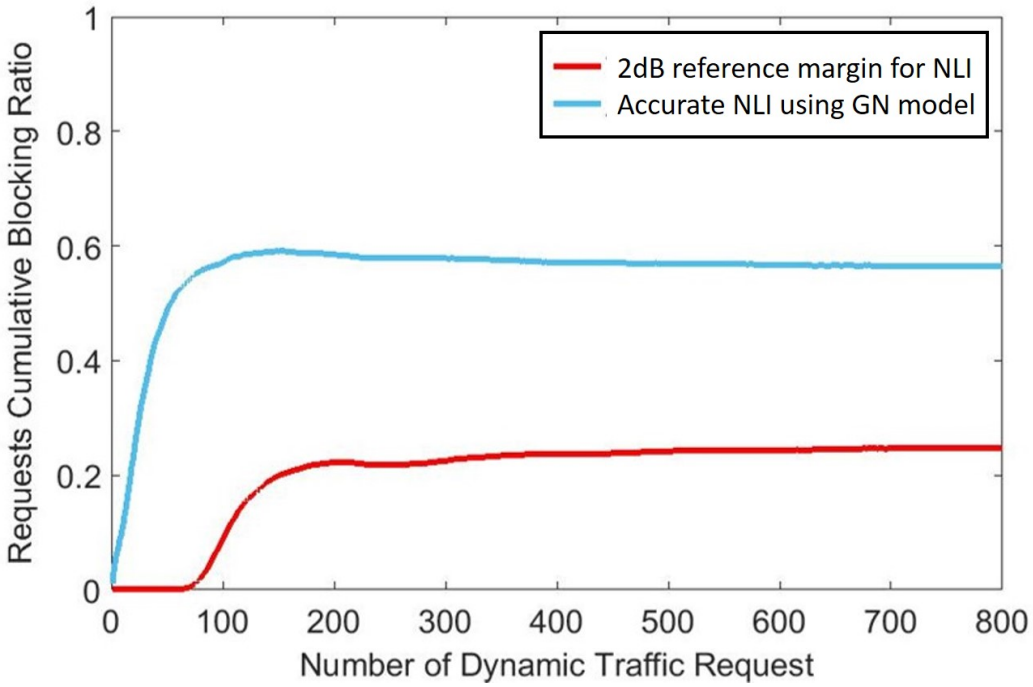

Fig. 4.2 Virtual optical network service requests blocking ratio with worst-case NLI analysis and the accurate NLI according to network status

.

or the worst-case NLI does not consider the signal power launch into the fibre, routing and spectrum allocation decision of lightpaths. Using these methods, the NLI is significantly overestimated in most cases. Therefore, some lightpath may adopt conservative modulation formats which reduces the overall spectral efficiency and hence underutilizing the optical network resources. Also, assuming a high margin for NLI often requires more powerful transceivers and more regenerators to be deployed in the network which further leads to an increase in the capital expenditure.

To unlock the potential capacity of the optical networks, we assume the existing service connections can adjust their assigned modulation formats dynamically according to the network status without considering the service-level agreement (SLA). In this case, the inter-channel blocking is not considered as the high-speed lightpaths can adjust to low-speed streams when suffering more NLI from newly established channels. Considering above assumption, we show the network throughput difference when adopting the exact NLI

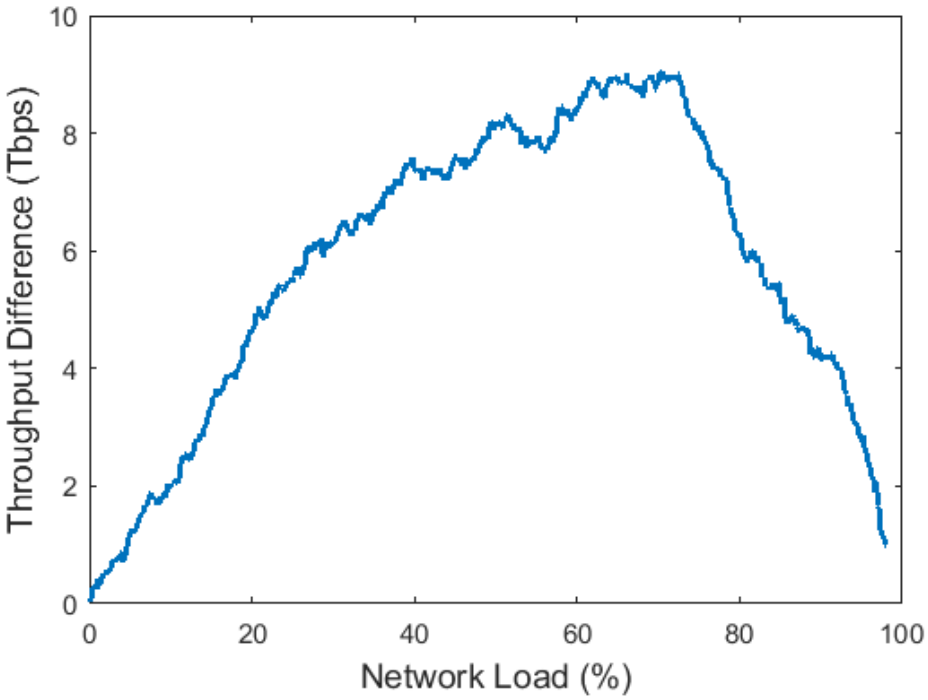

Fig. 4.3 Network capacity difference when adopting the actual NLI and 2 dB margin for NLI .

according to network status and adopting 2 dB margin to model the impact of NLI against the network loading in figure 4.3. The results are obtained by sequentially loaded the NSF network. It is observed the maximum 9.3 Tbps more network capacity is achieved by using accurate physical layer NLI without considering SLA. The accurate NLI can indeed help improve the network capacity in this case.

4.4 Proposed Hybrid Nonlinearity Model

The problem of high computation complexity, the accuracy lacking for small traffic flows, the inter-channel blocking of using accurate original GN model or simplified GN models as well as the conservative modulation formats with worst-case NLI or margin methods make them not a good candidate for NLI evaluation to enable physical layer impairments aware resource allocation in elastic optical networks.

To overcome the limitation of the aforementioned models in section 4.3, we propose a hybrid NLI model based on GN model for routing, modulation format and spectrum assignment problem in elastic optical networks. The proposed NLI model combines the features of both greedy accurate NLI estimation strategy and as it considers the channel loading conditions and the worst-case NLI method due to considering future service connections.

In hybrid NLI model, few concepts are introduced first. C continuous frequency slots are defined as a spectral window. Therefore, each window size is $C \cdot b$ where b is the per frequency slot bandwidth. For an optical network with F frequency slots in each link, there exist F/C windows. We set $LS = F/C$ representing the number of the windows, also known as the link loading states number. Then we define the loading state of a link as:

$$ls = \begin{cases} \left\lceil \frac{MF}{F} \cdot LS + \frac{1}{\mu} \right\rceil, & MF < F \\ LS, & MF = F \end{cases} \tag{4.4}$$

where MF is the maximum slot index among the allocated frequency slots of the link, μ is a very large number and $\lceil \rceil$ is a ceiling function giving the smallest integer greater than the input as the output. Factor μ is to make sure the link loading states to be 1 (minimum) when no spectrum slot of the link is assigned. By defining LS loading states, the spectrum occupation of the link can be divided into LS states. As the defined in equation 4.4, the link is of ls loading state when its maximum allocated frequency slot index MF is within range from $C \cdot (ls - 1)$ to $C \cdot ls - 1$ (except $MF = F$).

Figure 4.4 shows an example of two link loading states. In this example, we consider the network operates in 1 THz bandwidth, each slot width being 12.5 GHz and spectra window size is 100 GHz. As a result, there exist 10 loading states for a link ($LS = 10$). The red block stands for the actual spectrum allocation in the link. The maximum index of the actually allocated slot in figure 4.4 (a) is 7, thus the loading state of this link is 1 according to equation

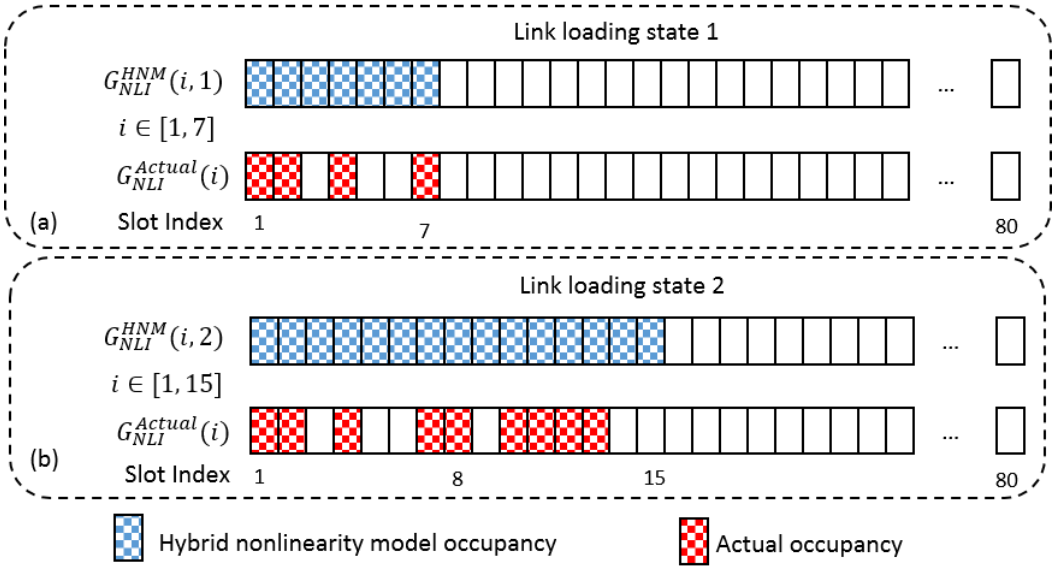

Fig. 4.4 An example of link loading states. (a) link of loading state 1; (b) link of loading state 2

.

4.4. Figure 4.4 (b) shows that the link loading state is 2 as the maximum actual occupied slot index is 13.

As the NLI is related to the spectrum assignment, the proposed hybrid NLI model is limited to using the first-fit assignment. Due to the definition of loading state in this work, first-fit spectrum allocation is adopted as it is shown as one of the best spectrum allocation schemes to achieve minimum blocking probability [109]. Considering the first-fit spectrum assignment, the loading state of a link reflects its loading condition. With higher loading states of a link, the higher indexed slots are allocated to the lightpaths. Hence, the link becomes more congested, resulting in higher NLI noise of all the channels propagating through that link. Therefore, ls is a key factor determining the NLI of the channels. As the NLI power spectral density does not fluctuate significantly within small bandwidth [42] [44], we choose the NLI PSD of the central frequency of a frequency slot as the NLI PSD for the slot. The single-span NLI PSD of each slot is calculated in advance for all link loading states ($ls^* = 1 \ldots LS$) assuming the full occupation of ls^* spectra windows from first frequency slot index to the last index $\frac{F}{LS} \cdot ls^*$ - 1 (except when the $MF = F$, $ls = LS$), as shown:

$$G_{NLI}(i\cdot b, ls^*) = \frac{16}{27}\cdot\cdot\gamma^2\cdot L_{eff}^2\cdot\int_0^{(\frac{F\cdot ls^*}{LS}-1)\cdot b}\int_0^{(\frac{F\cdot ls^*}{LS}-1)\cdot b} G_{sig}(f_1)\cdot G_{sig}(f_2)\cdot G_{sig}(f_1+f_2-i\cdot b)\cdot\rho(f_1,f_2,i\cdot b)\cdot df_1 df_2, \qquad \text{if } MF < F \tag{4.5}$$

$$G_{NLI}(i\cdot b, ls^*) = \frac{16}{27}\cdot\cdot\gamma^2\cdot L_{eff}^2\cdot\int_0^{B}\int_0^{B} G_{sig}(f_1)\cdot G_{sig}(f_2)\cdot G_{sig}(f_1+f_2-i\cdot b)\cdot\rho(f_1,f_2,i\cdot b)\cdot df_1 df_2, \qquad \text{if } MF = F \tag{4.6}$$

where G_{sig} is the power spectra density of signal, i is the frequency slot index $\in (1...\ \frac{F}{LS}\cdot ls^*$ - 1) if $MF < F$, otherwise $i \in (1...F)$, B is the total transmission bandwidth which equals to $F\cdot b$ and ρ is the '*four wave mixing*' factor in original GN model.

In figure 4.4 (a) and (b), the blue blocks represent how the NLI PSD is calculated using the proposed hybrid nonlinearity model assuming slot 1 to $\frac{F}{LS}\cdot ls^*$ - 1 fully occupied as depicted in equation 4.5 and 4.6. For the case that a link is within loading state 1, the NLI of assuming all the spectrum slot from 1 to 7 being allocated is calculated in advanced. Similarly, NLI PSD for all the spectrum slot from 1 to 15 is calculated for link loading state 2. When executing the first-fit spectrum assignment, for example: slot 10 – 13 are assigned where 13 is the maximum slot index allocated in the link, the link is within loading state 2, shown in above figure 4.4 (b). Thus, the NLI of those slots is decided according to the pre-calculated lookup table $(G_{NLI}^{HNM}(10,2), G_{NLI}^{HNM}(11,2), G_{NLI}^{HNM}(12,2), G_{NLI}^{HNM}(13,2))$ of slot 10 – 13 for link loading state 2. We still take these values from the lookup table to present their NLI even if slot 3, 5, 6, 9 are not allocated. By calculating and assign NLI $(G_{NLI}^{HNM}(10,2), G_{NLI}^{HNM}(11,2), G_{NLI}^{HNM}(12,2), G_{NLI}^{HNM}(13,2))$ of continuous occupied slot from 1 to 15 to the connection using slot 10 – 13 instead of their actual value $(G_{NLI}^{Actual}(10), G_{NLI}^{Actual}(11), G_{NLI}^{Actual}(12), G_{NLI}^{Actual}(13))$, the NLI is slightly overestimated compared to the exact NLI when slot 3, 5, 6, 9 are not assigned.

Above process can be seen that the NLI PSD value calculated from the hybrid NLI model (blue blocks) instead of the actual NLI (red blocks) in the link according to their index i and the link loading state ls^* are used for QoT evaluation. The assigned hybrid NLI value is always larger than or equal to the exact NLI value as the hybrid NLI model is the worst-case NLI for each link loading state.

The hybrid NLI model combines the features of worst-case NLI method due to full slots occupation within spectra windows of each loading state and the greedy exact NLI estimation strategy as it considers the channel loading conditions. The NLI PSD of each frequency slot not only depends on signal PSD G_{sig} but also relies on the loading state of the link and assigned frequency slot index. Due to the assumption that NLI adds incoherently, phase factor χ in original GN model is 1. This approach creates a lookup table for NLI according to the link loading state ls^* and the frequency slots indexes assigned to the lightpath. Due to rectangular spectra shape, the signal PSD $G_{sig}(f)$ is independent of f. Therefore, we can formulate the hybrid NLI lookup table by combining equation 4.5 and 4.6 to form a new equation written as:

$$G_{NLI}(i, ls^*) = G_{sig}^3 \cdot \xi_{i,ls^*} \tag{4.7}$$

where ξ_{i,ls^*} is the NLI PSD coefficient (unit: THz^2/mW^2) of frequency slot index i when the link is of ls^* loading state. ls^* present the particular loading state the link remains in while the ls is a variable ranging from 1 to LS. The factor ξ_{i,ls^*} is the integral results from equation 4.5 and 4.6 without the considering signal PSD G_{sig}, which is similar to nonlinear coefficient in [42].

By taking equation 4.7 into 4.2, the optimal signal PSD of a link within ls^* loading state can be expressed as:

$$G_{sig} = \sqrt[3]{\frac{G_{ASE}}{2 \cdot max(\xi_{i,ls^*})}} \tag{4.8}$$

where the function *max* takes the maximum value of the NLI PSD coefficients of the slot being ls^* loading state. The optimum signal PSD in equation 4.8 is the differential results of combing equation 4.2 and 4.7, aiming to minimize the linear SNR degradation of central frequency slot of link within ls^* loading state.

As the NLI PSD of each slot for different loading states is calculated based on given fibre parameters and signal transmission PSD, the model in equation 4.5 and 4.6 is more accurate than assigning SNR margins for NLI or the worst-case NLI analysis, especially for less congested links. As the proposed hybrid nonlinearity model is a step-wise model with links are associated with loading states, the nonlinearity is always slightly overestimated when the link remains in the same loading state. Thus, it also avoids inter-channel blocking problem and complex computation compared to using exact NLI information when the fibre links remain in the same loading state. The hybrid NLI model takes advantage of both the worse-case NLI method and calculating exact NLI to avoid their respective drawbacks. Since we use the original GN model, NLI estimation can be applied to a channel with less than 28 GHz bandwidth. In EON, the NLI PSD is frequency dependent and channel spacing is flexible. Therefore, for a channel occupying multiple frequency slots, we compute the NLI PSD by averaging the NLI PSD of all the frequency slots within the channel as:

$$G_{NLI}^{span,l} = \sum_{i=FS_{min}}^{FS_{max}} \frac{G_{NLI}(i, ls^*)}{FS_{max} - FS_{min} + 1} \tag{4.9}$$

where $G_{NLI}^{span,l}$ is the single-span NLI PSD for the channel of link l in loading state ls^*, the FS_{min} is the minimum frequency slot index of the lightpath and FS_{max} denotes the maximum

frequency slot index. Combining the nonlinearity incoherently from each span, the NLI PSD of the link l is expressed as:

$$G_{NLI}^{l} = \sum_{span=1}^{SP_l} G_{NLI}^{span,l} \tag{4.10}$$

where SP_l stands for spans number of the link l. By combining equation 4.1 – 4.3 and 4.4 – 4.10, we can calculate the end-to-end SNR to form the QoT evaluation of the lightpath in the elastic optical network, which is used in the following sections and chapters for the RMSA problem.

4.5 Accuracy Analysis of the Proposed Hybrid Nonlinearity Model

In this section, we analyse the accuracy of the proposed hybrid NLI model by comparing it with exact NLI using original GN model in [42]. The spectra window size is set to be 100 GHz with 12.5 GHz per slot width, thus the number of loading states LS being 10 for the link sequentially loaded from 0 to 1 THz bandwidth, which is evaluated in this section. Therefore, there are $8 \cdot i$ slots evaluated for link loading state i. Single mode fibre with loss coefficient of 0.22 dB/km, fibre nonlinearity coefficient $\gamma = 1.3\ W^{-1} \cdot km^{-1}$ and chromatic dispersion coefficient D of 16.7 $ps \cdot nm^{-1} \cdot km^{-1}$ is considered. Fibre span length are set to 80 km and 50 km which yields 17.6 dB and 11 dB loss per span respectively. Noise figure for all EDFAs is assumed to be 5 dB. A point-to-point transmission with 23 spans is assumed. The standard single mode fibre parameters used for the simulation are the same as shown in table 2.1 in chapter 2, as suggested by ITU-T G.652 and ITU-T G.650.2, while the EDFA noise figure is the typical noise figure which can also be found in [47] [107]. Throughout the thesis, the

calculation of the proposed hybrid nonlinearity model is based on the Matlab through Monte Carlo method instead of direct triple integration.

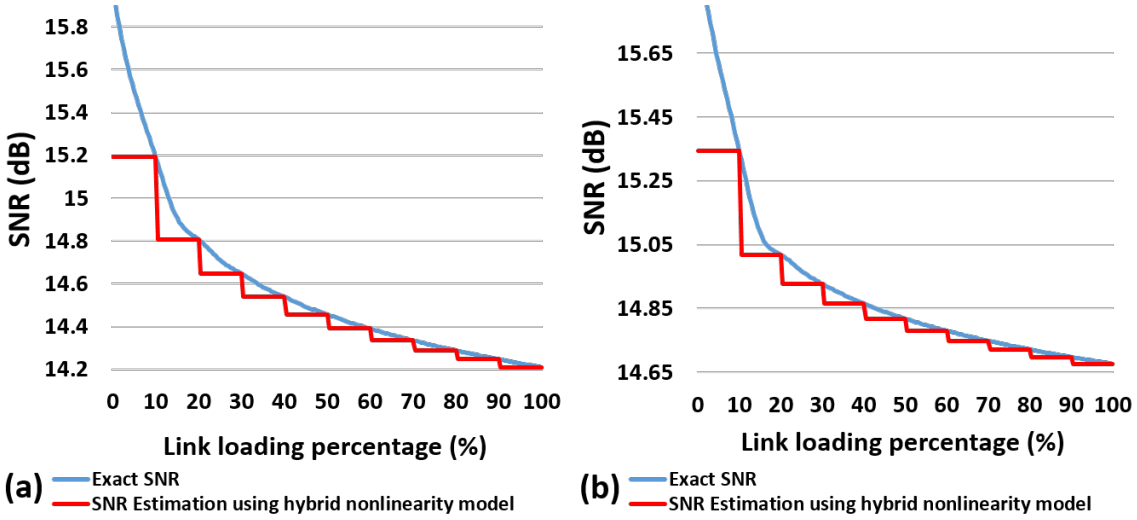

Fig. 4.5 SNR estimation of using the proposed NLI model and original GN model with PSD = 21.2 mW/THz, span length 80 km. (a) central frequency slot; (b) edge frequency slot.

We first fix the signal transmission PSD to be 21.2 mW/THz and span length to be 80 km. The SNR performance of central frequency slot which suffers the most nonlinear interference and edge frequency slot with the least nonlinear interference is evaluated and shown in figure 4.5 (a) and (b). It can be observed that the predicted SNR of using the proposed hybrid NLI estimation scheme has a very good approximation to the accurate SNR for this case.

Then the signal PSD is varied from 21.2 mW/THz to 15 mW/THz, the SNR results of using the proposed hybrid NLI model comparing with exact NLI for both central slot and edge slot are depicted in figure 4.6 (a) and (b) respectively.

We further vary the span length to 50 km instead of 80 km as mentioned above. Figure 4.7 (a) and (b) present the SNR of two slots using the proposed method and the exact NLI under this case.

From figures above, it can be observed that the proposed hybrid NLI model with a spectral window size of 100 GHz, can effectively approximate the real lightpath performance when the over 100 GHz spectrum is allocated for various signal PSDs and fibre span lengths.

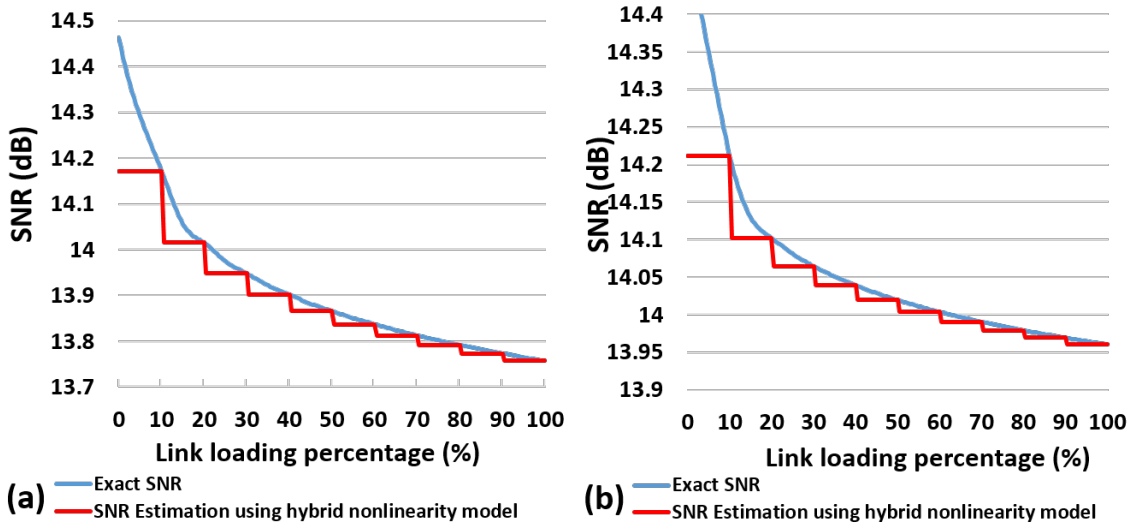

Fig. 4.6 SNR estimation of using the proposed NLI model and original GN model with PSD = 15 mW/THz, span length 80 km. (a) central frequency slot; (b) edge frequency slot.

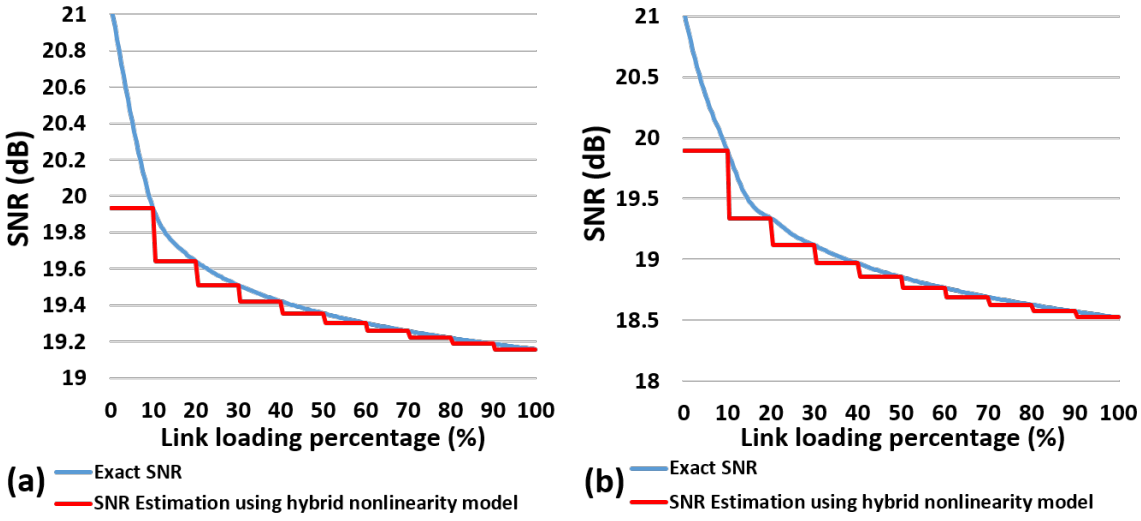

Fig. 4.7 SNR estimation of using the proposed NLI model and original GN model with PSD = 15 mW/THz, span length 50 km. (a) central frequency slot; (b) edge frequency slot.

Table 4.1 Optimal signal PSDs for central slot versus link loading states

ls^*	1	2	3	4	5
Signal PSD (mW/THz)	28.99	24.97	23.77	23.05	22.55
ls^*	6	7	8	9	10
Signal PSD (mW/THz)	22.18	21.88	21.63	21.42	21.24

Therefore, the proposed hybrid nonlinear impairments model proves to be useful and can be applied to different optical networks with different span lengths and signal PSDs. Despite the fact that proposed hybrid NLI cause slightly overestimation of the SNR, it is able to serve as an efficient and accurate tool for NLI evaluation as the NLI value of each slot for each link loading state is pre-stored.

Apart from fixed signal transmission PSD, we also investigate allocating dynamic signal PSD for each link based on its link loading state. The optimal signal PSD calculated according to equation 4.8 for different link loading states is shown in table 4.1. From the table, it can be seen that the optimal PSD decreases as the link loading state increases.

Figure 4.8 demonstrates the SNR performance of the proposed hybrid NLI model with span length = 80 *km* using the fixed optimal signal PSD = 21.24 mW/THz which is calculated as full 1 THz occupied, compared with flexible signal PSD according to table 4.1. Both the central frequency slot and edge frequency slot is evaluated. From the figure, we can observe the SNR improvement using flexible optimal signal PSD over using the fixed optimal signal PSD. The edge frequency slot benefits more SNR improvement with flexible signal PSD assignment according to its loading states compared to the central frequency slot due to the smaller NLI PSD coefficient. In the next section, a small simulation scenario is tested comparing the performance of the NSF networks using the proposed hybrid model with the NLI margin method.

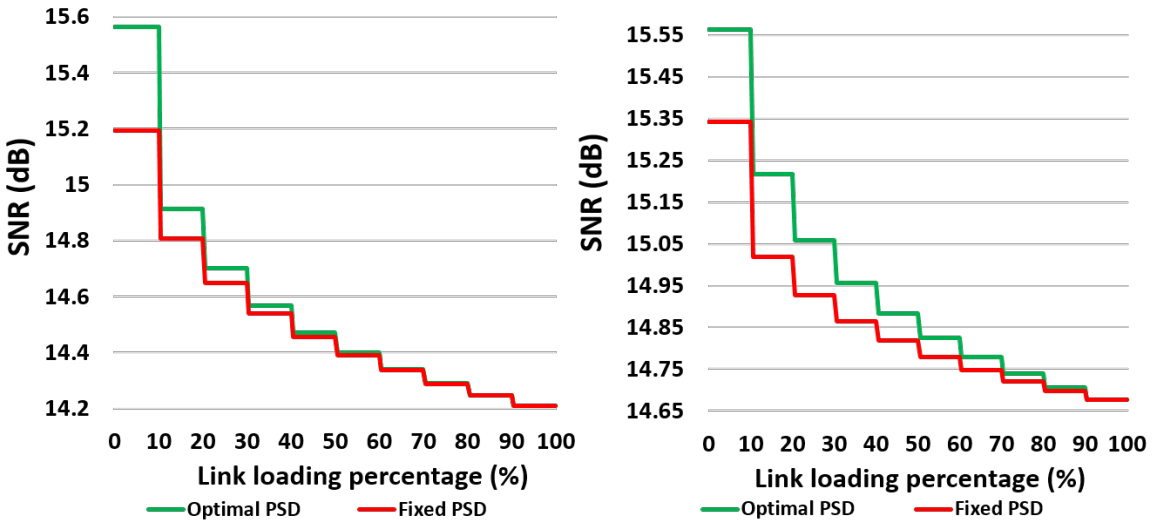

Fig. 4.8 SNR estimation performance comparison of the proposed hybrid NLI model using fixed PSD = 21.24 mW/THz with using flexible optimum signal PSD as shown in table 4.1. (a) central frequency slot; (b) edge frequency slot.

4.6 Hybrid Nonlinearity Model and LARA Algorithm

In order to preserve the existing services and allow future requests while improving the spectrum utilization, we integrate the proposed hybrid nonlinearity model into an RMSA scheme, which is named as Load and nonlinearity Aware Resources Allocation (*LARA*) algorithm. The flowchart of the algorithm is shown in figure 4.9.

LARA algorithm is able to find a proper path according to the routing algorithm for each connection request. After the path is selected, the algorithm will check if there is enough spectrum resource along the path to support the demanding traffic. When spectrum slots are available, the highest feasible modulation format is assigned to the lightpath based on the ASE noise and NLI noise of the hybrid nonlinearity model according to the links' loading states along the path and the assigned slots' index.

LARA algorithm also considers the case as the loading state of the link changes, NLI of the link changes and services provisioned based on previous loading state may be affected. The algorithm checks if any services blocked (SNR of lightpath drops below the threshold of the

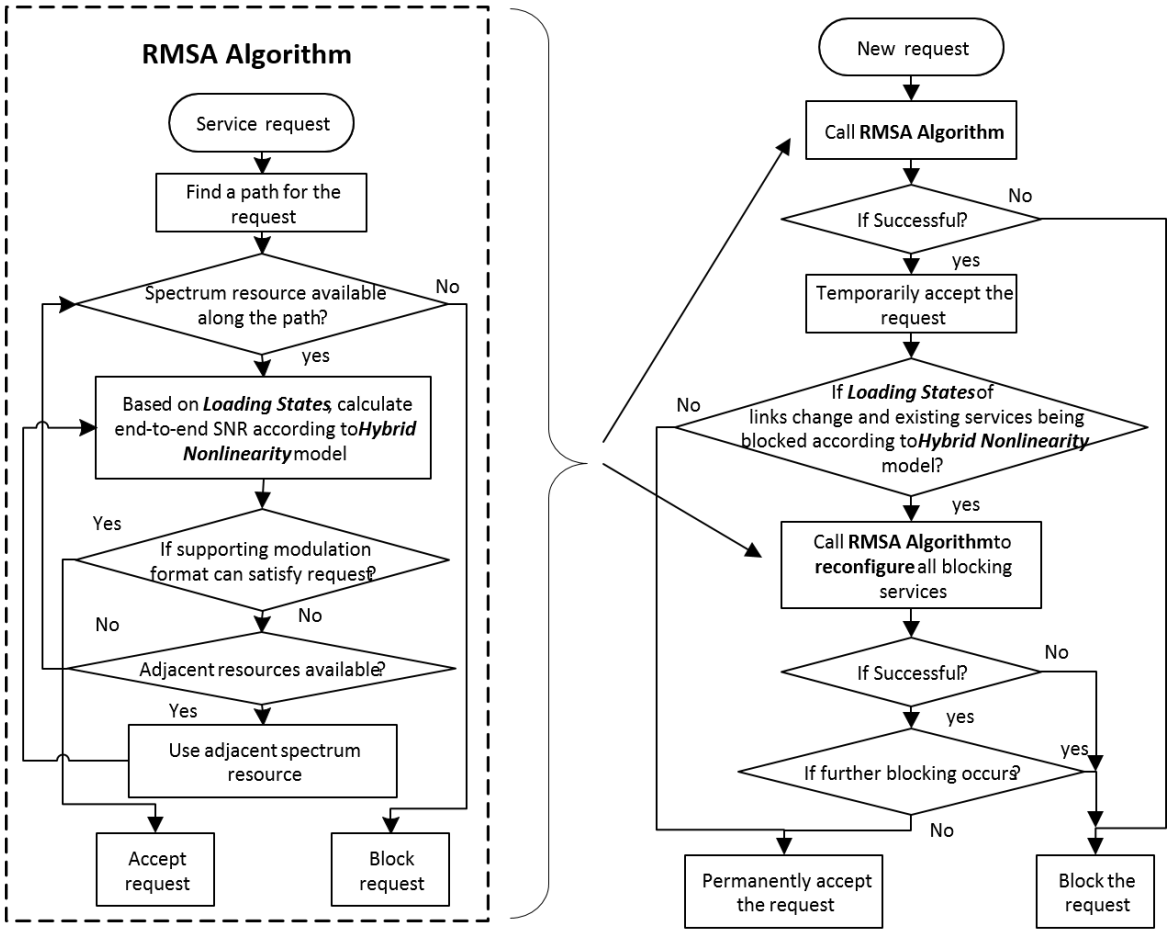

Fig. 4.9 The *LARA* algorithm

assigned modulation). In case inter-channel blocking occurs, *LARA* is able to make another routing, modulation format and spectrum decision for the affected services. *LARA* is also able to mitigate verify-reconfigure loop by blocking the request that triggers reconfiguration of multiple existing services that may be affected. Since our solution considers only 5 states, it requires a few numbers of service reconfigurations which does not add too much complexity to the optical network control plane.

To make the comparison of the proposed hybrid nonlinearity model, the NLI is assigned with the fixed reference margin of 0.5 dB for each of self-phase modulation, cross-phase modulation, four-wave mixing and stimulated Brillouin scattering/stimulated Raman scattering [6]. Similar to the fixed reference margin method, LOGON strategy in [50] calculates the NLI in the worst case, which also corresponds to approximate 2 dB due to NLI penalty.

For the proposed solution, 5 loading states are evaluated in this section over a total 5 THz bandwidth of C-band from 190.6 THz to 195.6 THz. As a result, 5 loading states correspond to 20%, 40%, 60%, 80% and 100% continuous occupied optical link. The whole 5 THz is divided into 400 frequency slots with 12.5 GHz width for each slot. For a channel occupying multiple slots, the NLI PSD of the channel of a single span is calculated using the equation 4.9 according to its loading states and the assigned slot indexes.

The signal launch power spectral density is chosen as 19 mW/THz, optimized according to equation 4.8 with each span length to be 80 km. We follow the symbol SNR threshold for different modulation formats to achieve 3.8 $\times 10^{-3}$ pre-FEC BER shown in 2.2. All nodes are transparent CDC BV-ROADMS with 7.25 dB insertion loss and all links in the network are assumed to be of identical span length of 80 km using single mode fibre. The NSFNET topology with 14 nodes, 21 links are used for evaluation with the same parameters as described in [47].

The traffic model is made up of symmetric bi-directional requests between randomly selected pairs of source and destination in the NSFNET topology. In this section, two types

of traffic scenarios are considered: 1) single line-rate 100 Gbps traffic requests and 2) mixed line-rate requests with the same portion of 400Gbps, 100Gbps, 40Gbps and 10Gbps requests. The mixed line-rate requests are to model the different data rate requests for various network services in the elastic optical network. In each traffic scenario, 5000 requests are randomly generated and sequentially provisioned into the network. 10000 instances of each scenario are examined and the results obtained are averaged over these 10000 instances. We compare the proposed *LARA* solution of using the proposed hybrid NLI model against using reference margin (RM) of 2 dB to model the impact of NLI and the exact NLI information. The evaluation is based on two routing algorithms: 1) Dijkstra physically shortest path routing and 2) congestion-aware routing in [107] and first-fit spectrum assignment as suggested in the above section. Matlab is used as the simulation tool for the routing computation, signal quality assessment, spectrum allocation and the modulation format assignment.

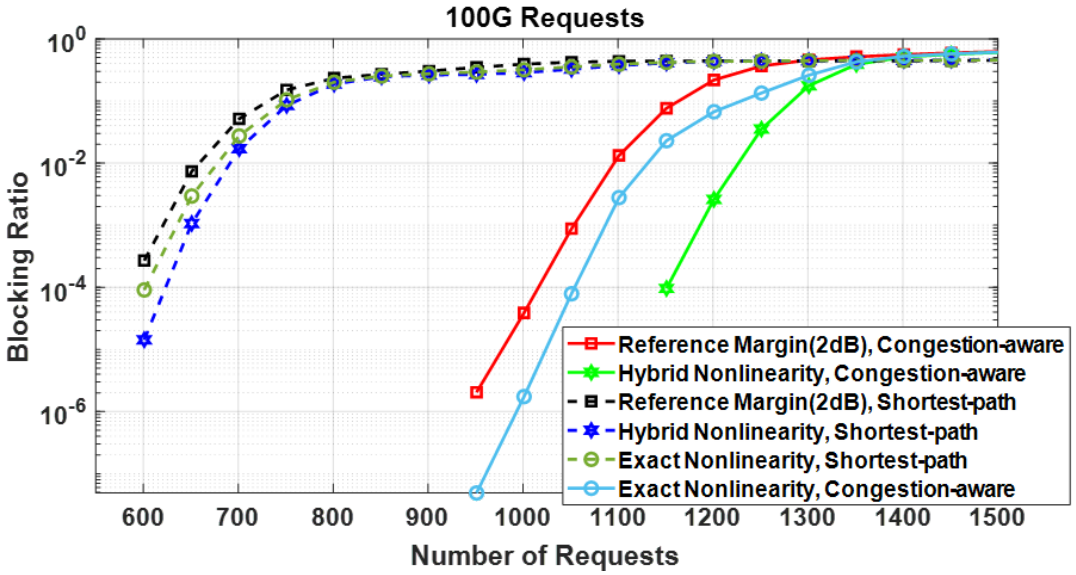

Fig. 4.10 Blocking probability for 100 Gbps request

Figure 4.10 shows the average blocking ratio of *LARA* solution using the hybrid nonlinearity model, the reference margin method and the exact NLI information for the number of requests for the single 100 Gbps requests. It indicates *LARA* is able to achieve higher service acceptance ratio than reference margin and exact NLI method. In the case of congestion-

aware routing strategy, *LARA* accepts approximately 130 and 100 more 100G requests than RM solution and using exact NLI information at 1% blocking ratio respectively. This yields 13 Tbps and 10 Tbps network capacity for the proposed solution. Similarly, as shown in figure 4.11, *LARA* accepts approximately 100 more requests in case of mixed line-rate traffic demands compared to using reference margin and around 30 more requests than using the exact NLI. The network capacity can be increased by 11.3 Tbps and 6.5 Tbps respectively.

When adopting the shortest path routing algorithm, the *LARA* solution can still achieve lower service blocking probability compared to using the reference margin NLI modelling method and using exact NLI information for both two traffic scenarios. The comparison between different solutions from figure 4.10 and 4.11 clearly shows that *LARA* solution with congestion-aware routing is optimal for both fixed line-rate and mixed line-rate demands.

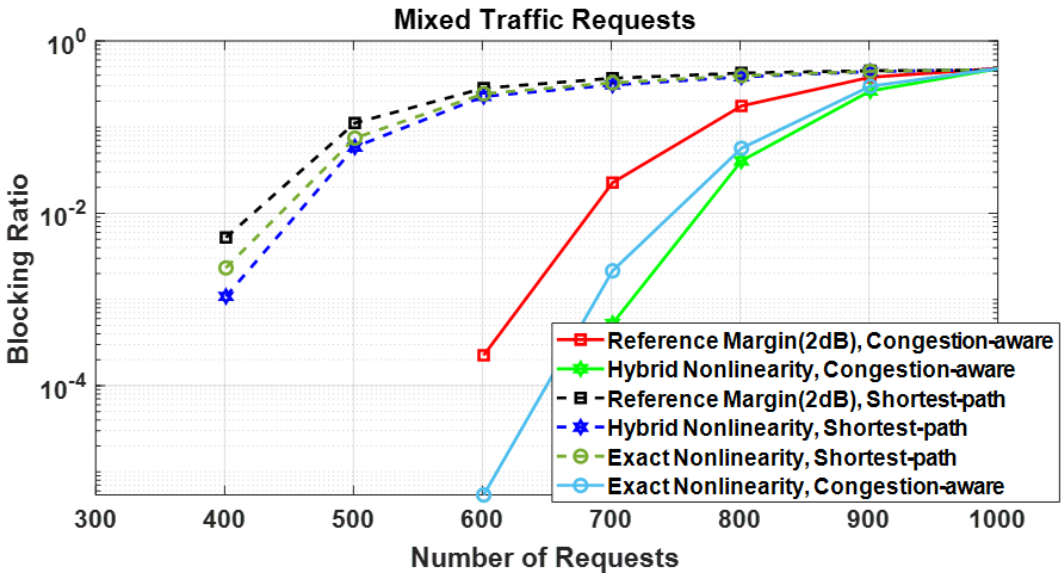

Fig. 4.11 Blocking probability for mixed traffic request

In figure 4.12 and 4.13, we showcase the average number of requests provisioned at different modulation formats for the *LARA* algorithm (using hybrid nonlinearity model), the 2 dB reference margin method, and the algorithm using the exact NLI knowledge at 1% network blocking ratio. It can be seen that *LARA* with hybrid nonlinearity model assigns higher modulation formats for more number of requests compared to RM method and using

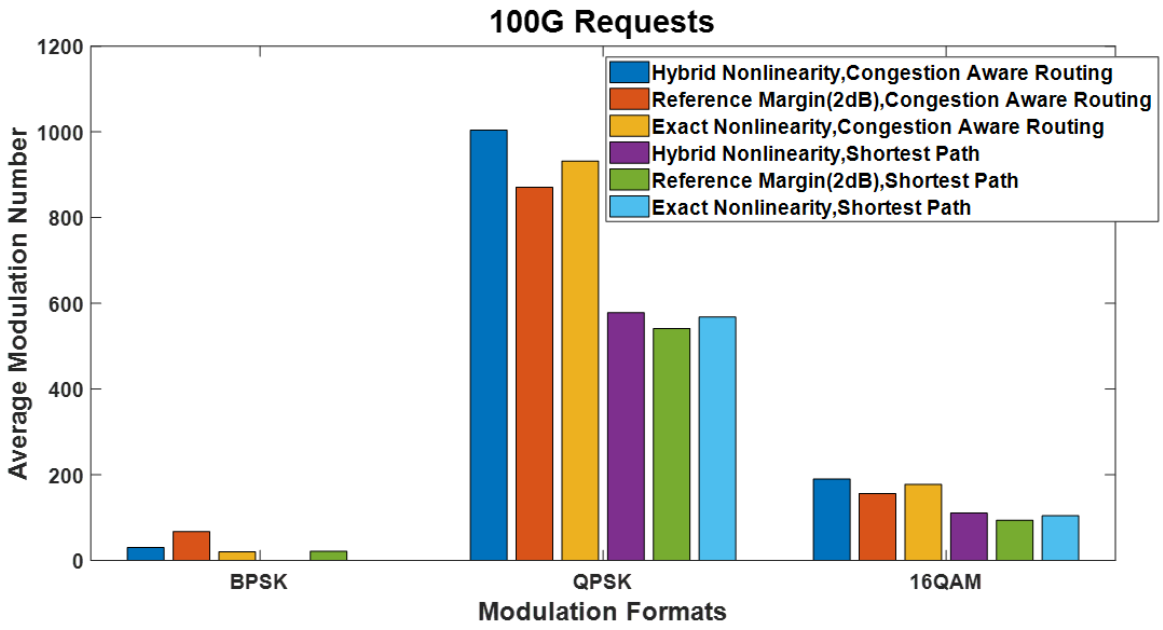

Fig. 4.12 Average number of modulation formats under 1% network blocking probability for 100 Gbps traffic

the exact NLI knowledge under all traffic scenarios and routing algorithms, thus achieving greater spectral efficiency. This is because the proposed hybrid nonlinearity model provides as an efficient tool with less conservative NLI estimation compared to assigning the impact of NLI a fixed reference margin. While for the algorithm using the exact NLI, it requires a significantly higher number of service replanning which reduces the network efficiency. In case of 100G requests, our solutions do not assign 8QAM as the modulation format to any requests as 8QAM is not a suitable modulation format for 100 Gbps requests compared to QPSK. As 8QAM consumes the same amount of spectrum slots as QPSK to deliver 100 Gbps traffic stream but QPSK can is more tolerant to NLI thus can achieve longer system reach distance. For the mixed line-rate traffic requests, the proposed *LARA* solution is able to utilize 8QAm as modulation format for the established lightpaths.

At 1% network blocking ratio, *LARA* only requires average 27.6 and 7.5 number of re-configurations for congestion-aware routing and shortest-path routing respectively. Similarly, 15.6 and 5.7 reconfigurations are needed in case of mixed traffic demands. The additional

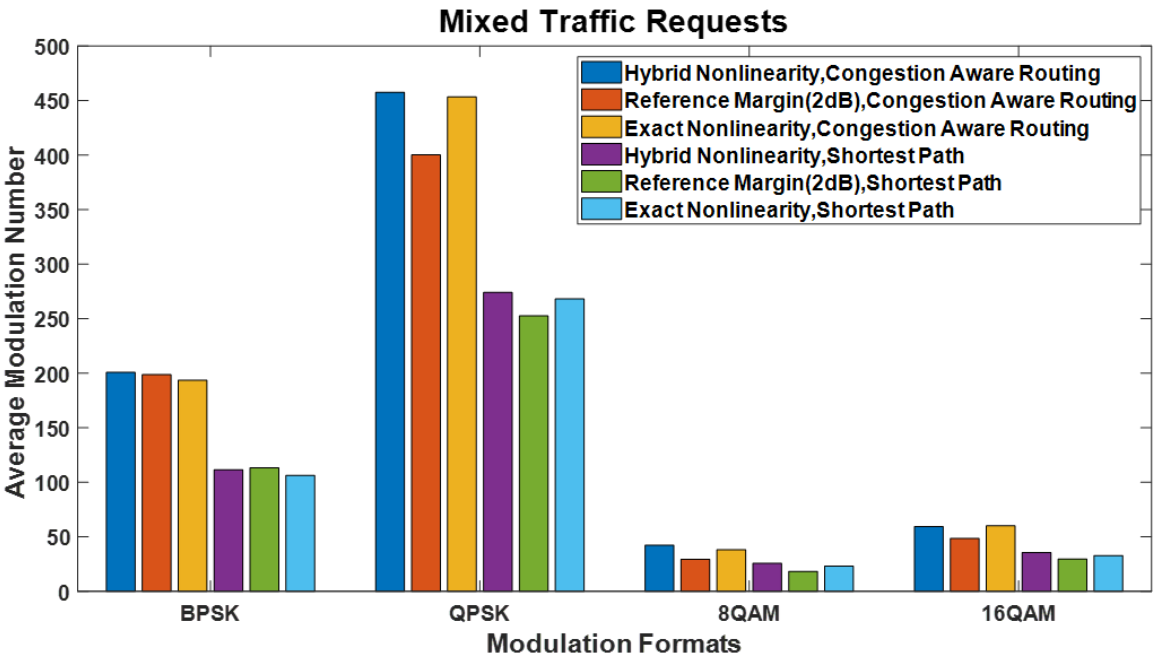

Fig. 4.13 Average number of modulation formats under 1% network blocking probability for mixed line-rate traffic

control plane complexity due to requests reconfiguration of using the *LARA* solution is affordable with over 100 lightpaths can be provisioned into the network. As a result, the *LARA* with the proposed hybrid nonlinearity model can achieve lower network blocking probability, higher spectrum efficiency.

4.7 Summary

In this chapter, we proposed the signal quality of transmission model in this work, which considers the ASE noise and the nonlinear impairments. State-of-art nonlinear impairments estimation methods: worst-case NLI or fixed reference margin method to model NLI and the accurate NLI using original GN model or simplified GN model is reviewed. The impact and of these state-of-art NLI models to the resource allocation and optimization in the optical network are discussed and quantified. Based on GN model, a novel load-aware NLI model is proposed for the RMSA problem. We first analyse and compare the accuracy

of the proposed hybrid nonlinearity model with accurate NLI model for a point-to-point transmission with various signal PSDs and fibre span lengths. The proposed NLI model shows a very good approximation to the original GN model. Further, we evaluate the performance of the proposed NLI model integrated with a simple RMSA solution. Comparing with the benchmark solution of using fixed reference margin for NLI, the RMSA with the proposed NLI model is able to provision significantly more service requests than traditional reference margin method while also achieving higher spectral efficiency. The proposed solution reduces the computational complexity of NLI estimation and also simplifies optical service provisioning with few numbers of re-planning. The proposed hybrid nonlinearity model is evaluated through extensive simulation studies under different traffic models and routing algorithms and the results verify the benefits of the solution.

Chapter 5

Sequentially Loaded Optical Network Optimisation

5.1 Introduction

Elastic optical networks have emerged as a promising technology to accommodate high-capacity and dynamic bandwidth demands of next-generation wireless networks. Resource allocation and optimisation in elastic optical networks are also considered as the main target in the view of network operators. It allocates the proper network resources to different traffic requests according to their demands and network status. In this chapter, we present a resource allocation algorithm for the sequentially loaded elastic optical networks using the proposed nonlinearity estimation scheme described in chapter 4. In case the newly embedded lightpath brings more nonlinearity, which blocks the existing connections, we propose a mixed integer linear programming model, and two heuristic algorithms using the proposed nonlinearity model as the service reconfiguration scheme for efficient resource allocation and traffic provisioning in elastic optical networks. The objective of the solution is to minimize the spectrum resource usage while satisfying the bandwidth demands of the connection requests and ensuring the quality of transmission. The proposed solutions are evaluated

using an extensive simulation model with off-line traffic requests and dynamic sequentially loaded requests against the benchmark solutions for two types of traffic profiles in the N6S9 network and the NSF network. The results presented in this chapter validate the benefits of the proposed nonlinearity estimation model and the corresponding algorithms to minimize the number of allocated frequency slots and service request blocking ratio while improving spectrum efficiency and overall network capacity. The idea of this chapter is submitted to Journal of Optical Communications and Networking for reviewing.

5.2 Hybrid Nonlinearity Model-based Resource Allocation Algorithm

In this section, we present several RMSA schemes in elastic optical networks taking nonlinear impairments effects into account. The hybrid nonlinearity model described in chapter 4 is integrated into the proposed resource allocation strategies to model the impact of NLI. The network is modelled as a directed graph $G = (V, E)$ where V is the set of optical nodes which in this case are bandwidth variable-reconfigurable optical add-drop multiplexers in the network while E presents the set of optical links. In this work, we set $L = |E|$ denoting the number of optical links. The available modulation format set in this chapter consists of DP-BPSK, DP-QPSK, DP-8QAM and DP-16QAM. We do not consider the insertion loss due to ROADMs in this chapter and the fibre span is assumed to be of equal length.

The set of traffic requests is denoted by $\boldsymbol{R}$, where each request $\boldsymbol{r_n} \in \boldsymbol{R}$ is modelled as a triplet (s_n, d_n, T_n). s_n and d_n present the source and destination of the connection request respectively while T_n is the bit rate demand between the source and destination. Since we consider the dual-polarization optical system with Nyquist rectangle spectral shaping [154] [155] in this work, each polarization mode carries the same amount of traffic. In this case, the number of frequency slots required to support request with data rate T_n with modulation

scheme m is calculated as:

$$B_{n,m}^{FS} = \left\lceil \frac{T_n}{2 \cdot m \cdot b} \right\rceil \tag{5.1}$$

where $B_{n,m}^{FS}$ is the number of frequency slots for request n using modulation format m while m = 1 denotes DP-BPSK, 2 denotes DP-QPSK, 3 for DP-8QAM and 4 for 16QAM. b is the per frequency slot bandwidth as suggested in equation 4.5. We consider the case where the traffic requests are sequentially loaded into the elastic optical networks. The pseudo code of the proposed algorithm is shown below in algorithm 1 as ***HM***.

For each request, $\boldsymbol{r_n}$, K least congested paths are calculated between the source and the destination of the request according to link congestion condition in the network. The congestion weight of each link is calculated as:

$$W_l = \sum_{n,f} \frac{PR_{l,f}^{n}}{F} \tag{5.2}$$

where $PR_{l,f}^{n}$ = 1 if connection n use link l and the frequency slot f of link l, 0 otherwise. The F is the same as defined in chapter 4, denoting as the total number of frequency slot of a link. For each candidate path, we first assume the connection travelling through that path can utilize the highest modulation format M by setting $m = M$, as shown in line 5. Then we search for the first-fit continuous and contiguous $B_{n,m}^{FS}$ frequency slots along the candidate path. In this case, the loading states of the links are updated temporarily given that $B_{n,m}^{FS}$ frequency slots are temporarily assigned to the request, shown in line 8. Then we determine NLI by searching the NLI lookup table using the updated loading states of the links and the indexes of $B_{n,m}^{FS}$ slots. The SNR of the request is computed according to equation 4.1 with corresponding ASE and NLI of the links along the candidate path. If the calculated SNR meets the SNR requirement for the selected modulation format m, we calculate the cost of

Algorithm 1 HM: Heuristic Algorithm Main

```
1: Set all the links loading states to 1;
2: for each traffic request r_n, do
3:     Find K least congested paths Path_{n,k} from source to destination according to equation
   5.2;
4:     for each candidate path do
5:         Set m = M;
6:         do
7:             Find first-fit continuous and contiguous B^{FS}_{n,m} slots along the candidate path;
8:             Temporally update link loading states assuming B^{FS}_{n,m} slots has been allocated;
9:             Determine the NLI of the connection according to NLI lookup table with the
10:            corresponding loading states of the links along the path and temporally
11:            assigned slots' index;
12:            Calculate the SNR of the request r_n according to equation 4.1;
13:            if Calculated SNR ≥ SNR_m then
14:                Calculate the cost of the candidate path according to equation 5.3;
15:            else
16:                m = m - 1; Cost_{n,k} = ∞;
17:            end if
18:        while Cost_{n,k} is ∞ & m ≠ 0
19:    end for
20:    if Cost_{n,k} is ∞ & m == 0 then
21:        Block the request r_n;
22:    else
23:        Choose the candidate path with the minimum cost;
24:        if any loading state changes? then
25:            Invoke SNR Checking Function;
26:            if no request blocked then
27:                Accept the request r_n;
28:            else
29:                Invoke service reconfiguration function
30:                if reconfiguration successful then
31:                    Accept the request r_n;
32:                else
33:                    Block the request r_n;
34:                end if
35:            end if
36:        else
37:            Accept the request r_n;
38:        end if
39:    end if
40: end for
```

the candidate path using equation 5.3, which is calculated as:

$$Cost_{n,k} = NL_{n,k} \cdot NSS_{n,k} \tag{5.3}$$

where $NL_{n,k}$ and $NSS_{n,k}$ is the number of links and number of required frequency slots of using candidate path k for connection request n respectively. Equation 5.3 captures the total number of allocated frequency slots along the path hence selecting the minimum cost path leads to better utilization of the network.

It is demonstrated in line 16 if the SNR requirement cannot be satisfied, we set $m = m - 1$, $Cost_{n,k} = \infty$ and repeat above process for a candidate path until one of the following three criteria is satisfied: 1) RMSA solution feasible for the candidate path k ($Cost_{n,k} \neq \infty$ in this case); 2) no frequency slots available for all applicable modulation formats (m == 0 and $Cost_{n,k} == \infty$); 3) candidate path is too long to support any modulation scheme (m == 0 and $Cost_{n,k} == \infty$). After searching for all the candidate paths, the algorithm selects one candidate path with minimum cost (utilize the least network spectrum resources).

The algorithm considers the NLI effects of new requests on established lightpaths. If the loading states of the links increase due to the provisioning of a new lightpath, we use the updated NLI information with increased loading states of the link for SNR calculation of the new lightpath. Similarly, we re-evaluate the QoT of the established lightpaths sharing the same fibre links using an **QoT Checking Function** with updated loading states of the links. The function is depicted below as algorithm 2.

The **QoT Checking Function** returns '*request blocked*' if the SNR of any established lightpaths drops below the SNR threshold for assigned modulation format which is regarded as blocked. In this case, the **Heuristic Algorithm Main** invokes the **Service Reconfiguration Function** to reconfigure all blocked requests. In this paper, we proposed 3 service reconfiguration schemes: 1) a MILP based service reconfiguration; 2) a MILP based heuristic service reconfiguration method; 3) a complete heuristic service reconfiguration scheme.

Algorithm 2 QoT Checking Function

```
for all existing traffic requests sharing the links with new established lightpath do
    Calculate the new SNR according to newly updated link loading states;
    if new calculated SNR is less than SNR threshold for assigned modulation format then
        return(request blocked);
    end if
end for
return(no request blocked);
```

Table 5.1 Constants of MILP model

Symbol	Meaning
N	Number of the requests
L	Number of the links
F	Number of the frequency slots
M	Number of the modulation formats
LS	Number of the loading states
K	Number of the shortest path

5.2.1 MILP based Service Reconfiguration

In case of existing connection blocked due to newly established lightpath bringing additional NLI, the MILP based service reconfiguration method reconfigures all the existing connections and new connection request. To limit the size of the MILP problem, we calculate K-shortest paths [156] for each request in advance. In table 5.1, it lists the size of the MILP considering the size of the network and the number of traffic requests.

Table 5.2 lists the input parameters of the MILP model. These parameters present such as the signal PSD, the NLI lookup table from the hybrid nonlinearity model, the ASE noise PSD

Table 5.2 MILP model input parameters

Symbol	Meaning
$G_{ASE} \in \mathbb{R} > 0$	Per span power spectrum density of ASE noise.
$G_{sig} \in \mathbb{R} > 0$	Signal PSD launched into the fibre.
$b \in \mathbb{R} > 0$	Bandwidth of each frequency slot.
$\mu \in \mathbb{N} > 0$	A very large number (10000 in this work).
$P_{n,k,l} \in \mathbb{B} = \{0,1\}$	Pre-calculated K paths, $P_{n,k,l} = 1$ if $k-th$ path of connection n uses link l.
$SP_l \in \mathbb{N} > 0$	The number of fibre spans of link l.
$SNR_m \in \mathbb{R} > 0$	SNR threshold for modulation scheme m.
$T_n \in \mathbb{R} > 0$	Bit rate request of connection n.
$B_{n,m}^{FS} \in \mathbb{N}$	Number of frequency slots required for connection n when assigned modulation scheme is m.
$G_{NLI}^{ls,f} \in \mathbb{R} > 0$	Per span NLI PSD of frequency slot f for a link of loading state ls (NLI lookup table).

due to EDFA in-line amplification, the pre-calculated K shortest paths, the SNR threshold for different modulation format, the traffic requests and etc.

Table 5.3 explains the decision variables of the MILP model. The proposed MILP is solved by giving the results of the decision variables with the given the size of the networks, input parameters and constraints. The details of the MILP model are described as follows.

The objective function 5.4 of the MILP problem aims at minimizing the highest allocated frequency slot index of the whole network. In this case, the highest link loading state is also minimized, which leads to reduced NLI estimation as well as better load balancing of the traffic. Furthermore, it also leaves more available capacity for the future requests with more

Table 5.3 MILP model decision variables

Symbol	Meaning
$x^n_{k,m,f} \in \mathbb{B}$	$x^n_{k,m,f} = 1$ if frequency slot f, modulation format m and $k-th$ path is assigned to connection n, 0 otherwise.
$z^n_{k,m} \in \mathbb{B}$	$z^n_{k,m} = 1$ if modulation format m and $k-th$ path is assigned to connection n, 0 otherwise.
$Mod_{n,m} \in \mathbb{B}$	$Mod_{n,m} = 1$ if connection n utilizes modulation format m, 0 otherwise.
$y_{ls,l} \in \mathbb{B}$	$y_{ls,l} = 1$ if link l is within ls loading state, 0 otherwise.
$PR^n_{l,f} \in \mathbb{B}\}$	$PR^n_{l,f} = 1$ if connection n use link l and frequency slot f, 0 otherwise.
$d_{l,f} \in \mathbb{B}$	$d_{l,f} = 1$ if frequency slot f is the maximum frequency slot index allocated in link l, 0 otherwise.
$H_{l,f} \in \mathbb{N}$	$H_{l,f} = f$ if f is occupied for link l, 0 otherwise.
$FS^n_{min} \in \mathbb{N}$	The minimum assigned frequency slot index of connection n.
$FS^n_{max} \in \mathbb{N}$	The maximum assigned frequency slot index of connection n.
$MF_l \in \mathbb{N}$	The maximum frequency slot index of link l.
$E^{n,l}_{NLI} \in \mathbb{R} \geq 0$	Nonlinearity PSD per span in link l of connection n.
$MF_{max} \in \mathbb{N}$	The maximum frequency slot index of all the link.

availability of continuous and contiguous frequency slots in the network.

$$\text{Objective:} \qquad \text{Minimize} \quad MF_{max} \tag{5.4}$$

The objective function subjects to following constraints. Constraint 5.5 ensures the maximum frequency slot index of each link does not exceed the maximum frequency slot index of the network.

$$MF_{max} \geq MF_l, \quad \forall l \tag{5.5}$$

Constraint 5.6 ensures that all the connection requests will be embedded.

$$\sum_{k,m,f} x^n_{k,m,f} \geq 1, \quad \forall n \tag{5.6}$$

Due to constraint 5.7 - 5.10, only one path, one modulation level is permitted for each connection request.

$$\sum_{k,m} z^n_{k,m} = 1, \quad \forall n \tag{5.7}$$

$$z^n_{k,m} \geq \sum_f x_{k,m,f}/\mu, \quad \forall n, k, m \tag{5.8}$$

$$\sum_m Mod_{n,m} = 1, \quad \forall n \tag{5.9}$$

$$Mod_{n,m} = \sum_k z^n_{k,m}, \quad \forall n, m \tag{5.10}$$

Constraint 5.11 ensures that non-overlapping of the spectrum for all the connection requests that share the same optical links.

$$\sum_{k,m,n} x^n_{k,m,f} \cdot P_{n,k,l} \leq 1, \quad \forall l, f \tag{5.11}$$

Constraint 5.12 makes sure that the number of frequency slots required allocated to the connection satisfies its bit-rate request according to the assigned path and modulation format.

$$\sum_{k,m,f} x^n_{k,m,f} = \sum_m Mod_{n,m} \cdot B^{FS}_{n,m}, \quad \forall n \tag{5.12}$$

Constraint 5.13 and 5.14 determine the lowest and highest frequency slot index allocated to each connection request respectively.

$$FS^n_{min} \leq \mu \cdot \left(1 - \sum_{k,m} x^n_{k,m,f}\right) + f, \quad \forall n, f \tag{5.13}$$

$$FS^n_{max} \geq f \cdot \sum_{k,m} x^n_{k,m,f}, \quad \forall n, f \tag{5.14}$$

Constraint 5.15 is required to satisfy the spectrum contiguity constraint in the transparent elastic optical network for each connection request.

$$FS^n_{max} - FS^n_{min} + 1 = \sum_{m} Mod_{n,m} \cdot B^{FS}_{n,m}, \quad \forall n \tag{5.15}$$

Constraint 5.16 determines the spectrum resource pool of each fibre link, $PR^n_{l,f} == 1$ if the request n utilizes the frequency slot f of link l.

$$PR^n_{l,f} = \sum_{k,m} \left(x^n_{k,m,f} \cdot P_{n,k,l}\right), \quad \forall n, l, f \tag{5.16}$$

Constraint 5.17 determines the frequency slot index allocated to each link.

$$H_{l,f} = \sum_{n} PR^n_{l,f} \cdot f, \quad \forall l, f \tag{5.17}$$

Constraint 5.18 – 5.22 determine the maximum frequency slot index MF_l of the link l when $\sum_f d_{l,f} = 1$. MF_l equals to zero if no frequency slot is allocated for the link l.

$$MF_l \geq H_{lf}, \quad \forall l, f \tag{5.18}$$

$$MF_l \leq H_{lf} + \mu \cdot (1 - d_{l,f}), \quad \forall l, f \tag{5.19}$$

$$\sum_{f} d_{l,f} \leq 1, \quad \forall l \tag{5.20}$$

$$MF_l \geq 0, \quad \forall l \tag{5.21}$$

$$MF_l \leq \mu \cdot \sum_{f} d_{l,f}, \quad \forall l \tag{5.22}$$

Constraint 5.23 ensures that each link can only be within one loading state.

$$\sum_{ls} y_{ls,l} = 1, \quad \forall l \tag{5.23}$$

Constraints 15.24 and 5.25 determine the loading states of the links according to their highest allocated frequency slot indexes. For unused links, the loading states of the links remain to be 1 as the minimum loading states according to equation 4.4.

$$\sum_{ls} \left(y_{ls,l} \cdot ls\right) \geq MF_l \cdot \frac{LS}{F} + \frac{1}{\mu}, \quad \forall l \tag{5.24}$$

$$\sum_{ls} \left(y_{ls,l} \cdot ls\right) \leq MF_l \cdot \frac{LS}{F} + 1 + \frac{1}{\mu}, \quad \forall l \tag{5.25}$$

Constraint 5.26 ensures SNR requirement is satisfied for assigned modulation format taking ASE and NLI into account.

$$G_{sig} \cdot \sum_{m} \frac{Mod_{n,m}}{SNR_m} \geq G_{ASE} \cdot \sum_{l} \left(PR^{n}_{l.f} \cdot SP_l\right) + \sum_{l} \left(E^{n,l}_{NLI} \cdot SP_l\right), \quad \forall n, f \tag{5.26}$$

Constraint 5.27 determines the NLI PSD of each connection using the hybrid nonlinearity model. The NLI of a request, in this case, depends on the allocated path, loading states of the links along the path and the index of assigned frequency slot.

$$E^{N,L}_{NLI} \geq \mu \cdot \left(PR^{n}_{l.f} - 1\right) + \sum_{ls} \left(y_{ls,l} \cdot G^{ls,f}_{NLI}\right), \quad \forall n, f, l \tag{5.27}$$

The size of above MILP formulation depends on the number of fibre links L, the number of connection requests N, the number of pre-calculated shortest paths K, the total number of modulation format schemes M, the number of frequency slots F and the number of loading states of a link LS. In our MILP formulation, there are $N \cdot L$ real (positive) variables, $L \cdot F + L + 2N + 1$ integer variables and $N \cdot K \cdot M \cdot F + N \cdot K \cdot M + N \cdot M + LS \cdot L + N \cdot L \cdot F + L \cdot F$ Boolean variables. As a result, there is $N + N \cdot K \cdot M + L \cdot F + L$ Boolean inequality constraints of the order of from constraint 5.6, 5.8, 5.11 and 5.20, $N + N + N \cdot M + N + N \cdot L \cdot F + L$ Boolean equality constraints with order of from 5.7, 5.9, 5.10, 5.12 , 5.16 and 5.23, $L + N \cdot F + N \cdot F + L \cdot F + L \cdot F + L + L \cdot F$ number of integer inequality constraint for 5.5, 5.13, 5.16, 5.18, 5.19, 5.21 and 5.22, $N + L \cdot F$ number of integer equality constraints for 5.15 and 5.17 and $L + L + N \cdot F + N \cdot F \cdot L$ number of real number inequality constraints for 5.24 – 5.27.

The above MILP problem is solved first to minimize the highest allocated frequency slot index in the network. Given the minimum MF_{max} value α obtained from solving the objective function of 5.4, the MILP model is again solved for the secondary objective as shown in 5.28:

$$\text{Objective:} \qquad \text{Minimize} \quad \sum_{n,l,f} PR^{n}_{l,f} \tag{5.28}$$

The new objective function subjects with previous constraints 5.5 – 5.27 and a new constraint 5.30 to ensure the minimum MF_{max}. In this case, the new objective is to minimize the total number of allocated frequency slots in the network by keeping the highest frequency slot index allocated on any link in the network to the minimum. As a result, the number of available frequency slots is maximized.

$$\text{Subject to:} \qquad \text{Constraint 5.5 - 5.27} \tag{5.29}$$

$$MF_{max} = \alpha \tag{5.30}$$

5.2.2 MILP based Heuristic Service Reconfiguration

The MILP formulation proposed previously is an NP-complete problem according to [98] [157]. Hence, it is challenging to solve the MILP model in real time for reasonably large networks and a large number of traffic requests. Therefore, to provide the RMSA reconfiguration solution for a large number of requests in large-scale networks, we propose a MILP based heuristic algorithms to reconfigure connections in a series of groups of requests. The order in which the requests are served first has a significant impact on the loading state of the links, NLI analysis of each request as well as the network spectrum utilization. Therefore, we apply the request reordering policy, described as **most spans number and most traffic demand first**. The traffic requests are reordered in the descending order of the number of spans in their shortest paths. For the requests with the same number of spans, we reorder

them in the descending order of the bit rate demands. The traffic demand with the greatest number of spans in its shortest path with maximum bit rate demand is served first.

For the MILP based heuristic service reconfiguration algorithm, we divide the traffic requests into several small subsets, with each subset A consisting of S traffic requests, except the last subset with size (N mod S) according to the request reordering policy mentioned above. To provision traffic request subset A_c, we denote A_{pre} as the collection of previous subsets A_1 ... A_{c-1}) that are already provisioned in the network. The proposed heuristic is a MILP based heuristic algorithm which provisions each connection request subset one by one solving the MILP formulation with the objective as follows:

$$\text{Objective:} \quad \text{Minimize} \quad \beta \cdot \sum_{l} MF_l + \big(1-\beta\big) \cdot \sum_{n,l,f} PR^n_{l,f}, \quad n \in (A_{pre} \cup A_c) \tag{5.31}$$

The objective function 5.31 of subset MILP problem includes minimizing the summation of the maximum allocated frequency slot index of each link and the total number of frequency slots occupied in the network. Especially when the weight factor $\beta = 0$, the objective is to minimize the overall number of allocated frequency slots. The objective aims to minimize the summation of the maximum frequency slot index assigned to each link when $\beta = 1$. For $0 < \beta < 1$, both features are minimized with the weight β.

The input parameters and the decision variables of modified sub MILP formulation are the same as listed in table 5.1, 5.2 and 5.3.

The objective function subjects to the following constraints.

$$MF_{max} \geq MF_l, \quad \forall l \tag{5.32}$$

$$\sum_{k,m,f} x^n_{k,m,f} \geq 1, \quad \forall n \in A_c \tag{5.33}$$

$$\sum_{k,m} z^n_{k,m} = 1, \quad \forall n \in A_c \tag{5.34}$$

$$z^n_{k,m} \geq \sum_{f} x_{k,m,f}/\mu, \quad \forall n \in A_c, k, m \tag{5.35}$$

$$\sum_{m} Mod_{n,m} = 1, \quad \forall n \in A_c \tag{5.36}$$

$$Mod_{n,m} = \sum_{k} z^{n}_{k,m}, \quad \forall n \in A_c, m \tag{5.37}$$

$$\sum_{k,m,n \in (A_{pre} \cup A_c)} x^{n}_{k,m,f} \cdot P_{n,k,l} \leq 1, \quad \forall l, f \tag{5.38}$$

$$\sum_{k,m,f} x^{n}_{k,m,f} = \sum_{m} Mod_{n,m} \cdot B^{FS}_{n,m}, \quad \forall n \in A_c \tag{5.39}$$

$$FS^{n}_{min} \leq \mu \cdot \left(1 - \sum_{k,m} x^{n}_{k,m,f}\right) + f, \quad \forall n \in A_c, f \tag{5.40}$$

$$FS^{n}_{max} \geq f \cdot \sum_{k,m} x^{n}_{k,m,f}, \quad \forall n \in A_c, f \tag{5.41}$$

$$FS^{n}_{max} - FS^{n}_{min} + 1 = \sum_{m} Mod_{n,m} \cdot B^{FS}_{n,m}, \quad \forall n \in A_c \tag{5.42}$$

$$PR^{n}_{l,f} = \sum_{k,m} \left(x^{n}_{k,m,f} \cdot P_{n,k,l}\right), \quad \forall n \in (A_{pre} \cup A_c), l, f \tag{5.43}$$

$$H_{l,f} = \sum_{n \in (A_{pre} \cup A_c)} PR^{n}_{l,f} \cdot f, \quad \forall l, f \tag{5.44}$$

$$MF_l \geq H_{lf}, \quad \forall l, f \tag{5.45}$$

$$MF_l \leq H_{lf} + \mu \cdot (1 - d_{l,f}), \quad \forall l, f \tag{5.46}$$

$$\sum_{f} d_{l,f} \leq 1, \quad \forall l \tag{5.47}$$

$$MF_l \geq 0, \quad \forall l \tag{5.48}$$

$$MF_l \leq \mu \cdot \sum_{f} d_{l,f}, \quad \forall l \tag{5.49}$$

$$\sum_{ls} y_{ls,l} = 1, \quad \forall l \tag{5.50}$$

$$\sum_{ls} \left(y_{ls,l} \cdot ls\right) \geq MF_l \cdot \frac{LS}{F} + \frac{1}{\mu}, \quad \forall l \tag{5.51}$$

$$\sum_{ls} \left(y_{ls,l} \cdot ls\right) \leq MF_l \cdot \frac{LS}{F} + 1 + \frac{1}{\mu}, \quad \forall l \tag{5.52}$$

$$G_{sig} \cdot \sum_{m} \frac{Mod_{n,m}}{SNR_m} \geq G_{ASE} \cdot \sum_{l} \left(PR^{n}_{l.f} \cdot SP_l\right) + \sum_{l} \left(E^{n,l}_{NLI} \cdot SP_l\right), \quad \forall n \in (A_{pre} \cup A_c), f \quad (5.53)$$

$$E^{N,L}_{NLI} \geq \mu \cdot \left(PR^{n}_{l.f} - 1\right) + \sum_{ls} \left(y_{ls,l} \cdot G^{ls,f}_{NLI}\right), \quad \forall n \in (A_{pre} \cup A_c), f, l \quad (5.54)$$

The meaning of constraint 5.32 - 5.54 are similar to constraints 5.5 - 5.27 shown in subsection 5.2.1. for constraint 5.33 - 5.37 and 5.39 - 5.43, we apply the range of n as $\forall n \in A_c$ to replace its original range $\forall n$ in original MILP problem. This is to ensure that only traffic requests in the subset A_c will be provisioned. In this case, the knowledge of RMSA results from previous subsets or the demands of future request subsets are not required. For constraints 5.38, 5.53 and 5.54, the range of request n is replaced by $\forall n \in (A_{pre} \cup A_c)$ instead of $\forall n$. The modified constraint 5.38 ensures that the allocated frequency slots of current subset A_c do not overlap with the spectrum used by previously provisioned subset A_{pre}. The modified constraint 5.53 and 5.54 ensure SNR requirements are met for both current subset A_c and previous subset A_{pre}.

Apart from modified constraints, two more constraints 5.55 and 5.56 are added for the subset MILP formulation. The constant $XInput^{n}_{k,m,f}$ in 5.55 is the RMSA solution from previous request subset A_{pre}. Constraint 5.55 guarantees that the results of solving decision variable $x^{n}_{k,m,f}$ of the current subset is equivalent to the previous solution for the requests from A_{pre}.

$$x^{n}_{k,m,f} = XInput^{n}_{k,m,f} \quad \forall n \in A_{pre}, k, m, f \quad (5.55)$$

$$\sum_{ls} \left(y_{ls,l} \cdot ls\right) \leq \sum_{ls} \left(YInput_{ls,l} \cdot ls\right), \quad \forall l \quad (5.56)$$

$YInput_{ls,l}$ in 5.56 is the pre-estimated loading state of each link in the main MILP based heuristic algorithm. It is a Boolean parameter and it equals to 1 when link l is estimated to be loading state ls; 0 otherwise. $YInput_{ls,l}$ is an input parameter for the sub MILP while the constraint 5.56 ensures that the actual loading states of the links of solving the sub MILP problem do not exceed the pre-estimated loading states $YInput_{ls,l}$.

The proposed MILP based heuristic service reconfiguration is depicted as algorithm 3 using the proposed subset MILP.

Algorithm 3 PH1: MILP based Heuristic Service Reconfiguration

1: Reorder the connection requests according to reordering policy;
2: Divide the traffic subset according to its subset size S and service reordering policy;
3: Initialize all the loading states by setting $\sum_{ls}\left(YInput_{ls,l}\cdot ls\right)=1,\forall l$;
4: **for** each request subset A_c, c = 1, 2, 3, ..., $\lceil\frac{N}{S}\rceil$ **do**
5: Solve the subset MILP formulation 5.28 according to constraints 5.32 - 5.56;
6: **if** a solution is found **then**
7: Accept the request subset;
8: Record the RMSA solution $x^n_{k,m,f}$ as $XInput^n_{k,m,f}$, as the input for the next subset
9: MILP iteration;
10: **if** $c_{ug}\neq\varnothing \quad \& \quad c==c_{ug}$ **then**
11: Recalculate $YInput_{ls,l}$ according to RMSA solution $x^n_{k,m,f}$;
12: Set $c_{ug}=\varnothing$;
13: **end if**
14: $c=c+1$;
15: **else**
16: **if** $YInput_{ls,l}$ == 1 $\forall l \in$ *candidate paths in subset* A_c **then**
17: Upgrade link loading states $YInput_{ls,l}$ to next level $\forall l \notin$
18: *candidate paths in subset* A_c;
19: **else**
20: Upgrade link loading states $YInput_{ls,l}$ to next level $\forall l \in$
21: *candidate paths in subset* A_c;
22: Record c by assigning its value to c_{ug}, $c_{ug}=c$;
23: Set c = 1; Jump to step 4;
24: **end if**
25: **end if**
26: **end for**

As $YInput_{ls,l}$ is pre-estimated loading states of all the links in the network, the actual corresponding loading states of the links of solving the RMSA problem should not exceed the pre-estimated values, as shown in 5.56. When the pre-estimated links loading states $YInput_{ls,l}$ are too large, the sub MILP assigns higher NLI to the lightpaths, causing severe NLI overestimation. On the other hand, when pre-estimated links loading states $YInput_{ls,l}$ are too small, it leads to infeasible RMSA solution with links of such low loading condition to serve all the traffic. According to this principle, the proposed MILP based heuristic

reconfiguration scheme aims to yield a proper pre-estimated $YInput_{ls,l}$ to accommodate all the request subsets as well as to minimize the two features mentioned in the subset MILP optimisation target.

Since there is no traffic in the network before the first request subset is provisioned, we set pre-estimated loading states of the every link $\sum_{ls}\left(YInput_{ls,l} \cdot ls\right) = 1, \forall l$ for every link l, as shown in line 3. We then dynamically adjust the estimated $YInput_{ls,l}$ according to the traffic of request subsets. For each request subset Ac consisting of a set of bit rate demands, the algorithm invokes the MILP solver to solve the problem in 5.32 - 5.56 to obtain the RMSA solution. Line 5 – 9 show that when a solution is found, the RMSA result $x^n_{k,m,f}$ with $\forall\, n \in A_{pre} \cup A_c$ (the solution of the decision variable) is recorded and we set $XInput^n_{k,m,f} = x^n_{k,m,f}$ as the input parameter for the following request subsets. The input $XInput^n_{k,m,f}$ enables the constraint 5.55 to ensure that the consistency of RMSA solution of previous request subsets.

If the solution is infeasible, the allocated maximum frequency slot index of the request subset exceeds the bounds of $YInput_{ls,l}$, resulting in violation of constraint 5.56. In this case, the pre-estimated loading states of the links of associated paths need to be upgraded to satisfy constraint 5.56. Since there is no knowledge about which paths to be selected from the candidate paths for the request subset A_c, we upgrade the loading states of all the links of all the candidate paths in the subset A_c to the next level ($ls = ls + 1$, for all associated links), as shown in line 19 – 21. Line 22 shows the request subset index c is recorded as c_{ug} when the link loading states upgrade occurs. Then we reset $c = 1$ to repeat the algorithm from first request subset with updated $YInput_{ls,l}$ until $c == c_{ug}$, as shown in line 10.

We also consider the situation where the MILP solver gives different RMSA results using updated $YInput_{ls,l}$. In this case, the RMSA solution might be again beyond the $YInput_{ls,l}$ of the rest optical links to next level until subsets A_1, ..., $A_{c_{ug}}$ are completely provisioned as shown in line 16 – 18. Line 11 – 12 shows that after successfully provisioning subset A_1, ...,

$A_{c_{ug}}$, we re-calculate $YInput_{ls,l}$ according to the RMSA results and set c_{ug} as the empty set. The process, as summarized in the algorithm 3, is repeated until a proper $YInput_{ls,l}$ is found to accommodate all the request subsets.

5.2.3 Complete Heuristic Service Reconfiguration

To further reduce the complexity of service reconfiguration, a complete heuristic service reconfiguration scheme is proposed in algorithm 4. Unlike previous MILP based reconfigurations, the heuristic service reconfiguration function only reconfigures the blocked traffic requests. It works similar to the main algorithm by using K least congested paths. It starts searching from the highest modulation format and assigning the corresponding first-fit spectrum slots along each candidate path. The details of the heuristic service reconfiguration function are shown in the pseudo-code below.

The service reconfiguration function stops searching for the modulation-spectrum combination for a candidate path when the temporally allocated spectrum leads to further blocking of the requests. In this case, the path is discarded from the candidate set by setting a very high-cost value (infinity in this work). This strategy prevents reconfiguration loops where the reconfiguration function triggers further reconfigurations. This technique is able to reduce the overall complexity of the algorithm. If all candidate paths fail, the function returns *reconfiguration failure* to the main algorithm as **HM**. The function returns *reconfiguration success* only when all blocked requests are reconfigured successfully. The new lightpath will not be permanently established unless all blocked requests are successfully reconfigured.

Algorithm 4 PH2: Heuristic Service Reconfiguration Algorithm

```
1: Reorder the connection requests according to reordering policy;
2: for all blocked traffic requests, q = 1,... do
3:     Find K least congested paths;
4:     for each candidate path do
5:         for m = M; m > 1; m - - ; do
6:             Search for the first-fit B^FS_{q,m} for the blocked service q;
7:             Temporally update corresponding loading states of the links;
8:             if any loading state changes then
9:                 if any existing lightpath blocked then
10:                    Set the cost of path k to be ∞;
11:                    break for;
12:                else
13:                    Calculate the SNR of the request q;
14:                    if SNR ≥ SNR_m then
15:                        Calculate the cost of the path according to equation 5.3;
16:                        break for;
17:                    end if
18:                end if
19:            else
20:                Jump to step 13 - 17;
21:            end if
22:        end for
23:    end for
24:    if any cost of K paths not equals to ∞ then
25:        Choose the path with the minimum cost;
26:        Temporally accept the reconfigured lightpath;
27:        Temporally release the initial spectrum resources of service q;
28:    else
29:        return(service reconfiguration failure);
30:    end if
31: end for
32: Accept service reconfiguration;
33: return(service reconfiguration success);
```

5.3 Simulation Environment Setup

We evaluate the performance of our proposed approaches in two network topologies to validate their effectiveness in both small network and large network: 1) a small network with 6 nodes and 9 links (N6S9); 2) national science foundation (NSF) network with 14 nodes 21 links, as shown in figure 5.1 and 5.2.

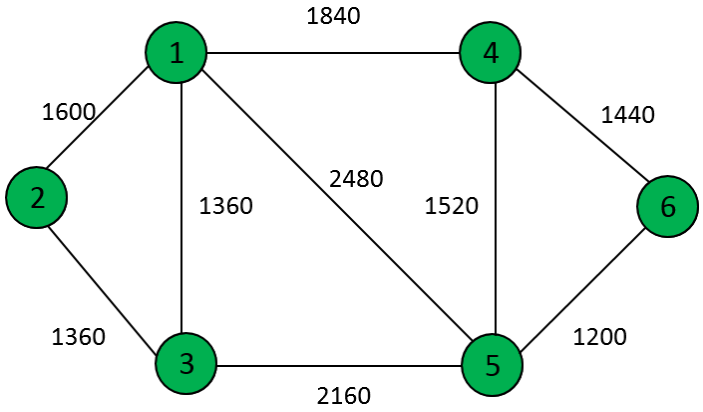

Fig. 5.1 N6S9 network topology (unit: *km*).

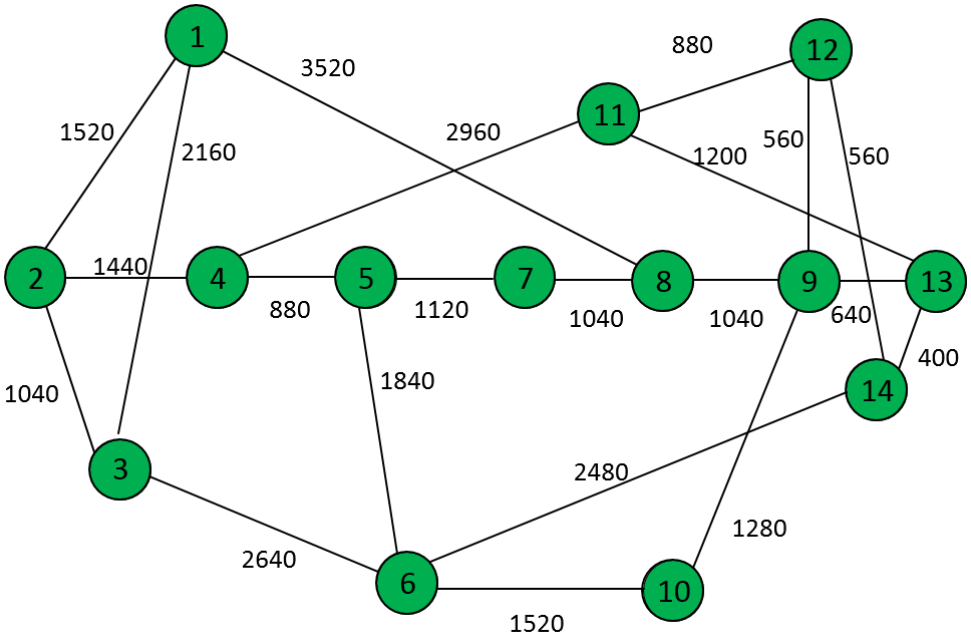

Fig. 5.2 NSF network topology (unit: *km*).

Each optical link is of bi-directional using a pair of fibres. We consider that the network operates in the C-band of 193.6 THz and frequency slot bandwidth b = 12.5 GHz as per ITU-T [79]. Total bandwidth B is 4 THz, thus the number of frequency slots F equals to 320. M is 4 corresponding to four modulation levels while the number of shortest paths per connection, K = 3 for the main RMSA algorithm and the corresponding service reconfiguration algorithms. The spectra window size of the proposed hybrid NLI model is 100 GHz and 200 GHz, hence the number of loading states LS corresponds to 20 and 40 for comparison.

The same parameters of fibre and EDFA described in section 4.5 of chapter 4 are used. The fibre spans are of equal length with 80 km/span. Pre-FEC bit error rate requirement of all the traffic requests is set to 3.8×10^{-3} for error-free transmission. The SNR threshold for each modulation format to achieve the pre-FEC BER target is calculated according to [71] which is 5.46 dB for DP-BPSK, 8.47 dB for DP-QPSK, 12.45 dB for DP-8QAM and 15.13 dB for DP-16QAM. For the proposed MILP based heuristic service reconfiguration, the subset size S is set to be 2 and weight factor β is 0.5. We evaluate two types of traffic requests for the simulation: low-to-medium bandwidth requests that are uniformly distributed between 40 Gbps and 400 Gbps and medium-to-high bandwidth requests that are uniformly distributed between 100 Gbps and 600 Gbps. Both traffic types are unidirectional.

To evaluate the performance of the proposed resource allocation algorithm with different service reconfiguration schemes, we use the ILP method and the sequential RMSA heuristic algorithm described in [98] as the benchmark. An ILP for the RMSA problem is formulated and an RMSA heuristic scheme is presented allocating the resource for connection requests in a sequential manner in the benchmark method.

The benchmark method adopts the maximum transmission distance method with a guard band for the modulation level assignment to model the impact of the physical layer impairments. The maximum permitted transmitted distance is different for each modulation level of m. For a higher modulation level, the reach distance is shorter while the reach

Table 5.4 Reach distance for different modulation format with different signal PSD (unit: km)

Signal PSD (mW/THz)	DP-BPSK	DP-QPSK	DP-8QAM	DP-16QAM
10.64	9680	4800	1920	1040
13.40	11600	5760	2240	1200
16.87	13120	6560	2560	1360
21.24	13760	6880	2720	1440
26.73	13040	6480	2560	1360
33.66	10960	5440	2160	1120
42.38	8240	4080	1600	880

distance increases with lower modulation formats. The benchmark method pre-calculates K shortest paths for each pair of source-destination for both ILP and the RMSA heuristic algorithm, while the routing decision is chosen among the K candidate paths. However, it only indicates transmission distance for each modulation format regardless of signal power. If the signal PSD changes, the pre-defined reach distance may no longer support error-free transmission for the assigned modulation format.

Therefore, in our approach, we first calculate the worst-case NLI PSD assuming full channel occupancy of all the 4 THz bandwidth for different transmission PSDs. The maximum transmission distance of each modulation format is then calculated to achieve pre-set pre-FEC BER for different signal PSDs using equation 4.1 and 4.2 with worst-case NLI. Table 5.4 shows the longest transmission distance of each modulation format for error-free transmission with fibre parameters described earlier. The guard band for the benchmark is set to 12.5 GHz (one frequency slot) as similar to [98].

5.4 Simulation Results

We first evaluate the performance of the proposed service reconfiguration algorithms against benchmark methods in terms of network utilization and spectrum efficiency. Later, the complete algorithms are also performed for sequentially loaded NSF network to measure the network blocking probability.

5.4.1 Performance Comparison of Service Reconfiguration Approaches

Results for N6S9 Network with low-to-medium bandwidth requests

For the N6S9 network, we evaluate and compare the results of the proposed MILP reconfiguration, referred to as **PM** in this chapter, the benchmark ILP (**BI**), the proposed MILP based heuristic reconfiguration algorithms (**PH1**) and the proposed complete heuristic service configuration (**PH2**) and the benchmark heuristic (**BH**). Service reconfiguration algorithms have the knowledge of all the existing traffic thus they are regarded as off-line algorithms.

To make the comparison of reconfiguration algorithms, the results are averaged over 20 traffic profiles where each traffic profile consists of 20 connection requests between randomly selected pairs of nodes. The **PM** and the **BI** are simulated on a desktop with 3.1 GHz Intel i7-3770s CPU and 16 GB memory using IBM ILOG CPLEX version 12.7.1. The running time for the **PM** is between 1 minute to 10 minutes for low-to-medium bandwidth requests with proper upper bound and lower bound of the MF_{max}. The running time for $LS = 40$ is 1.5 - 2 times more than the case when $LS = 20$ due to higher MILP complexity. The BI requires approximately 2-3 times more time to find an RMSA solution than the PM reconfiguration scheme. For medium-to-high bandwidth requests, it takes longer to obtain the optimal results compared to low-to-medium bandwidth requests. The time required for the PH1 is less than the PM and the BI by calculating the RMSA results within 1 minute.

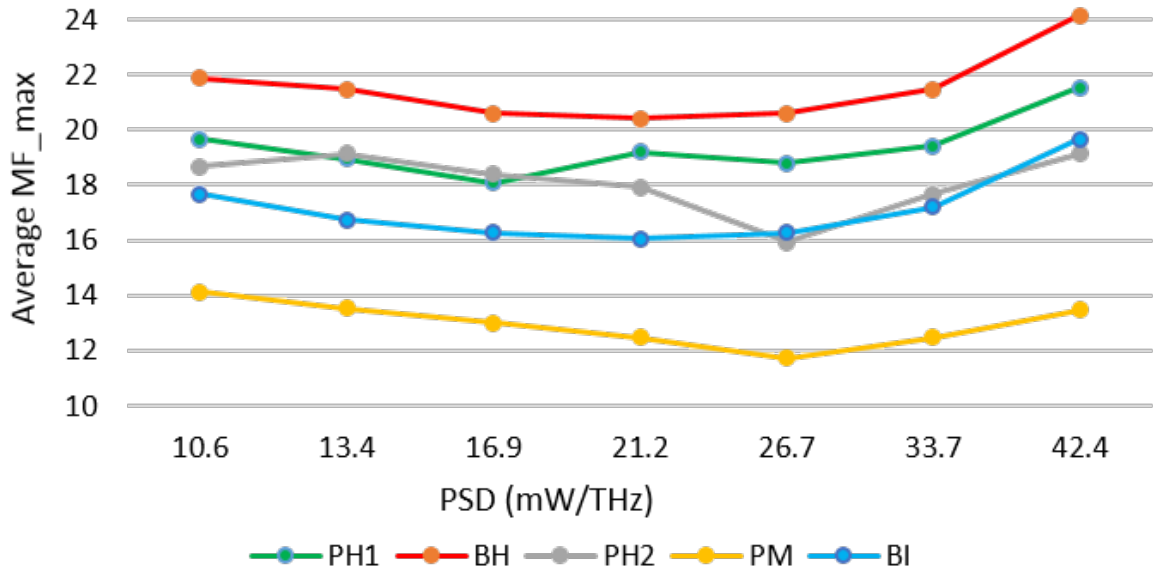

Fig. 5.3 Average maximum allocated frequency slot index in the network versus different signal PSDs of different reconfiguration algorithm with low-to-medium bandwidth requests.

First, we consider the case where traffic profiles are low-to-medium bandwidth requests. In figure 5.3, the average maximum allocated slot index in the network MF_{max} is compared between different algorithms for each transmission PSD when $LS = 40$. It can be seen that the PM achieves the least MF_{max} for all transmission PSDs. Compared to the BI, it reduces MF_{max} from 24 % to 46% for different PSDs. The results are as expected since we use a more accurate hybrid nonlinearity model for **PM** as compared to the maximum transmission distance method in the **BI**. The reduction of MF_{max} leads to potentially higher available capacity by leaving more continuous and contiguous frequency slots available in the network. In this case, the reduction of MF_{max} also results in less loading states of the links which may account for less NLI estimation for the proposed NLI model. It can be observed from figure 5.3 that the 16.9 mW/THz is the best PSD among the options for **PH1** while 21.2 mW/THz is the best PSD for two benchmark methods to obtain minimum MF_{max}. The rest of the strategies achieve the smallest MF_{max} for PSD 26.7 mW/THz.

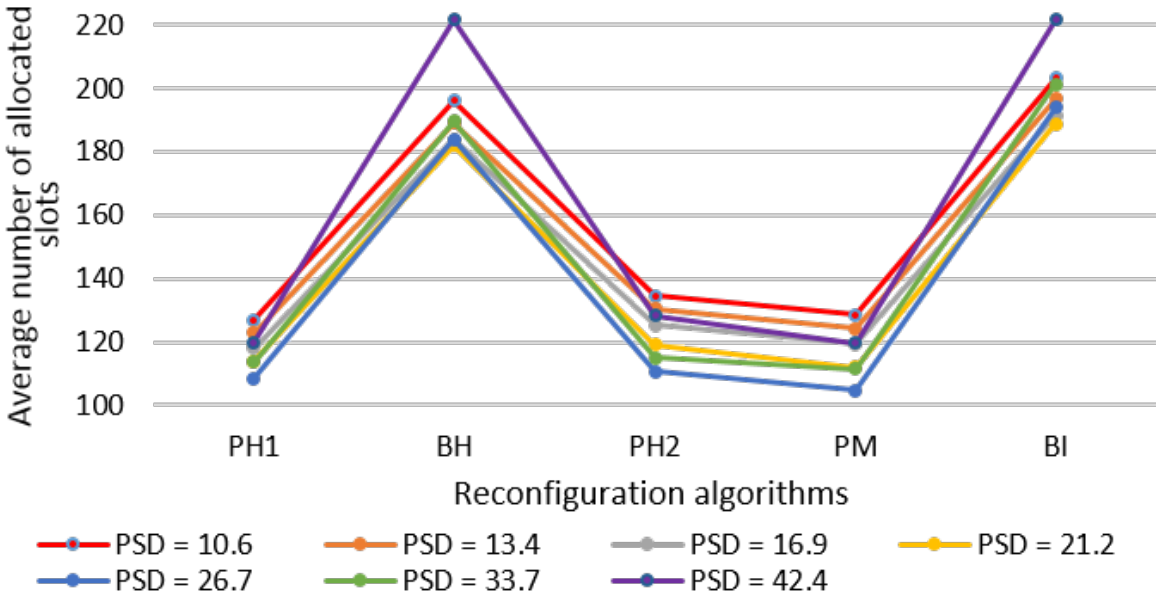

Fig. 5.4 Average number of allocated frequency slot in the network versus different signal PSDs of different reconfiguration algorithm with low-to-medium bandwidth requests.

Figure 5.4 shows the average number of allocated frequency slots in the network using different algorithms for different PSDs (LS = 40 for the proposed algorithms) under low-to-medium bandwidth requests. Although two proposed heuristics require the similar amount of spectrum resources, the MILP based heuristic (**PH1**) allocates 1.7% - 7% fewer number of frequency slots than the complete heuristic reconfiguration function (PH2) for different PSDs. In this case, the PM utilizes the least spectrum resources due to its secondary goal of minimizing the number of allocated frequency slots.

The proposed MILP and two heuristics allocate approximate 40% - 45% fewer frequency slots compared to BI and BH when PSD = 21.2 mW/THz. The benefits of the proposed solutions are again due to the hybrid NLI model, which makes a less conservative NLI estimation. Thus, the lightpaths can utilize more high modulation formats with accurate NLI information, which is shown in figure 5.5 with two transmission PSDs. In this case, it leaves more free frequency slots in the network for future connection requests.

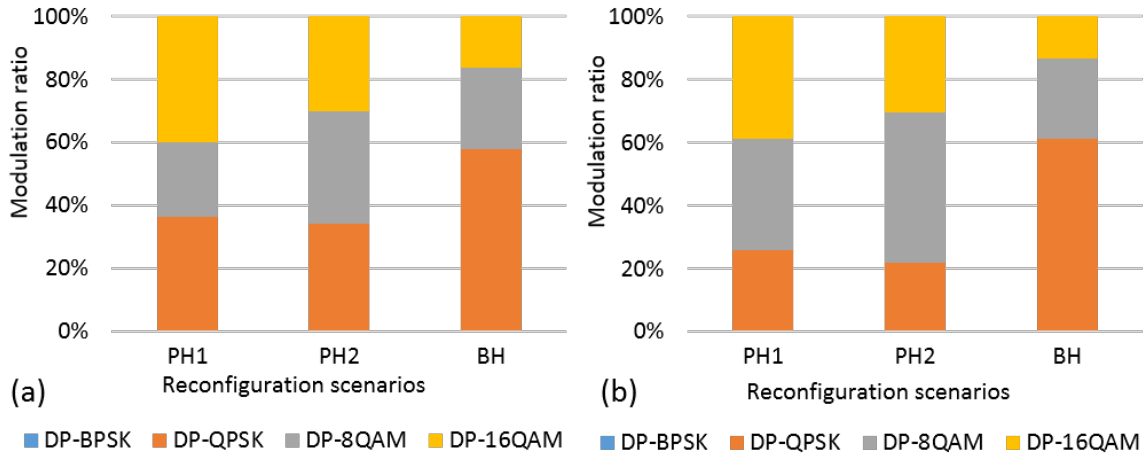

Fig. 5.5 Modulation format ratio versus different algorithms. (a) PSD = 21.2 mW/THz; (b) PSD =26.7 mW/THz with low-to-medium bandwidth requests.

The ratio of different modulation formats used for provisioning low-to-medium bandwidth requests using two proposed heuristics (both with LS = 40) and benchmark heuristic for transmission PSD = 21.2 mW/THz and PSD = 26.7 mW/THz is illustrated in figure 5.5. It can be observed that both proposed heuristic approaches utilize high modulation schemes for more requests compared to the benchmark method, leading to higher spectrum efficiency. In the case of two proposed heuristic algorithms, approximately 36% of the connection requests use DP-QPSK when PSD = 21.2 mW/THz and approximately 26% requests utilize DP-QPSK when PSD = 26.7 mW/THz. Rest of the connection requests use higher modulation schemes. Again, it shows that in the N6S9 network with 20 low-to-medium bandwidth requests, PSD = 26.7 mW/THz achieves better spectrum efficiency for proposed heuristic algorithms than PSD = 21.2 mW/THz.

The best PSD among the options for two benchmark methods is 21.2 mW/THz which maximizes the transmission distance assuming the worst-case NLI. However, the best PSD for the 3 proposed service reconfiguration solutions to achieve minimum spectrum usage is 26.7 mW/THz. This is because less congested link yields less NLI compared to the worst-case NLI. Therefore, PSD of 26.7 mW/THz leads to better SNR performance.

To understand the effect of granularity of spectra window size defined in the proposed hybrid NLI model on the network, we compare the performance of the PM and the PH2 where LS = 40 (window size of 100 GHz) with the case where $LS = 20$ (window size of 200 GHz) for 4 THz bandwidth. Figure 5.6 illustrates the percentage saving on the number of allocated frequency slots for the case with $LS = 40$ over $LS = 20$ with low-to-medium bandwidth requests. It shows that the case $LS = 40$ requires fewer spectrum resources than $LS = 20$ for both PH2 and PM. This is because with smaller spectra windows size defined (more link loading states number LS), the more NLI estimation accuracy can be obtained. The improved NLI accuracy results in less spectrum waste for RMSA solution. On the other hand, the complexity of 3 proposed service reconfiguration solutions grows with the increasing number of the defined link loading states LS.

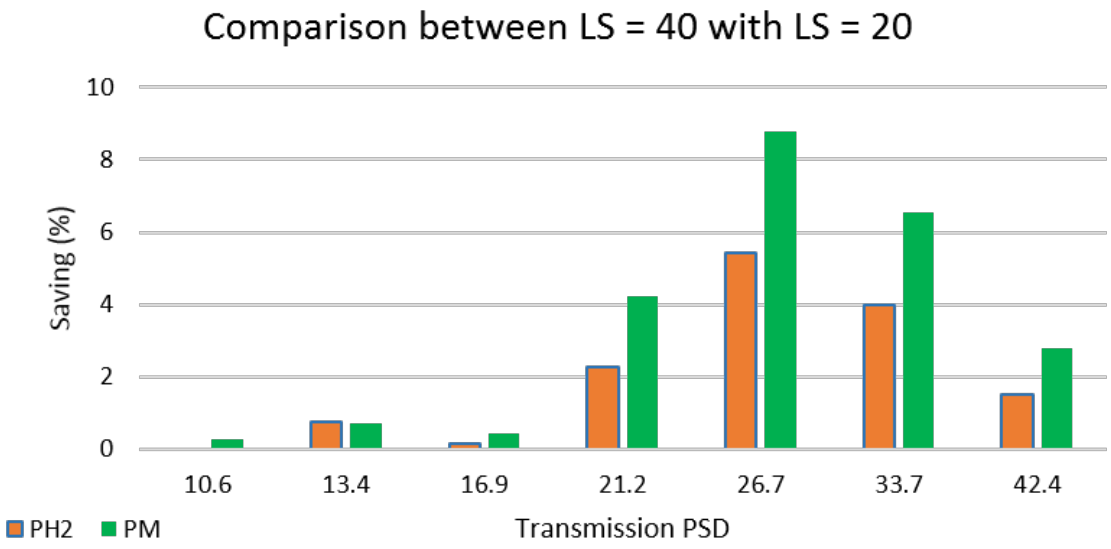

Fig. 5.6 Allocated slots number saving for LS = 40 over LS = 20 with low-to-medium bandwidth requests.

The parameters β and MILP subset size S defined in the MILP based heuristic service reconfiguration (PH1) have a considerable impact on its performance. In this section, we also vary the subset size S from 2 to 1, the β value from 0.5 to 0 and 1 respectively and compare their performance with the proposed $\beta = 0.5$ and $S = 2$ shown above.

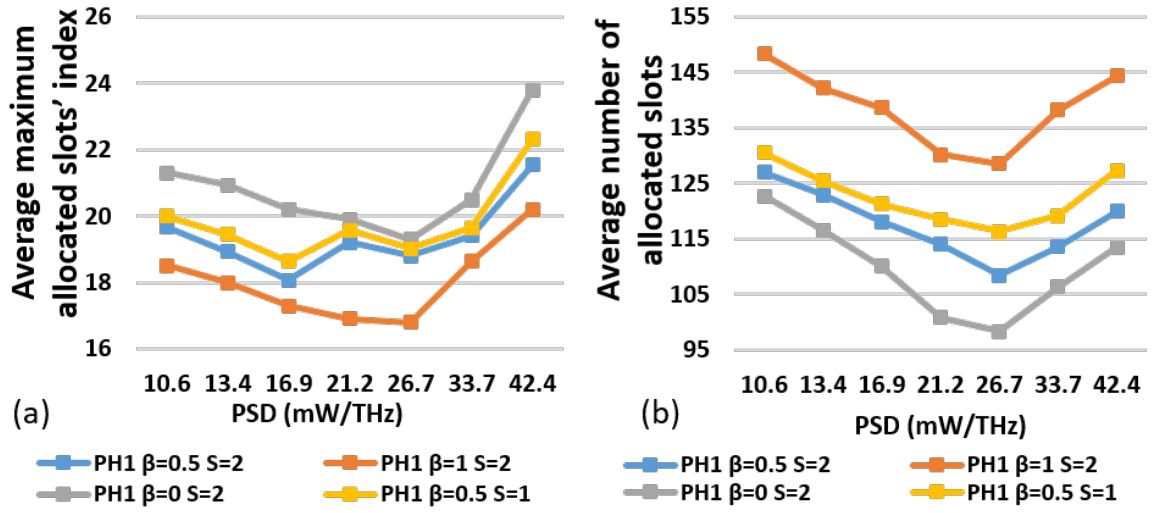

Fig. 5.7 Allocated slots number saving for LS = 40 over LS = 20 with low-to-medium bandwidth requests.

Figure 5.7 (a) shows the average maximum allocated slot index MF_{max} against the increasing signal PSDs. As with $\beta = 1$, PH1 aims at minimizing the summation of maximum slot index among all the links. Therefore, the combination with $S = 2$ and $\beta = 1$ of PH1 achieves the minimum MF_{max}. On the other hand, PH1 with $\beta = 0$ and $S = 2$ leads to the highest MF_{max} among the tested combinations as its optimisation target is irrelevant to MF_{max}. We also vary the S to be 1 and result depicts that $S = 2$ can yield slightly less MF_{max} compared to the PH1 with $S = 1$.

Figure 5.7 (b) shows the average number of allocated slots against the signal PSDs for different S and β combinations. Contrast to the results in figure 5.7 (a), PH1 with $\beta = 0$ requires the least spectrum slots number while $\beta = 1$ uses the most spectrum resources. This is because $\beta = 0$ of PH1 is to minimize the number of slots assigned in the network. For the case PH1 with subset size $S = 1$, the algorithm assigns slightly more slots compared to $S = 2$. The larger subset size of PH1 can achieve better results than smaller subset size in terms of the less maximum slot index and lower number of allocated slots. However, it also needs more time to solve the sub MILP problem, with approximate 1 minute for $S = 2$ and 20 - 30 seconds for $S = 1$.

Results for N6S9 Network with medium-to-high bandwidth requests

The important performance metrics such as the average MF_{max}, the number of allocated slots and the modulation format ratio show similar characteristics and trends for medium-to-high bandwidth requests in NSF network compared to low-to-medium bandwidth requests in the N6S9 network. Due to the space constraints, we do not show all these results in this work. The table presents the average number of allocated frequency slots for PH1, PH2, PM, BI and BH. Again, the proposed off-line service reconfiguration solutions utilize 40% - 70% fewer frequency slots compared to the benchmark methods. The PH1 approach is observed to use fewer spectrum resources even compared to PM when PSD $\neq$ 26.7 mW/THz. This is because the primary objective of PM is only to minimize MF_{max} while the PH1 minimizes both features (summation of MF_l and the number of allocated frequency slots) with weight β.

Table 5.5 Average number of allocated slots in N6S9 network for medium-to-high bandwidth requests.

Signal PSD (mW/THz)	10.6	13.4	16.9	21.2	26.7	33.7	42.4
PH1	198	194	186	180	176	183	192
PH2	206	202	196	189	180	185	198
PM	216	196	198	190	171	194	203
BI	290	286	282	281	289	290	317
BH	288	277	270	262	270	280	335

Results for NSF Network for Both Traffic Profiles

We also apply the two traffic requests to the large NSF topology to study how the proposed reconfiguration algorithms perform for a large network. Due to the size of the NSF network, the number of traffic requests for each traffic profile is set to 30. The results are calculated and averaged based on 20 traffic profiles. The PM and BI consume a significant amount of time to provide solutions for the NSF network due to the computational complexity of solving MILP (software aborted after 6-10 hours searching). For large complex networks, it is infeasible to implement BI or PM approaches for practical timescale. Therefore, in this sub-section, we compare the results of the PH1, PH2 with the BH in the NSF network.

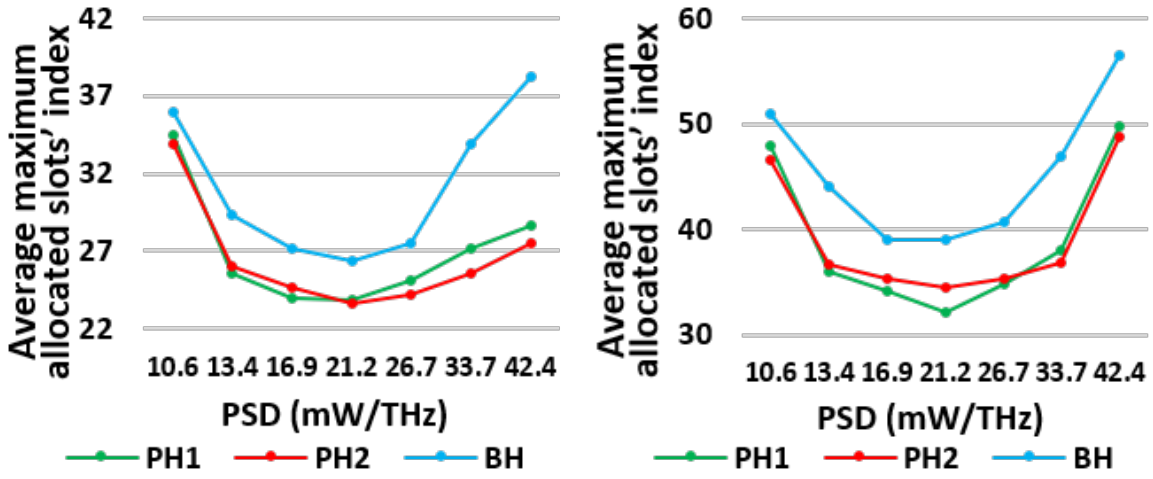

Fig. 5.8 Average maximum frequency slot index versus transmission PSD. (a) 40 Gbps – 400 Gbps requests; (b) 100 Gbps – 600 Gbps requests.

The average MF_{max} of each algorithm as a function of transmission PSDs is shown in figure 5.8. It indicates that the PH1 and PH2 achieve similar performance for two types of traffic scenarios. Similarly, the proposed solutions can leave more continues and contiguous spectrum resources in the NSF network compared to BH.

In figure 5.9, we present the number of allocated frequency slots as a function of PSDs for both traffic scenarios. The curve of BH (brown triangle markers) is associated with a left side blue vertical axis and curves of PH1 and PH2 (circle markers) are associated with the

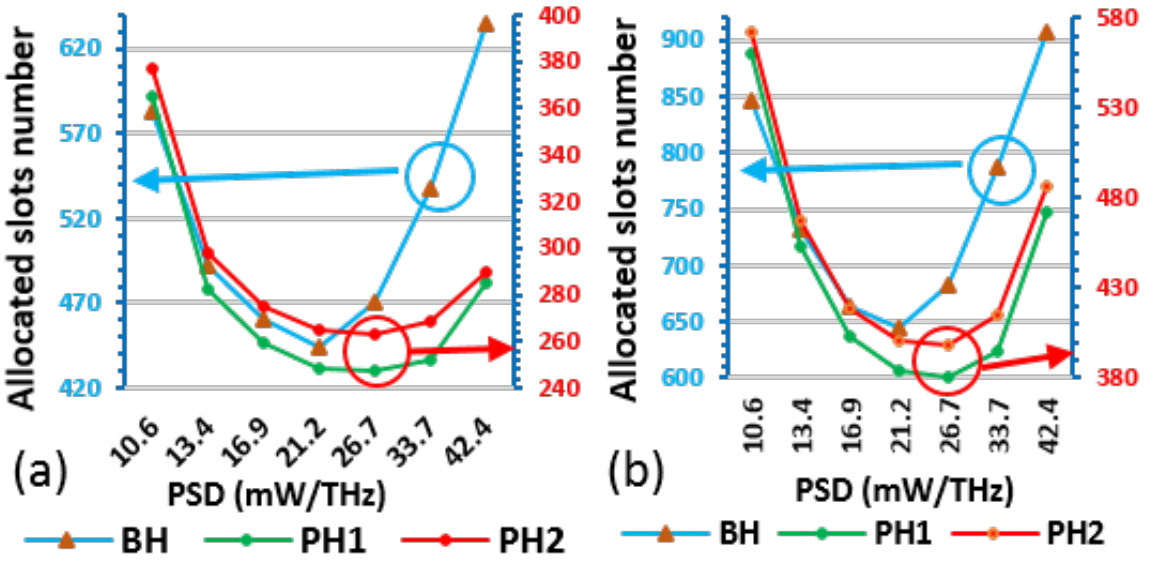

Fig. 5.9 Average number of allocated frequency slots versus transmission PSD. (a) 40 Gbps – 400 Gbps requests. (b) 100 Gbps – 600 Gbps requests.

right side red vertical axis. The PH1 approach saves slightly more slots compared to PH2, due to better resource optimisation of sub-MILP formulation. The PH1 and PH2 can save up to 80% and 70% number of slots, compared to BH, for low-to-medium and medium-to-high bandwidth requests respectively when the PSD is between 21.2 mW/THz and 26.7 mW/THz. It shows the number of slots saving increases when PSD increases. In the NSF network, the best PSD among the tested options for PH1 and PH2 to achieve minimum spectrum usage is 26.7 mW/THz for both traffic scenarios.

5.4.2 Performance Evaluation of the Complete Proposed RMSA Algorithm in Sequentially Loaded NSF Network

To evaluate the performance of the proposed schemes in a realistic scenario with dynamic incremental traffic requests, we sequentially load the NSF network with low-to-medium bandwidth requests and medium-to-high bandwidth requests. The traffic requests are randomly generated respectively following the same traffic distribution described earlier. We evaluate the request blocking ratio and spectrum efficiency of the proposed solutions. The

service request blocking probability is expressed as:

$$BP_i = \frac{Block_i}{i} \tag{5.57}$$

where $Block_i$ is the average number of blocked requests after provisioning i_{th} request. To build statistical results of the service blocking probability and network utilization, the complete RMSA algorithm is repeated 2000 times. Apart from the previous benchmark method, we further include the congestion-aware RMSA described in [107] as the second benchmark (**CA-BH2**) in this section. The CA-BH2 utilizes the congestion-aware routing strategy and the first-fit spectrum assignment. NLI modelling in CA-BH2 considers using the GN model assuming full channel occupied within C band. Details of the NLI model is referred to as equation (1) – (3) in [107].

To obtain the statistical results, the simulation needs to be performed thousands of time. Therefore, the PM and BI approach cannot provide a feasible solution for service reconfiguration due to their complexity (software aborted) for NSF network. As the algorithm is repeated thousands of times, PH1 is not able to give the results in a reasonable amount of time. Therefore, we compare the performance of the **proposed heuristic algorithm main** using PH2 as the service reconfiguration (LS = 40) with the sequential RMSA of the **BH** and **CA-BH2**.

Figure 5.10 shows the requests blocking probability against the number of requests when PSD = 19.3 mW/THz. The results clearly show that the proposed scheme with PH2 using hybrid NLI model accepts approximately 300 and 200 more low-to-medium bandwidth requests at 1% blocking probability compared to the BH and CA-BH2 respectively. Average 148 and 51 more requests can be accepted at 1% blocking probability for medium-to-high bandwidth requests compared to BH and CA-BH2 respectively.

The average network throughput when the network reaches 1% blocking ratio for two algorithms is shown in figure 5.11. The results indicate that the proposed solution with PH2

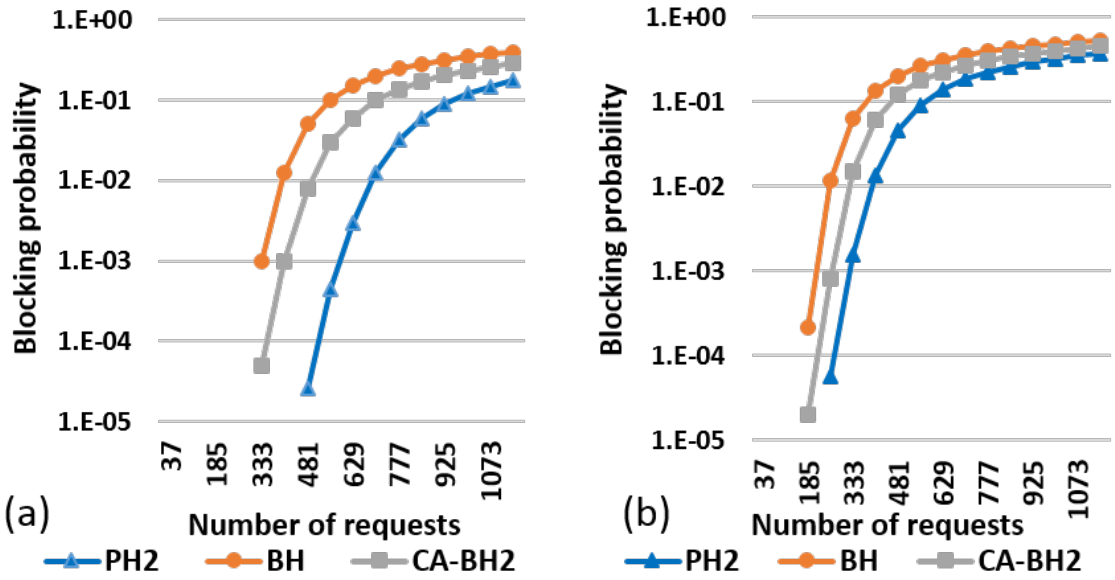

Fig. 5.10 Blocking probability versus the number of loaded requests when PSD = 19.3 mW/THz. (a) 40 Gbps – 400 Gbps requests; (b) 100 Gbps – 600 Gbps requests.

as service reconfiguration scheme can serve 25.5 Tbps – 55.7 Tbps more capacity than both benchmark solutions at 1% blocking ratio for low-to-medium bandwidth requests. Similarly, 15.86 Tbps – 42.1 Tbps more network throughput can be achieved using the proposed solution for different PSDs with medium-to-high bandwidth requests.

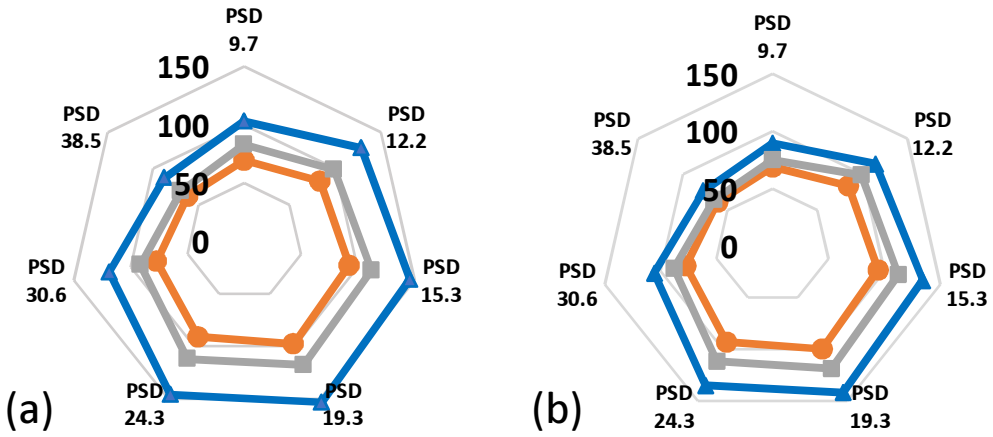

Fig. 5.11 Network throughput when NSF network reaches 1% blocking probability. (a) 40 Gbps – 400 Gbps requests; (b) 100 Gbps – 600 Gbps requests.

Figure 5.12 demonstrates the probability of service requests reconfiguration of using PH2 as the reconfiguration scheme against the increasing number of loaded traffic for both traffic profiles. Both figure 5.12 (a) and (b) show that the network requires more reconfiguration as the signal PSD increases. This is obvious as the network operates in high NLI regime, making the NLI the dominant noise. Therefore, the NLI effect on the signal QoT is stronger than the low signal PSD, which requires more reconfiguration due to more QoT degradation with increasing link load.

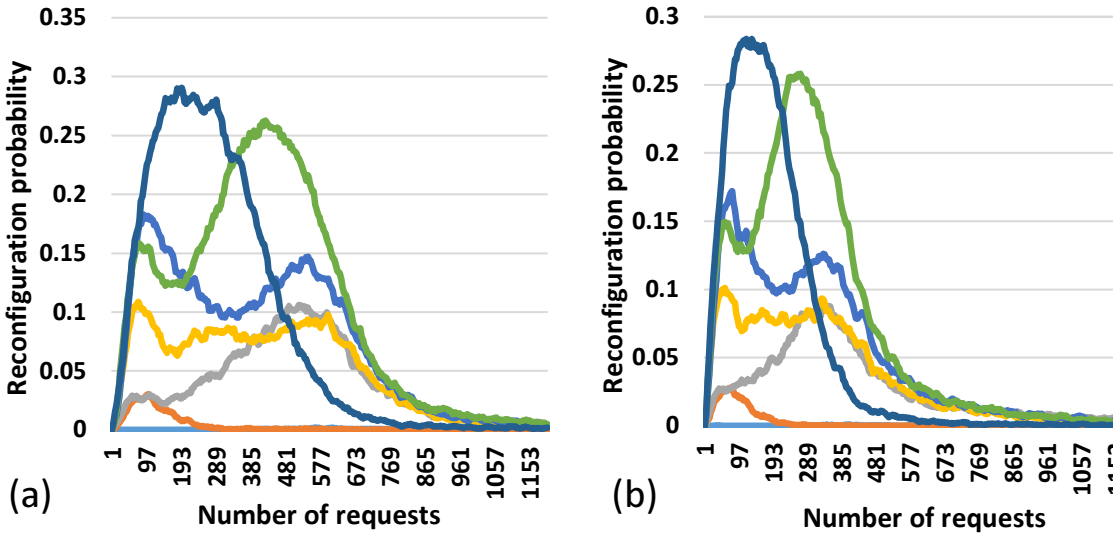

Fig. 5.12 Service requests reconfiguration probability of PH2 against the increasing number of traffic. (a) 40 Gbps – 400 Gbps requests; (b) 100 Gbps – 600 Gbps requests.

In table 5.6, we list the number of service reconfiguration required to provision 800 service requests sequentially into the NSF network with different signal PSDs for both traffic patterns. Similar to the results in figure 5.12, the number of service reconfiguration increases as the signal PSD raises. However, fewer number of reconfigurations are performed with PSD = 38.5 mW/THz compared to PSD = 30.6 mW/THz. This is understandable as the network is in high NLI regime with PSD equals to 38.5 mW/THz, suffering from significantly higher network blocking probability than the network with PSD = 30.6 mW/THz. As a result, a fewer number of requests can be accepted for PSD 38.5 mW/THz compared to

Table 5.6 Average service reconfiguration number for PH2 to provision 800 requests.

Signal PSD (mW/THz)	9.7	12.2	15.3	19.3	24.3	30.6	38.5
Low-to-medium traffic	0.07	1.3	17	21	33	53	45
Medium-to-large traffic	0.02	1	12	14	21	34	26

PSD = 30.6 mW/THz, making the overall reconfiguration number smaller. Moreover, the successful reconfiguration rate for network operating within the high nonlinear regime due to high signal PSD is reduced as well.

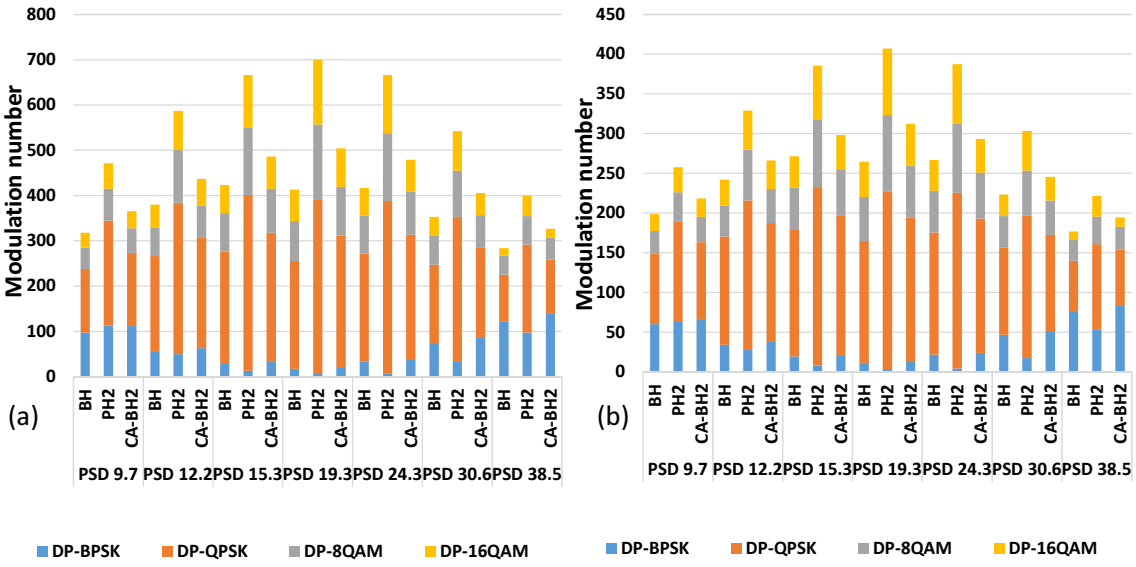

Fig. 5.13 Modulation format number when NSF network reaches 1% blocking probability. (a) 40 Gbps – 400 Gbps requests; (b) 100 Gbps – 600 Gbps requests.

Figure 5.13 shows the stacked bar charts of each modulation format number at 1% blocking probability for two traffic types. It indicates the PSD = 19.3 mW/THz to be the best PSD in sequentially loaded NSF network with 4 THz bandwidth to achieve the maximum spectrum efficiency and network throughput for both traffic scenarios. In this case, the best PSD option is different compared to PH2 in the N6S9 network shown earlier to achieve maximum spectral efficiency (PSD = 26.7 mW/THz) for static low-to-medium bandwidth

requests. This is because the NLI of the lightpaths increases as link utilization increases. As a result, PSD = 19.3 mW/THz yields to better SNR performance than PSD = 26.7 mW/THz.

The link utilization in the sequentially loaded network is sufficiently high when blocking starts to occur compared to traffic reconfiguration scenarios above with relatively less congested links. Therefore, more NLI should be assigned to new lightpaths that are using the more congested links. As a result, the high network utilization leads to lower PSD to maximize end-to-end SNR compared to the low network utilization. It is observed that the network accepts more low-to-medium bandwidth requests than medium-to-high bandwidth requests at 1% blocking probability. But the percentage of each modulation format when the network reaches 1% blocking probability is similar for both traffic.

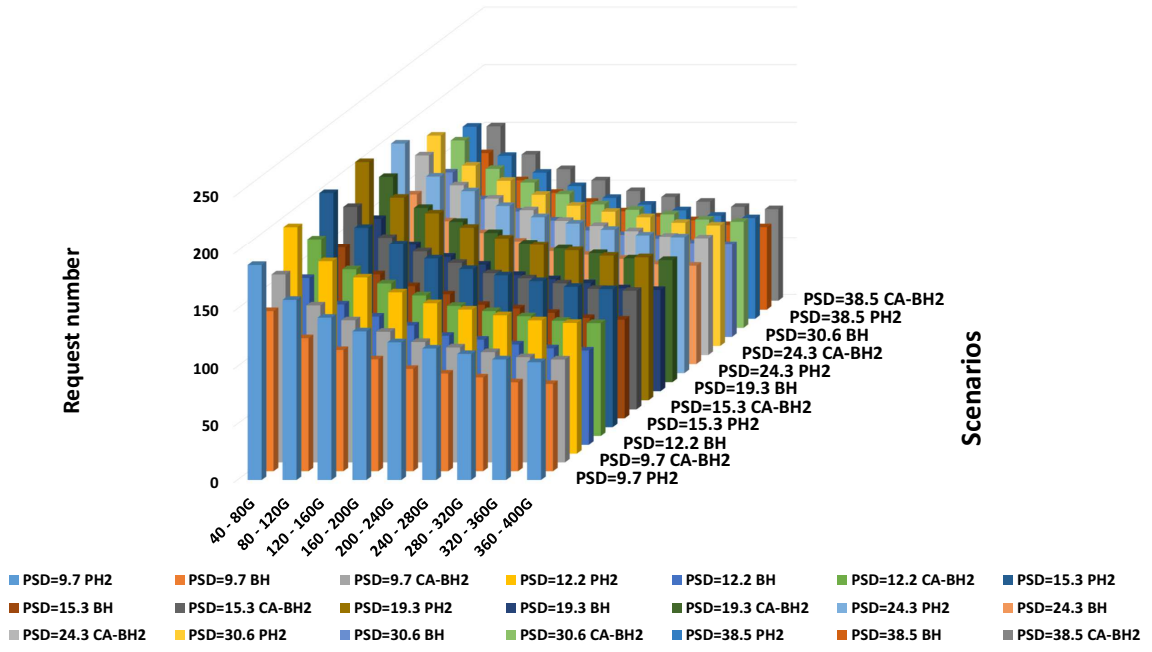

Fig. 5.14 Bit-rate distribution of accepted requests for low-to-medium bandwidth traffic requests.

Figure 5.14 presents the average bit-rate distribution of all accepted low-to-medium bandwidth requests. When PSD = 19.3 mW/THz, the proposed solution accepts approximately 40% and 16.3% more different bit-rate requests compared to BH and CA-BH2 respectively. The graph also implies small bit-rate requests have better acceptance ratio than the large bit-rate request. The case of the medium-to-high bandwidth traffic also shows a similar trend regarding the bit-rate distribution of accepted request. Therefore, we do not show the results due to the limitation of space.

5.5 Summary

In this chapter, we propose a complete algorithm with 3 service reconfiguration schemes to solve the RMSA problem in EON based on the proposed hybrid NLI model. The results show that compared to the benchmark methods, the proposed solutions are able to save a significant amount of spectrum resource, achieve better spectrum efficiency, provide lower blocking probability and higher network capacity with different signal PSDs in our evaluation of two types of networks. The results also indicate that to achieve minimum spectrum usage, the optimal PSD of the proposed solutions decreases as the amount of network traffic increases.

Chapter 6

Dynamic Resource Allocation and Traffic Grooming in Elastic Optical Networks

6.1 Introduction

In this chapter, we first further analyse the effect of inter-channel blocking problem due to nonlinear impairments to the lightpaths and the networks. Based on the effect, we further propose the dynamic resource allocation scheme for dynamic traffic requests in the optical networks considering the inter-blocking problem of using the proposed hybrid nonlinearity model. The online heuristic algorithm accommodates each request according to their time of arrival where the future requests are unknown to the algorithm. The spectrum slots resources are dynamically allocated to different requests and the loading states defined in chapter 4 keeps fluctuating. The objective of the proposed heuristic algorithm is to accommodate more request so as to maximise the network utilisation. Another objective in this chapter is to improve the network capacity by utilising the excess SNR margin of the different lightpaths in the network. We combine the capability of bandwidth-variable transponders and the traffic grooming techniques to efficiently use the excess margin. The proposed strategy is evaluated and the performance is compared with other baseline algorithms. The ideas of this

chapter were presented in the 2017 International Conference on Optical Network Design and Modeling in Budapest [153] and 2017 European Conference on Optical Communication in Gothenburg [158].

6.2 Effect of Inter-Channel Blocking due to Nonlinear impairments

The inter-channel blocking problem of SNR degradation of existing lightpaths due to new lightpaths being established is simply analysed in chapter 4. In this section, we will have a detailed discussion of the impact of the inter-channel blocking and how to avoid inter-channel blocking with the proposed algorithm for dynamic traffic scenarios.

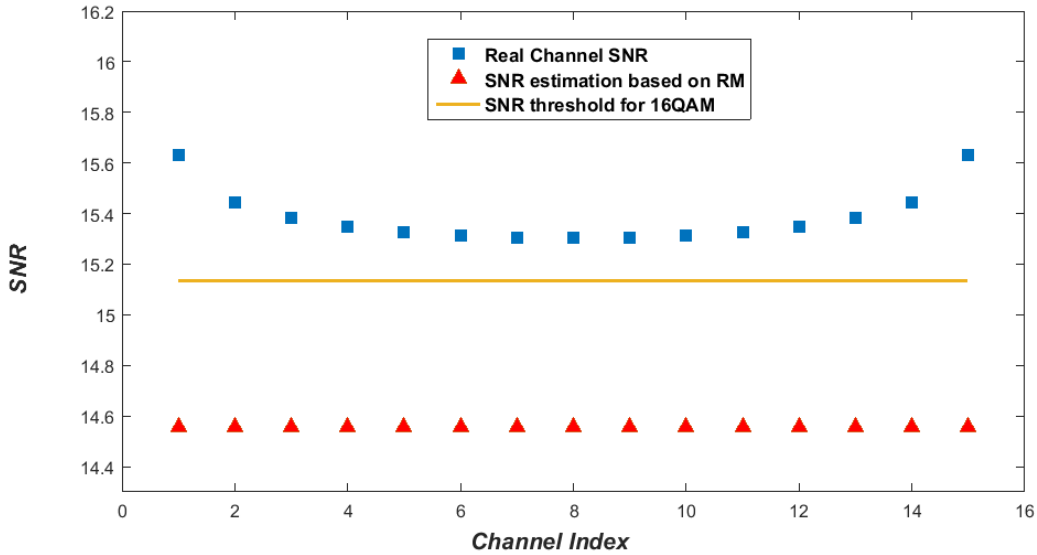

Fig. 6.1 SNR estimation of using the reference margin method and the actual SNR of 15 channels provisioned.

In figure 6.1, we showcase the effects of real NLI of using original GN model and 2 dB reference margin (RM) method to model the impact of NLI on the SNR of the lightpaths provisioned on the same link. Lightpaths are deployed over a link within total 18 spans

fibre with 80 kilometres per fibre span. The single mode fibre is considered with the same fibre parameters described in table 2.1. We assume the signal PSD to be 19 mW/THz with rectangular Nyquist shaping. From figure 6.1, it is observed that when 15 lightpaths or channels (shown as blue blocks with channel index 1-15) are allocated, all the lightpaths can transmit with 16QAM as the modulation format based on their real NLI. However, using the reference margin NLI estimation scheme does not allow 16QAM as the modulation format as it largely overestimates the NLI.

However, when lightpaths with channel index of 16-30 are allocated, the nonlinear impairments of the existing lightpaths 1 - 15 increases while 16QAM becomes infeasible for those lightpaths. It is also known as the inter-channel blocking shown in the previous chapter. The inter-channel blocking issue is shown in figure 6.2. Again, utilising reference margin method to estimate the worst-case nonlinear impairments makes 16QAM impossible modulation format for all the lightpaths in both cases due to overestimating the NLI impacts.

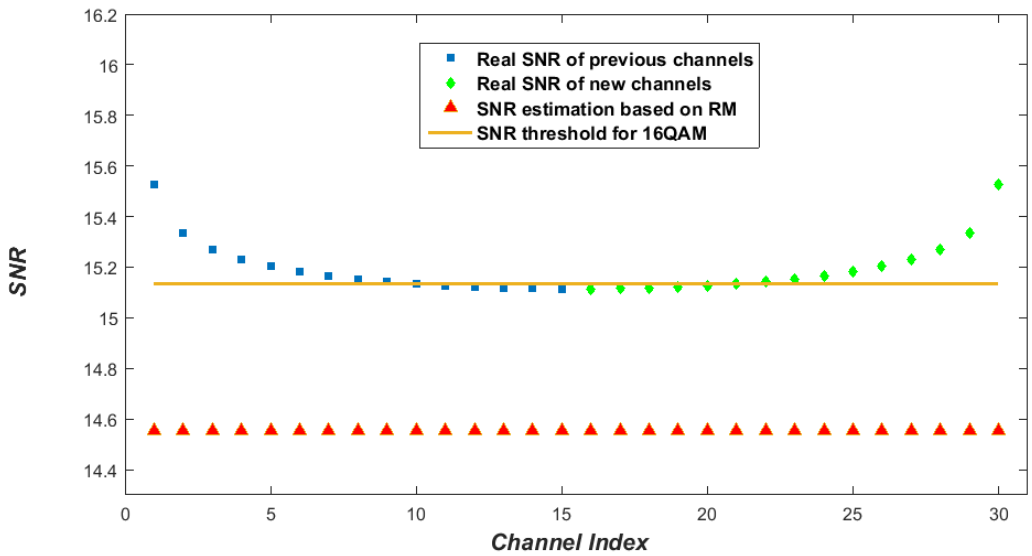

Fig. 6.2 SNR estimation of using the reference margin method and the actual SNR of 30 channels provisioned.

6.3 Nonlinearity-Aware Resource Allocation for Dynamic Traffic

The hybrid nonlinearity model is proposed in chapter 4 to overcome the drawback of using a conservative reference margin scheme and to avoid inter-channel blocking problem when adopting exact nonlinearity information for dynamic traffic in EON. In this chapter, we propose a hybrid nonlinearity model based resource allocation scheme with dynamic traffic with a certain interval of arriving time and holding time. In this work, we assume a link of 5 loading states (LS = 5) for 5 THz in C-band. As a result, the loading states are classified as being 20%, 40%, 60%, 80% and 100% of frequency slots continuous occupied.

6.3.1 The proposed Algorithm

To protect existing lightpaths from inter-channel blocking problem and to allow provision future traffic while improving the spectrum utilisation in the dynamic elastic optical network, we present a load and nonlinear impairments aware resource allocation algorithm, known as NARA algorithm. NARA searches for K-least congested routing paths for each traffic demand while using the proposed hybrid nonlinearity model as the nonlinear impairments model for the quality of service evaluation. The sub-algorithm is shown as KLC with HN. The KLC with HN algorithm assigns the first available frequency slots to the dynamic traffic requests. Similar to congestion-aware routing in [107], the weight W_j of the link j in the KLC with HN is expressed as:

$$W_j = \frac{N_{span,j}}{1 - \frac{Fs_j^{oc}}{F}} \tag{6.1}$$

where $N_{span,j}$ is the span number of j_{th} link, F is the number of frequency slots shown in chapter 4 and Fs_j^{oc} is the number of allocated frequency slots of j_{th} optical link .

For the dynamic traffic request, we assume that each service request R consists of bit-rate demand r bps from source node S to destination node D with a certain time of arrival interval

and a certain amount of holding time. We define the concept of network state (*NS*) used for computation in the algorithm, which includes link loading states, the weight of each optical link and spectrum allocation condition in the optical network.

Algorithm 5 :NARA Algorithm

Input: Service request, network states *NS*.
Output: RMSA solution for the request.
for request R_i **do**
    Invoke KLC with HN algorithm as shown in 6 for R_i;
    Reconfigure blocked services using the KLC with HN algorithm according to their provisioning order in case inter-channel blocking occurs;
    if configuration of R_i and reconfiguration of all blocked services (if necessary) are successful **then**
        AcceptR_i and the reconfiguration of blocked services;
        Update network states;
    else
        Reject request R_i;
    end if
    Release the connections and their corresponding spectrum resources when service expired;
end for

To provision each lightpath request, the proposed NARA algorithm shown as in algorithm 5 computes the RMSA solution using proposed KLC with HN algorithm shown as algorithm 6. NARA algorithm considers the increasing nonlinear impairments effects of the new lightpaths provisioning on the existing lightpaths if the link loading states of the chosen candidate routing path alter. When link loading states vary and the SNR of provisioned lightpaths fall below the threshold of assigned modulation format, inter-channel blocking occurs. NARA algorithm will then reconfigure the affected services using the KLC with HN algorithm. However, the reconfigured lightpath may also result in inter-channel blocking problem. In this case, the NARA algorithm will choose the one path among the K candidate paths that do not trigger the further blocking. If all the K candidate paths are infeasible, we reject the service request thus it can avoid complex reconfiguration loops. As 5 loading states are defined in this chapter for each link, a few numbers of service reconfiguration are needed.

Only when all the blocked lightpaths are reconfigured successfully, the new lightpath demand R_i can be finally provisioned to the network.

Algorithm 6 KLC with HN Algorithm

Input: Request R_i, network states NS.
Output: RMSA solution for request R_i.
Find K least congested paths $P_{k,i}$ for r_i using graph edge weight given in equation 6.1, (k = 1,2, ...,K);
for each candidate path $P_{k,i}$ **do**
    for $MF_{k,i} = M$; $MF_{k,i} > 1$; $MF_{k,i}$ - -; **do**
        Search for first-fit spectrum resources $SR_{k,i}$ with modulation format $MF_{k,i}$ that can satisfy traffic demand of r_i;
        Calculate estimated $SNR_{k,i}$ based on the proposed hybrid nonlinearity model;
        if Calculated SNR *geq* $SNR_{MF_{k,i}}$ **then**
            Record $P_{k,i}$, $MF_{k,i}$ and $SR_{k,i}$;
            Calculate the cost of path $P_{k,i}$ according to equation 5.3;
        end if
    end for
    if no spectrum resource available for path $P_{k,i}$ **then**
        Set the cost of path $P_{k,i}$ to be ∞;
    end if
end for
if Minimum cost of K paths not ∞ **then**
    choose the minimum cost path;
else
    Reject the request R_i;
end if

As indicated in the KLC with HN scheme 6, K candidate paths are computed between S_i and D_i based on the NS for lightpath with bit-rate demand of R_i. Further, for each calculated path $P_{k,i}$, we start with assigning the highest modulation format level M. The algorithm search for the first-fit spectrum resource $SR_{k,i}$ for modulation $MF_{k,i}$ to accommodate the request with bit rate demand of r_i. Then we calculate $SNR_{k,i}$ according to the proposed hybrid nonlinearity model. Then the optimal modulation format $MF_{k,i}$ is selected to reduce the number of allocated frequency slots as well as maximising the SNR margin for higher NLI tolerance. The first available continuous frequency slots along the routing path $SR_{k,i}$ is then temporally assigned to the lightpaths.

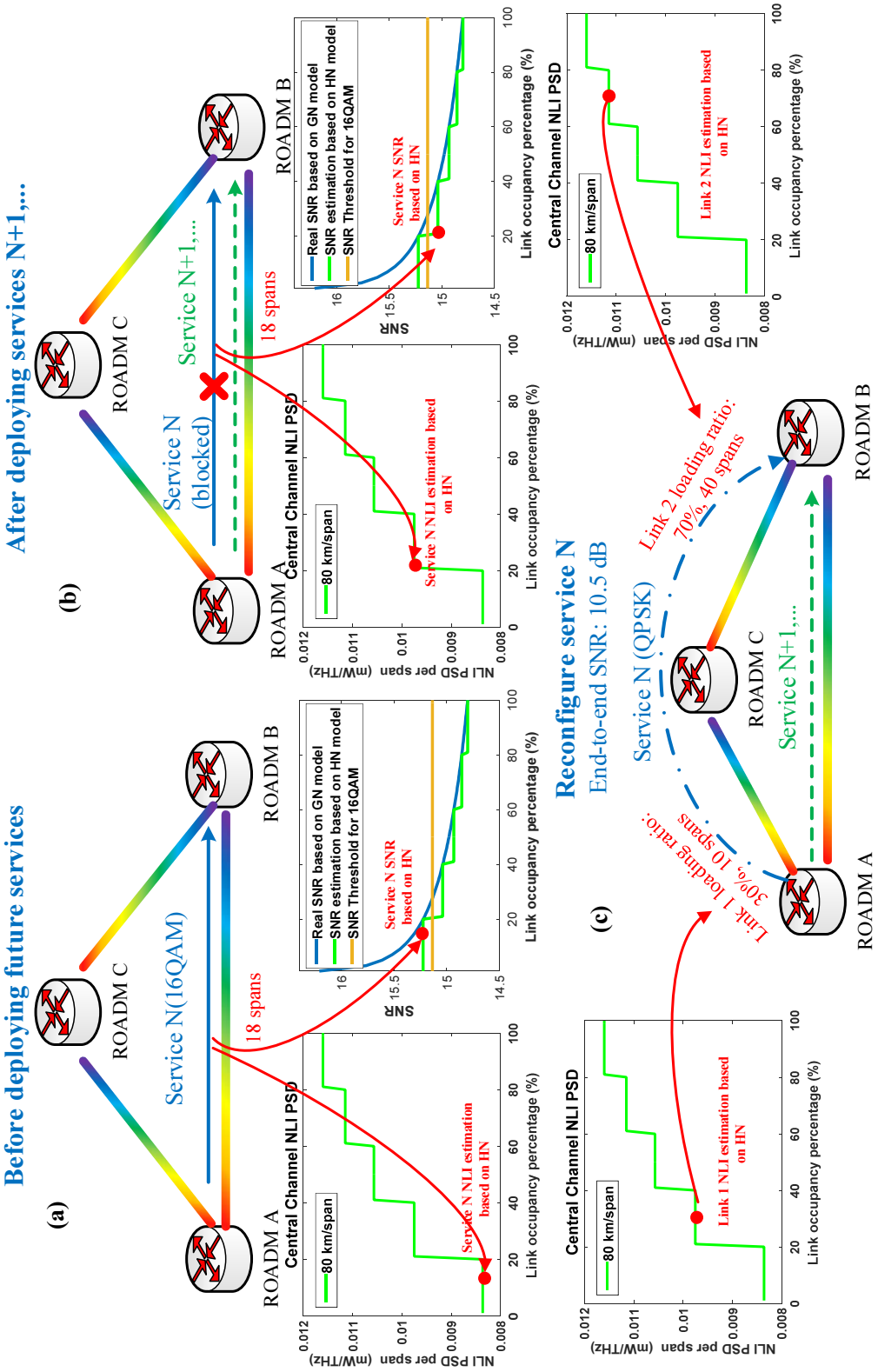

Fig. 6.3 A showcase example of service reconfiguration of using proposed NARA algorithm.

Figure 6.3 shows the lightpath reconfiguration process according to the proposed NARA scheme. As depicted in figure 6.3 (a), connection request *N* is provisioned on the link A-B with 15% resource occupied. The link load state, in this case, is 1 according to the hybrid nonlinearity model. As a result, the NLI PSD of the central channel of this link is 0.0084 mW/THz per span based on the hybrid nonlinearity model which indicates the SNR to be 15.22dB for connection *N*. Service *N* is able to transmit a 16QAM signal from A to B as shown in the figure. In figure 6.3 (b), when more lightpaths are established on that link A-B, the link loading states varies which triggers the NARA algorithm to examine if any established lightpaths using the same link are blocked due to the increasing amount of nonlinear impairments. In this case, lightpath *N* cannot adopt 16QAM as modulation format thus it needs to be reconfigured. The NARA algorithm calculates a new path A-C-B, as shown in figure 6.3 (c) and determines the NLI for each link along the selected path according to their respective loading state. The SNR of the lightpath is then derived as per equation 4.1 and 4.2 in chapter 4..

6.3.2 Simulation and Performance Evaluation

In this section, we discuss the evaluation approach for the NARA algorithm and the simulation setup. We compare the performance of the NARA algorithm with the benchmark method that uses physically shortest-path routing algorithm with 2dB reference margin accounting for the impact of NLI (known as benchmark shown below) and the one using the exact NLI information. The reconfiguration is not needed for the benchmark solution as nonlinear impairments are assumed to be the worst case while for the algorithms using the exact NLI, we do not consider the service replanning. For NARA algorithm, the *K* is set to 5 for selecting the candidate paths. The cumulative blocking ratio of requests and network spectrum utilisation are evaluated in this work. In this chapter, we use Matlab as the simulation tool to evaluate the proposed RMSA scheme against the benchmark.

In the simulation setup, we consider that the network operates in the 5THz bandwidth of C-band and 12.5 GHz granularity as per ITU–T G.694.1 v2.0 [79] corresponding to 400 frequency slots. Multiple continuous frequency slots can form a wide bandwidth channel as one of the features in EON. We use the same set of fibre parameters as presented in chapter 5. The pre-FEC BER is set to be 3.8×10^{-3} while the required SNR for different modulation formats to achieve this pre-FEC BER is the same as shown in table 2.2. The colourless, directionless and contentionless, bandwidth-variable reconfigurable optical add-drop multiplexer is assumed with an insertion loss of 7.25 dB.

In the simulation, the NSF topology is evaluated as shown in figure 5.2. Each lightpath request consists of a randomly selected pair of nodes as source and destination with symmetric bi-directional bit rate requirement, which includes the FEC overhead. 2 types of traffic requests are evaluated: 1) single line-rate 100 Gbps request and 2) mixed line-rate requests with 10% of them being 400 Gbps, 40% being 100 Gbps, 30% being 40 Gbps and 20% being 10 Gbps to study the effects of different bandwidth granularity requirements.

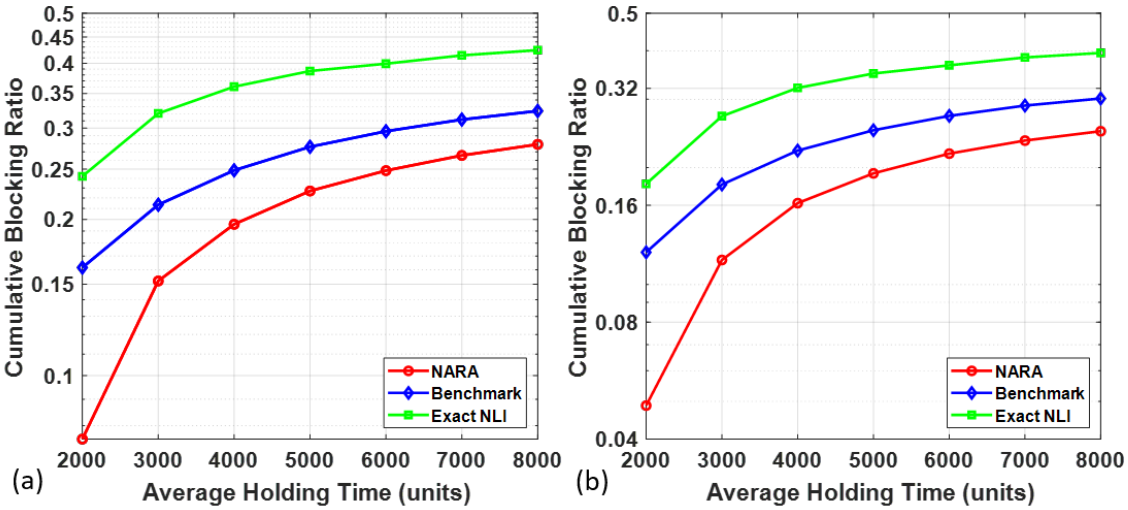

Fig. 6.4 Cumulative blocking ratio of traffic with different holding time. (a): 100 Gbps request. (b): mixed line-rate request

The arrival interval time between connection requests is assumed to follow the Poisson distribution and the holding time of the request is assumed to be exponentially distributed. We vary both average interval time of arrival and the average requests holding time to evaluate different traffic patterns. For each traffic pattern, 10000 connection requests are randomly generated. The dynamic traffic requests are established according to their arrival time and the lightpaths are tear down when expiring. In this case, the cumulative blocking ratio is evaluated and compared with each traffic pattern. The simulation is repeated 1000 times for each traffic pattern to obtain statistically relevant results of both proposed RMSA scheme and benchmark solution.

In figure 6.4, it shows the cumulative blocking probability for traffic requests with different amount of holding times. We set the average request interval time to be 1 time unit while the average holding time is varied from 2000 time units to 8000 time units with 1000 time units increments for each case. From the figure, the proposed NARA scheme achieves 5% - 15% higher connection request acceptance ratio compared to the benchmark solution for a different amount of service holding times. It also shows the around 12% - 22% lower service blocking ratio than the RMSA using the exact NLI information given by the original GN model. The lower blocking probability of the proposed solution yields 15 Tbps - 45 Tbps network capacity compared to benchmark solution and 36 Tbps - 66 Tbps capacity compared to using the exact NLI information. As the average holding time increases, the blocking ratio increases as services with less average holding time expire earlier which leaves more available frequency slots for other requests. It also can be observed that the proposed NARA algorithm performs better in case of shorter average holding times compared to longer holding time under both traffic scenarios.

To evaluate the effect of interval time, the average holding time is set to be 8000 time units and the interval time of arrival connection requests is set from 1 time unit to 6 time units. Figure 6.5 depicts that the proposed NARA scheme experiences 5-10% less blocking

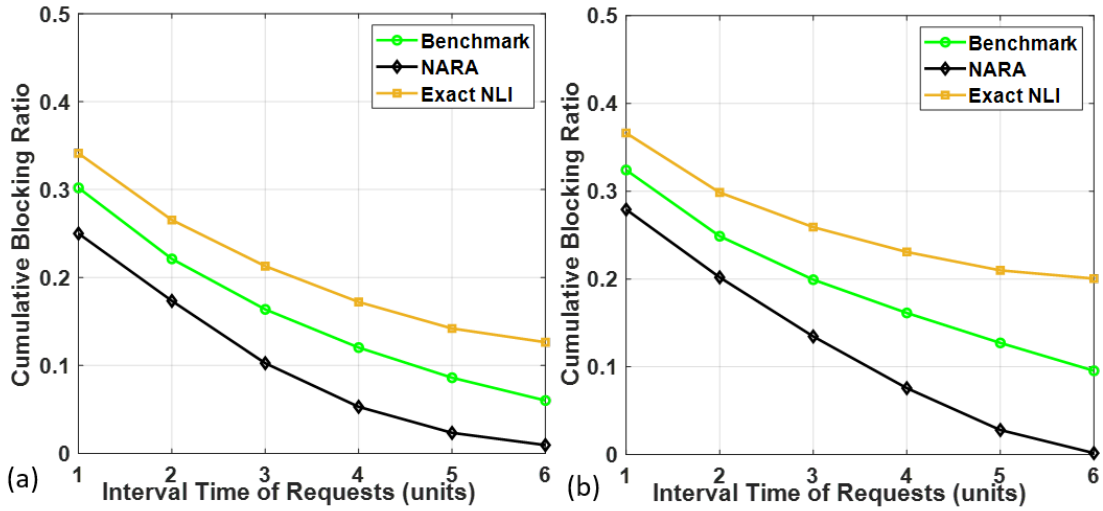

Fig. 6.5 Cumulative blocking ratio of traffic with different interval of arrival time. (a): mixed line-rate request. (b): 100 Gbps request

ratio compared to the benchmark method and 10 - 18% less blocking ratio compared to using exact NLI for single line-rate 100 Gbps request. The benefit of the algorithm in terms of blocking ratio increases as the requests interval time increases. Similar to the case with different service holding time, it happens because, with shorter average interval time, more requests need to be established in the network within a fixed range of time, which leads to more congested network. Therefore, when the network becomes highly congested, fewer requests can successfully be provisioned even with the NARA algorithm. On the other hand, fewer spectrum resources are required within the same amount of time when the average interval time increases, due to fewer demands of bandwidth. It results in a less congested network and therefore higher request acceptance ratio is achieved with the proposed NARA RMSA scheme. When comparing to the RMSA using the exact NLI from the original GN model, it requires fewer service replanning number, thus making the spectrum highly fragmental. Moreover, the inter-channel blocking problem mentioned earlier limits the number of lightpaths to be provisioned. From the figure, the blocking ratio is approximate 0 using NARA RMSA scheme when the interval time of requests is 6 whereas

the benchmark method suffers 10% service blocking probability. For mixed line-rate traffic requests, the NARA algorithm achieves approximately 5% improvement over the benchmark solution and 10% over the RMSA using the exact NLI information for all interval time. The proposed NARA solution is able to achieve maximally 60 Tbps and 31 Tbps network throughput compared with the reference margin benchmark and using the original GN model respectively for 100 Gbps traffic requests. Similarly, it achieves 45 Tbps and 22 Tbps over two baseline RMSA schemes for the mixed traffic requests.

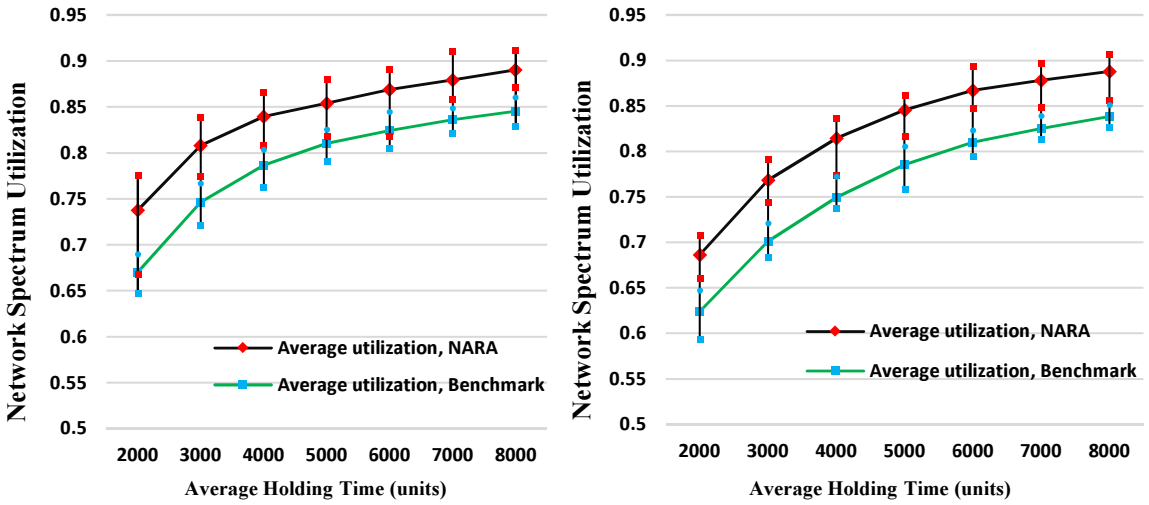

Fig. 6.6 Average network spectrum utilization of different holding time. (a): 100 Gbps request. (b): mixed line-rate request

Figure 6.6 depicts the average spectrum utilisation ratio in the optical network using the proposed NARA scheme and the benchmark method for various requests average holding time. The maximum and minimum spectrum utilisation for each scenario is also shown with the results of all a thousand instances of the traffic patterns. The spectrum utilisation in the network (NU) evaluated is expressed as:

$$NU = \frac{\sum_l F s_j^{oc}}{F \cdot NL} \tag{6.2}$$

where NL is the number of links in the network. The NU in equation 6.2 is the ratio of the number of allocated frequency slots in the network over the overall number of slots.

The NARA algorithm can yield 4.5% - 6.7% higher spectrum utilisation in the network at the point of the 10000 requests compared to the benchmark method for single line-rate 100 Gbps requests. For the mixed line-rate traffic, 4.9% to 6.2% higher spectrum utilisation can be achieved for the proposed algorithm achieves with different holding times. The higher spectrum utilisation in NARA is primarily due to the use of the proposed hybrid nonlinearity model for more accurate nonlinear impairments estimation but also the proposed K-least congested path routing makes better path selection to yield the better traffic engineering as well.

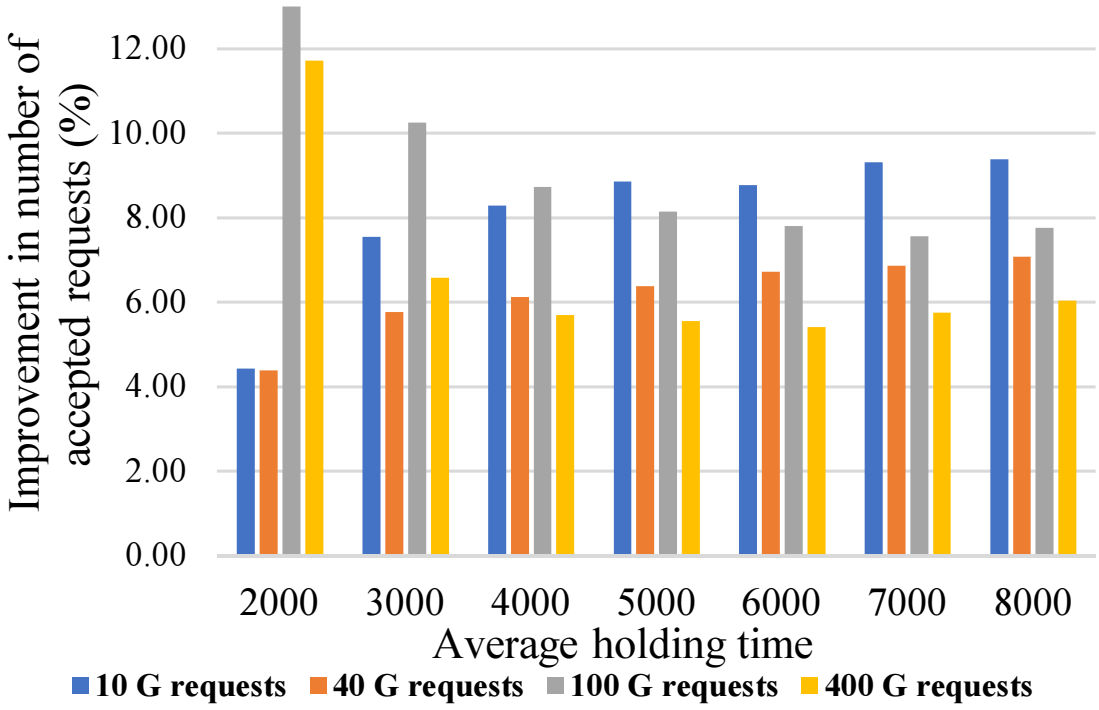

Fig. 6.7 Accepted traffic improvement for NARA compared to benchmark for mixed line-rate request.

The improvement in the number of accepted requests for the NARA scheme over the benchmark solution for the mixed line-rate requests is depicted in figure 6.7. The graph

demonstrates that at least 5% more requests can be achieved for all traffic patterns. In case of smaller service holding time, the improvement in larger traffic requests (100 Gbps and 400 Gbps) is 11% - 13% higher as the NARA solution is able to serve more requests which require more continuous frequency slots compared to the benchmark. As the average holding time increases, the optical network becomes highly congested thus reducing the amount of available continuous frequency slots in the network. As a result, large bandwidth requests that require more continuous frequency slots become more difficult to provision compared to small bandwidth requests. This effect is also evident from figure 6.7 where the NARA solution favours the small bandwidth traffic requests (10 Gbps and 40 Gbps) over large bandwidth requests and achieves 7% - 9% improvement in the acceptance of small traffic requests.

6.4 Traffic Grooming Technique for Nonlinear Elastic Optical Networks

The significant challenge faced by service providers is to support the exponential growth of dynamic traffic towards access, metro as well as core networks. Traffic grooming scheme was proposed to aggregate amount of small traffic streams into a large group unit in optical networks The traffic grooming technique enables high capacity transmission thus results in network throughput improvement. In this section, we propose a novel routing, modulation format and spectrum assignment scheme combined with traffic grooming technique for the elastic optical networks operating in the nonlinear regime.

In this chapter, we also consider the NLI noise and ASE noise are the dominant impairments in the network. The modulation format level is chosen from DP-BPSK, DP-QPSK, QP-8QAM, DP-16QAM, DP-32QAM and DP-64QAM to achieve 3.8×10^{-3} pre-FEC bit error rate.

6.4.1 RMSA algorithm with Traffic Grooming

We assume that each request R consists of bi-direction bit-rate demand r from source s to destination d, sequentially loaded into the network. A least congested path P is calculated. According to the path P, the average link loading condition lc is written as:

$$lc = \sum_{l=1}^{NL} \frac{W_j}{NL} \tag{6.3}$$

where NL is the number of optical links along the selected path P and W_j is congestion weight of link j along the path P. The concept of lc is the average value of link loading states of selected path and it is implemented in the proposed traffic grooming algorithm, as shown in algorithm 7.

Algorithm 7 Traffic Grooming Algorithm

1: **Input:** Request R_i, network states NS.
2: **Output:** RMSA solution for request R_i.
3: Find a least congested paths P_i for r_i from source s_i to destination d_i;
4: Calculate average link loading condition lc_i according to equation 6.3 and the selected path P_i;
5: **if** $lc_i \leq sthd$ **then**
6: Execute **Strategy 1**;
7: **else**
8: Execute **Strategy 2**;
9: **end if**

The algorithm begins with computing the least congested path between the source and destination for the traffic demand. Then the average loading condition of the computed path is calculated using equation 6.3. When the average loading condition of the path lc is smaller than or equal to the pre-set threshold $sthd$, the algorithm will invoke **Strategy 1** to allocate resource to the connection request. In case that the average loading condition $lc > sthd$, the **Strategy 2** is executed.

The **Strategy 1** shown in 8 is also named as the '*new lightpath first*'. It aims to establish new lightpath when the calculated path of the main algorithm 7 is not congested as the

Algorithm 8 Traffic Grooming Strategy 1

Input: Request R_i, network states NS, calculated path P_i.
Output: RMSA solution for request R_i.
for modulation format MF_i = DP-BPSK to DP-64QAM **do**
    Calculate required number of spectrum slots sr_i for request r_i with modulation format MF_i;
    Find sr_i free contiguous frequency slots along the path P_i using first-fit assignment;
    if spectrum slots available **then**
        Denote slots' index as $F_i = [f_i, ..., f_i + sr_i - 1]$;
        Calculate the SNR_i according to assigned slots in F_i;
        if $SNR_i \geq SNR$ threshold for modulation format MF_i **then**
            Accept the request and set up a new lightpath for r_i;
            Record the highest available modulation format and maximum capacity of the new lightpath;
            Break for;
        end if
    end if
end for
if no spectrum slots available along the path or QoT fails **then**
    if any active lightpath between source s_i and destination d_i **then**
        Denote the active lightpath as $ALP_i = [lp_1, ..., lp_q]$;
        for $j = 1 : q$ **do**
            if remaining capacity (maximum possible capacity - current capacity) of lightpath lp_j can accommodate r_i **then**
                Accept Request R_i;
                Upgrade modulation format of lp_j for request R_i;
                Update the remaining/current capacity of lightpath lp_i;
                Break for;
            end if
        end for
    end if
end if

average loading condition is below certain level $sthd$. In this case, **Strategy 1** searches for the first finds spectrum slots F_i for the connection request R_i when assigning modulation format MF_i (from DP-BPSK to DP-64QAM). We start from the lowest modulation format DP-BPSK as it gives the maximum potential capacity. In this case, a huge bulk of continuous and contiguous spectrum will be allocated. The large bulk of spectrum is actually to reserve the capacity with modulation format upgrade to accommodate more requests in case no spectrum can be found in the future when the network is highly congested. It starts with the largest spectrum 'bulk' of using DP-BPSK. When no spectrum available for DP-BPSK, it starts to search for a smaller spectrum 'bulk' with DB-QPSK to accommodate the requests and then DB-8QAM...

If the spectrum slots are available, then the ASE and NLI PSD are calculated. We compute the SNR to check whether it satisfies the SNR requirement for modulation format MF_i. The service request is accepted, the maximum capacity with its highest available modulation format of the new lightpath is recorded when it meets the SNR requirement.

In case of no contiguous spectrum resources available or quality of transmission (QoT) constraint cannot be satisfied, **Strategy 1** checks if any active lightpath between the source s_i and destination d_i has enough SNR margin to upgrade its modulation format level to allow the new request r_i groomed into the existing lightpath. When there is existing lightpath has the potential SNR margin to accommodate new requests, the request will be accepted and corresponding information such as lightpath remaining capacity, which equal to (maximum possible capacity - current capacity).

The **Strategy 2** shown in 9 is named as the '*Grooming first*'. The traffic grooming main algorithm invokes **Strategy 2** when the average loading condition lc is higher than the pre-set threshold of $sthd$. This is because when the network is heavily loaded, to find contiguous and continuous spectrum becomes difficult. In contrast to **Strategy 1**, **Strategy 2** first examine if any existing lightpath of the same source and destination with the request

Algorithm 9 Traffic Grooming Strategy 2

Input: Request R_i, network states NS, calculated path P_i.
Output: RMSA solution for request R_i.
if any active lightpath between source s_i and destination d_i **then**
    Denote the active lightpath as $ALP_i = [lp_1, ..., lp_q]$;
    for $j = 1 : q$ **do**
        if remaining capacity (maximum possible capacity - current capacity) of lightpath lp_j can accommodate r_i **then**
            Accept Request R_i;
            Upgrade modulation format of lp_j for request R_i;
            Update the remaining/current capacity of lightpath lp_i;
            Break for;
        end if
    end for
else if no active lightpath between s_i and d_i or failure of R_i grooming to existing lightpath **then**
    for modulation format MF_i = DP-BPSK to DP-64QAM **do**
        Calculate required number of spectrum slots sr_i for request r_i with modulation format MF_i;
        Find sr_i free contiguous frequency slots along the path P_i using first-fit assignment;
        if spectrum slots available **then**
            Denote slots' index as $F_i = [f_i, ..., f_i + sr_i - 1]$;
            Calculate the SNR_i according to assigned slots in F_i;
            if $SNR_i \geq SNR$ threshold for modulation format MF_i **then**
                Accept the request and set up a new lightpath for r_i;
                Record the highest available modulation format and maximum capacity of the new lightpath;
                Break for;
            end if
        end if
    end for
end if

R_i has enough remaining capacity to support the bit rate demand r_i. The service will be accepted and aggregated into existing lightpath when traffic grooming is possible. In the case of grooming failure, **Strategy 2** will calculate a path and search for the spectrum resources for the requests.

The objective of the algorithm of using **Strategy 1** is able to establish lightpath with potential to upgrade modulation format level as the priority to accommodate more requests from large spectrum 'bulk' to small spectrum 'bulk' when network is not highly loaded. When the network becomes congested. **Strategy 2** aims to utilise these spectrum 'bulks' to release their capacity potential by upgrading the modulation level as the priority.

6.4.2 Simulation Results and Analysis

We examine the proposed solution with the following parameters and assumptions. The network is considered to operate in 5 THz C-band with 193.6 THz as central frequency. The 5 THz bandwidth is divided into 400 frequency slots in a single optical link with 12.5 GHz each. 7.5 dB insertion loss is assumed with the ROADM and the noise figure of EDFA is set to be 5 dB. We use NSFNET topology with 14 nodes and 21 links deploying single mode fibre for evaluation. The fibre span length is of 80 km and the SSMF parameters are the same as shown in previous chapters.

Bi-direction 100 Gbps traffic requests are assumed and generated between randomly selected pairs of nodes while the bit-rate requests contain FEC overhead in this work. We randomly generate 3000 service requests, incrementally provision them into the networks. To build the statistic results, the process is repeated 1000 times. To make a fair comparison, the same set of traffic requests are repeated for all the benchmark scenarios. In this work, we choose 2 benchmark method as the baseline. The benchmark 1 [107] is a non-traffic grooming RMSA strategy using the least congested path routing technique and the first-fit spectrum assignment while the benchmark 2 [152] is a traffic grooming enabled algorithm.

We set the pre-set threshold *sthd* factor as 0.4 for our proposed traffic-grooming enabled RMSA scheme.

Figure 6.8 shows the network blocking ratio of the proposed traffic-grooming enabled RMSA scheme and 2 benchmark methods against the increasing number of traffic requests for signal power spectral density of 19 mW/THz. It indicates the proposed traffic-grooming RMSA scheme achieve higher service acceptance ratio compared to 2 benchmark method. From the figure, it can be observed that the proposed algorithm can accept approximate 100 and 300 more requests respectively compared to benchmark 1 and benchmark 2.

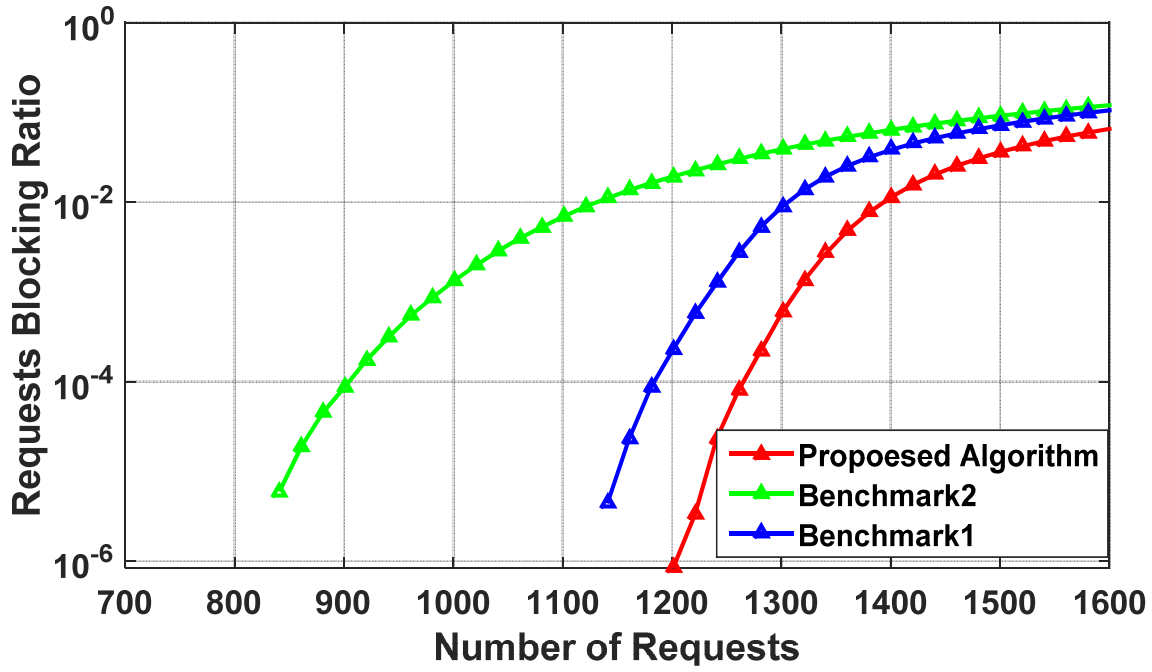

Fig. 6.8 Service blocking ratio versus number of requests.

In figure 6.9, we show the average number of transponders required for each algorithm over the increasing network traffic load. The proposed traffic-grooming enabled algorithm can save up to 50% transponders compared to using benchmark 1. The numbers of required transponders in both benchmarks grows linearly with increasing overall throughput in the network. As benchmark 2 is a traffic-grooming enabled method, its first target is to groom

the new bandwidth request into the existing lightpath. Therefore, it can significantly reduce the number of transponders.

when the network is less congested with a fewer number of lightpath provisioned, the number of transponders that the proposed scheme and benchmark 1 require is similar. However. when the network becomes more congested, the increasing number of required transponders for the proposed algorithm gradually drop down. Therefore, the numbers of transponders needed for the proposed algorithm and benchmark 2 are approaching. Although the benchmark 2 method needs slightly fewer number of transponders, it experiences a significantly higher network blocking ratio as depicted in figure 6.8.

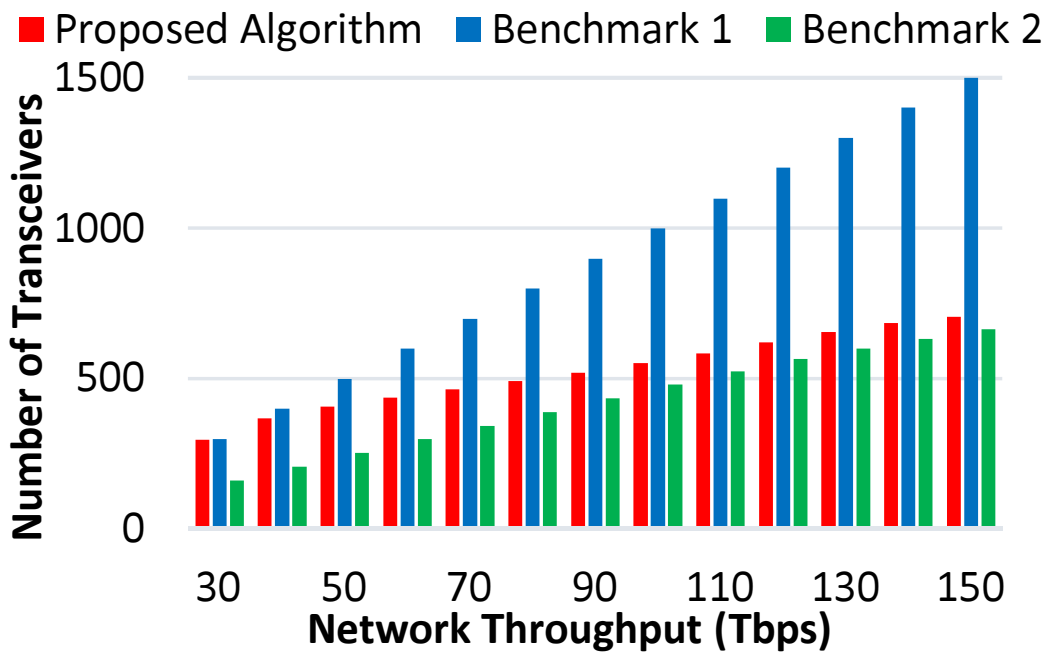

Fig. 6.9 Number of transceivers versus increasing network load (PSD: 19 mW/THz).

Figure 6.10 shows the overall network capacity at 1% network blocking probability against the increasing signal PSD for the proposed traffic-grooming enable RMSA scheme and 2 benchmark solutions. For all 3 algorithms, the network capacity increases as the signal PSD increases from 10 mW/THz to 19 mW/THz. However, the network capacity drops down gradually as the signal PSD continuously raises higher than 19 mW/THz. The graph

indicates 19 mW/THz yields the highest network capacity and it is optimal signal PSD for the 3 RMSA schemes. When signal PSD is 19 mW/THz, the proposed solution achieves 7% and 26% more capacity compared to benchmark 1 and benchmark 2 respectively.

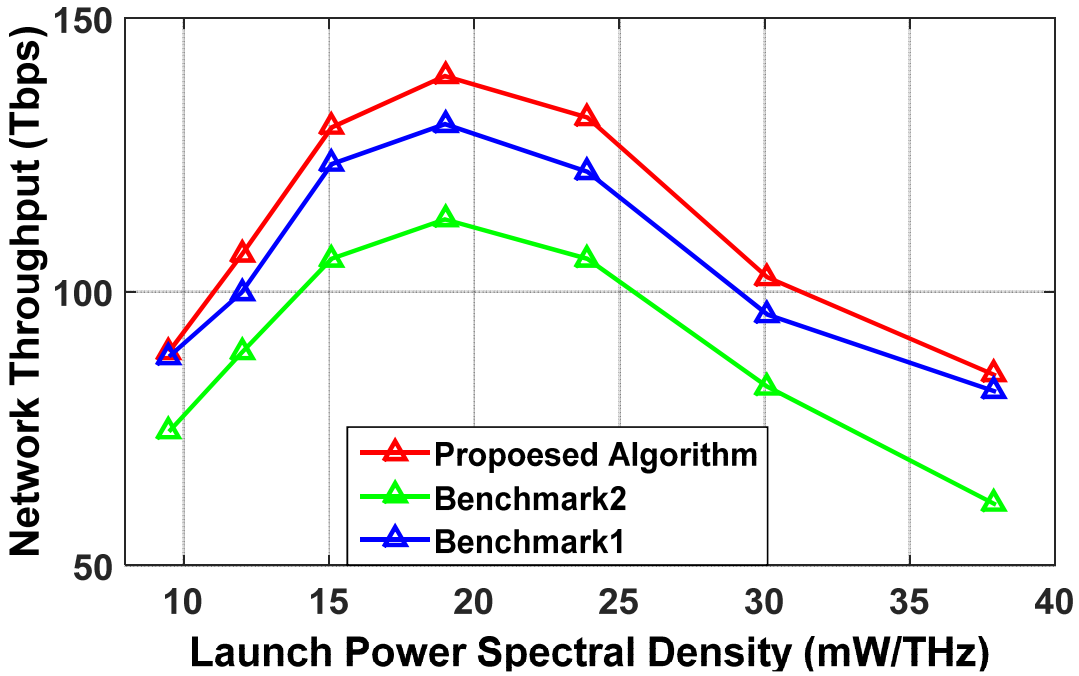

Fig. 6.10 Network throughput at 1% blocking probability versus increasing PSD.

6.5 Summary

In this chapter, we have shown the effect of inter-channel blocking due to using accurate NLI information. Based on the proposed hybrid nonlinearity model in the previous chapter, we further proposed a nonlinearity-aware resource allocation algorithm proposed with a sophisticated K-least congested path routing strategy for the dynamic traffic scenarios. The proposed NARA algorithm is compared with a benchmark solution using extensive simulation studies for different traffic models. The results show that the NARA algorithm significantly improves service acceptance ratio and network spectrum utilization which makes it appropriate for elastic optical network planning and operation.

According to the hybrid nonlinearity model in terms of loading states of link, we define the concept of loading condition of a path. The loading condition concept is then integrated into the proposed traffic grooming enabled routing, modulation format and spectrum assignment algorithm. Through an extensive simulation study, the proposed scheme outperforms two benchmark methods in the paper. We also show the tremendous number of transceivers saving over non-traffic grooming benchmark solution and significantly better service acceptance ratio over traffic grooming benchmark solution at the cost of utilizing only 6% more transceivers. The results verify the benefits of the proposed traffic grooming solution with different PSD values.

Chapter 7

Load-Aware Power Optimisation

7.1 Introduction

It is important to accurately model, monitor and manage the impairments in the future optical networks to meet the requirement of providing flexible, high bandwidth demands. Apart from impairments from optical links, it is also a great challenge to manage the impairments generated by reconfigurable optical add-drop multiplexers (ROADMs), due to the requirement of additional amplifiers to compensate the insertion loss. In current optical networks, optical signal with a constant power is launched across multiple fibre spans and ROADMs, where any power loss is completely compensated by the amplifiers. The traditional approach cannot efficiently manage the impairments as it neglects the characteristics of different spans and ROADMs, such as fibre type, span length, loading condition due to add-drop, noise figure (NF) of amplifiers and insertion loss, making it an inefficient use of the network. In the context of software-defined networking, the power of each span and ROADM can be dynamically optimised according to network status to improve network throughput. Therefore, in this chapter, we proposed a coordinated fibre span and ROADM input power optimisation strategy to minimize the SNR degradation of nonlinearity and ASE noise in the coherent optical network. The benefit of the proposed model is verified through experiment

and the simulation. The idea of this chapter is presented at the 2018 European Conference on Optical Communication in Rome [159].

7.2 Power Optimisation Model

It is well known that optical networks consist of optical links and optical nodes. Launching signal in optical network can cause impairments from optical links and optical nodes, such as ROADM. The impairments from optical links and ROADM pose significant challenges to the optical systems and networks, which affect the signal BER reach distance and the network capacity. ASE noise and NLI are the dominant impairments in optical network deployed with coherent transmission. Therefore, end-to-end SNR of a lightpath can be expressed as:

$$SNR = \Bigg(\sum_{n}^{N_{rd}} \Big(\frac{P^{rd}}{h\nu B \cdot 10^{\frac{NF_n^{rd}}{10}} \cdot IL_n} \Big)^{-1} + \sum_{i}^{N_{sp}} \Big(\frac{P^{i}}{h\nu B \cdot 10^{\frac{NF_i}{10}} \cdot LO_i + P_i^3 \cdot \chi_i} \Big)^{-1} + SNR_{TRx,b2b}^{-1} \Bigg)^{-1} \tag{7.1}$$

The first part $\sum_{n}^{N_{rd}} \Big(\frac{P^{rd}}{h\nu B \cdot 10^{\frac{NF_n^{rd}}{10}} \cdot IL_n} \Big)^{-1}$ on the right side of equation 7.1 represents the SNR degradation from post-amplifiers compensate the power loss of ROADM insertion loss. P^{rd} is the per channel input power of the ROADM, NF_n^{rd} is the noise figure as the post-amplifier of ROADM n, IL_n is the insertion loss of ROADM n and N_{rd} is the number of ROADM along the lightpath.

The second part on the right side of equation $\sum_{i}^{N_{sp}} \Big(\frac{P^{i}}{h\nu B \cdot 10^{\frac{NF^{i}}{10}} \cdot LO_i + P_i^3 \cdot \chi_i} \Big)^{-1}$ indicates the SNR degradation of optical links due to in-line ASE noise and NLI, where P_i is the per channel power launched into fibre span i, h is the Planck constant, ν is the carrier frequency, NF_i is the noise figure of EDFA at the end of span i, LO_i is the power loss in dB of span i, χ_i is the nonlinearity coefficient determined by GN model and N_{sp} is the number of fibre span along the lightpath.

The third part on the right side of equation 7.1 $SNR^{-1}_{TRx,b2b}$ stands for the SNR degradation due to transponders quantified as the back-to-back transmission performance. As SNR degradation of transponder only depends on its own performance, we do not consider its optimisation due to the irrelevancy of the optimisation target. The parameters are shown in figure 7.1.

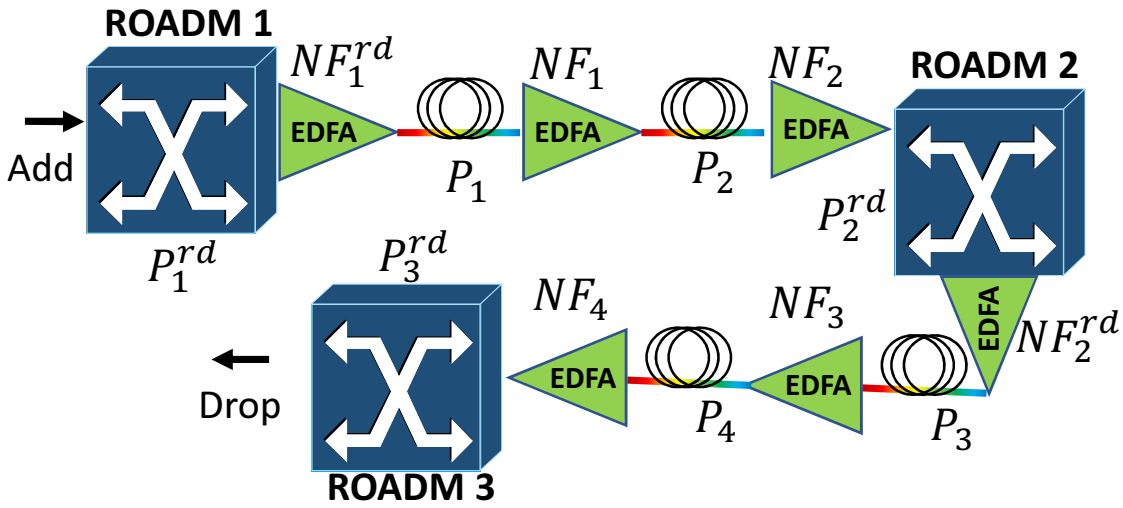

Fig. 7.1 A simple network with physical layer parameters.

In current optical networks, the optical signal is launched with a constant power across multiple fibre spans and the ROADMs. The power loss is completely compensated by distributed EDFAs to ensure the same level of power.

From equation 7.1, the SNR degradation due to compensating ROADM insertion loss decreases as the per channel input power of ROADM P_{rd} increases. Therefore, increasing the ROADM input power can help improve the end-to-end SNR performance of the lightpath. Therefore, the per channel power of the signal from different ports of the ROADM is amplified to an equal but high value of P_{rd}. This is to ensure the different lightpaths of the same power level before and after space-wavelength switching. The high power P_{rd} is then attenuated due to the ROADM insertion loss. Before launching into the following fibre span, post-amplifiers of ROADM re-amplify the signal to an optimal power level of the span afterwards.

Despite optical signal traversing through the ROADM operating in the linear regime, the NLI in the fibre spans grows cubically as the signal per channel power increases. As a result, there exists an optimum launch power for each span. From equation 7.1 above, the power of each fibre span can be optimized individually which is expressed as:

$$P_i = \sqrt[3]{\frac{h\nu B \cdot 10^{\frac{NF_i}{10}} \cdot LO_i}{2 \cdot \chi_i}} \tag{7.2}$$

From equation 7.2, it can be seen that the optimum power of each span does not only depend on its associated attenuation and the noise figure of the EDFA at the end of the span but also relies on the nonlinearity coefficient. In this work, we apply the load-aware nonlinearity coefficient which is calculated in chapter 4 to replace the individual nonlinearity coefficient of different channels. The optimum per channel launch power of each span is higher when the link is lightly loaded. The optimum power gradually reduces as the optical link becomes congested. Therefore, we optimise the per span channel power using the equation 7.2 by considering the noise figure of EDFA, fibre attenuation and the loading condition of each span. We also set the signal power launching into ROADM with a sufficiently high value according to EDFA capability to reduce the impact of the ROADMs insertion loss. This forms the theoretical foundation of this chapter.

7.3 Experimental Setup and Results Analysis

To validate the performance of the proposed power optimization strategy, we set up the field trial testbed, as shown in 7.2. The testbed consists of 2 optical links. In total 314 km fibre in the lab make up the 5 spans of the first link and 236 km UK National Dark Fibre Infrastructure Service (NDFIS) from University of Bristol and looped back from Froxfield forms the second optical links. Three WSSs in the trial experiment is to emulate the ROADM to add and drop optical signal. Apart from the insertion loss of the WSSs, additional 7 dB

loss is applied to emulate the loss of the ROADM in the network with 2 stages of WSSs for add/drop.

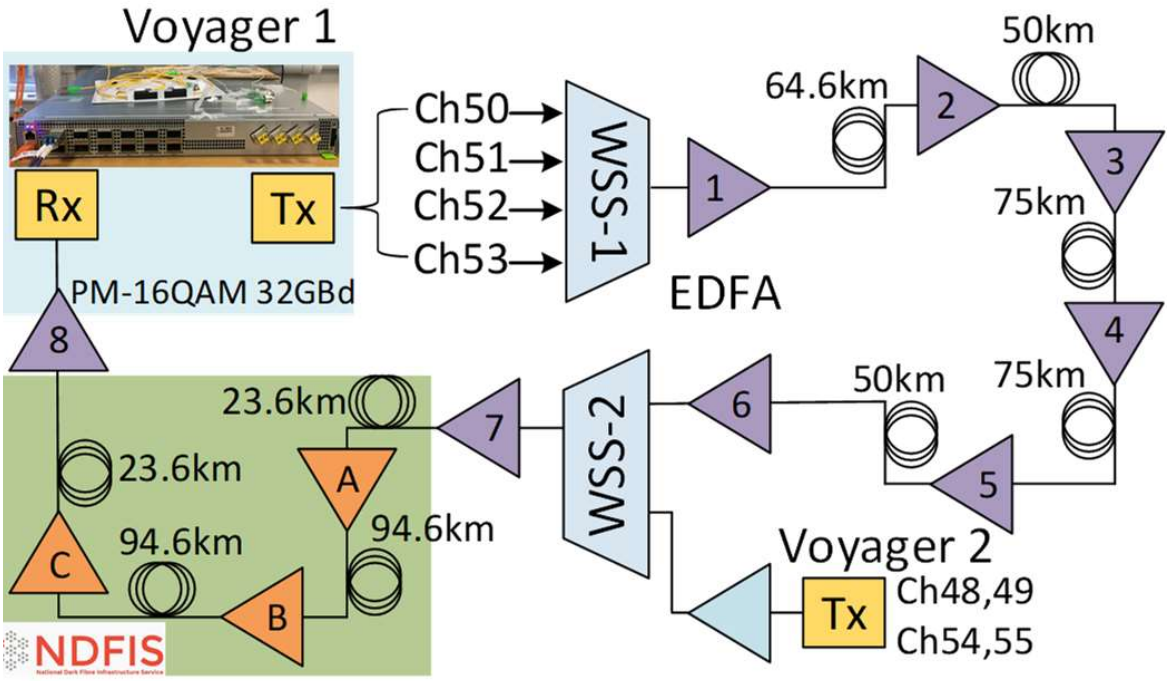

Fig. 7.2 Field trial experiment testbed.

Voyager switch is an optical white box, served as the coherent transponders in our experiments. In our scenario, the voyager switch is configured to use DP=16QAM as the modulation format with 25% FEC overhead. The signal pulse is shaped by a root raised cosine match filter with 0.3 roll-off factor.

Four 50 GHz spacing Nyquist shaped channels, namely Ch50 - Ch53 in the figure 7.2 with frequency 193.6 THz - 193.75 THz respectively, are launched into the first optical link through WSS1. Another four channels (Ch48, 49, 54, 55) are added to the second link through WSS2 to emulate diverse loading conditions of different links.

We first consider the case that each EDFA completely compensate the span loss and the WSS loss. Thus, the launch power of each channel into every fibre span and WSS is equivalent. The constant per channel launch power varies from -4 dBm to 5 dBm. The

pre-FEC bit error rate as a function of signal launch power of Ch51 and Ch52 is plotted in figure 7.3. The pre-FEC difference between two channels is due to the different performance of the two TRx of back-to-back transmission performance. From figure 7.3, it is observed that both channels achieve the lowest pre-FEC BER when the launch power is 0 dBm, which corresponds to 6.48 $\times 10^{-3}$ for Ch51 and 4.31 $\times 10^{-3}$ for Ch52.

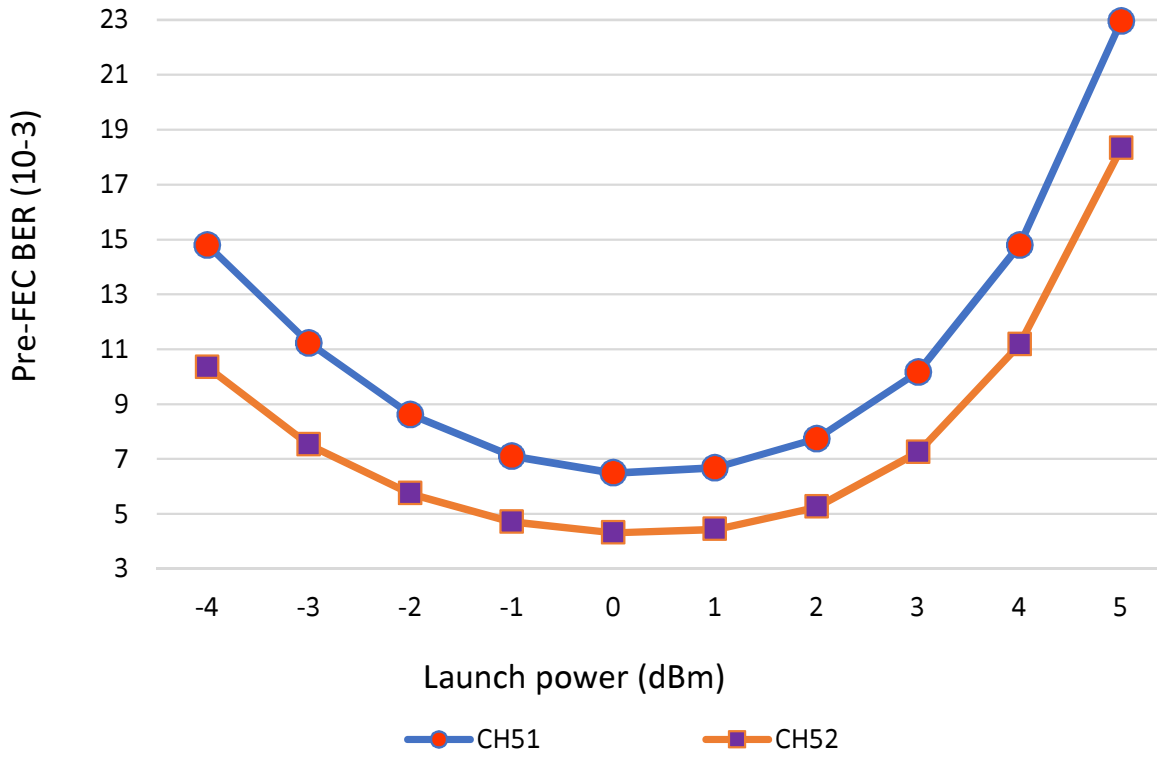

Fig. 7.3 The pre-FEC bit error rate of the benchmark against various per channel launch power.

The per channel launch power achieving the lowest pre-FEC bit error is regarded as the benchmark for the span power optimisation. We start the fibre span level power optimisation from the first span with 0 dBm as the per channel launch power across all the spans and the WSSs. At each step, the optimum power launched into the span is calculated based on equation 7.2. According to the equation, the optimal per channel launch power is related to the noise figure of the EDFA. However, the noise figure of EDFA may change with different levels of input power and different amplification gain. To solve this problem, we need to

measure the accurate noise figure while maintaining the power to be optimum. Therefore, we propose a span power optimization strategy shown in algorithm 10.

Algorithm 10 Per EDFA power optimisation flowchart

1: **for** span i = 1, 2, ... **do**
2: Determine the nonlinearity coefficient χ_i according to the loading condition of the span;
3: Set the noise figure of span i NF_i = 5 dB;
4: Calculate the optimum power P_i according to equation 7.2;
5: Adjust the gain of EDFA i of span i to make sure per channel output power $P_{out,i}$ == P_i;
6: Measure the EDFA noise figure $NF_{i,ms}$;
7: **if** $|NF_{i,ms} - NF_i| \leq 0.2$ dB **then**
8: Power Optimization competed;
9: $P_i^{optimum} = P_i$;
10: **else**
11: $NF_i = NF_{i,ms}$;
12: Repeat step 4 - 7;
13: **end if**
14: **end for**

For span i, the power P_i is calculated according to equation 7.2 assuming the noise figure NF_i of EDFA i to be 5 dB with corresponding load-aware NLI coefficient χ_i of the span. The calculated span power P_i is then applied to the network by adjusting the EDFA gain. In this case, we measure the noise figure of EDFA i and denote the measured value as $NF_{i,ms}$. The technique to measure the noise figure is shown in figure 7.4.

The parameter P^1_{ASE} and P^2_{ASE} stands for the average power of out band ASE noise after EDFA amplification and before EDFA amplification respectively. The noise figure is calculated as:

$$NF = 10log_{10}\left(\frac{P^1_{ASE}}{Gh\nu \cdot B} + \frac{1}{G} - \frac{P^2_{ASE}}{h\nu \cdot B}\right) \tag{7.3}$$

where G is the gain of the EDFA, h is the Planck constant, ν is the carrier frequency, B is the bandwidth of effective noise bandwidth or the resolution taken from the optical spectrum analyser.

We then compare the measured noise figure value $NF_{i,ms}$ with NF_i. The optimization for span i is completed when value of measured value of $NF_{i,ms}$ with assumed value NF_i converge to the same value, as shown in line 7 and 8 of algorithm 10. In case of convergence failure, the new assumed noise figure value is updated by setting $NF_i = NF_{i,ms}$. The new assumed noise figure is feed into equation 7.2 to calculate new optimal power and repeat the above steps. The process is repeated until the noise figure value converges and the optimum per channel launch power of span i is derived with the accurate noise figure of EDFA i.

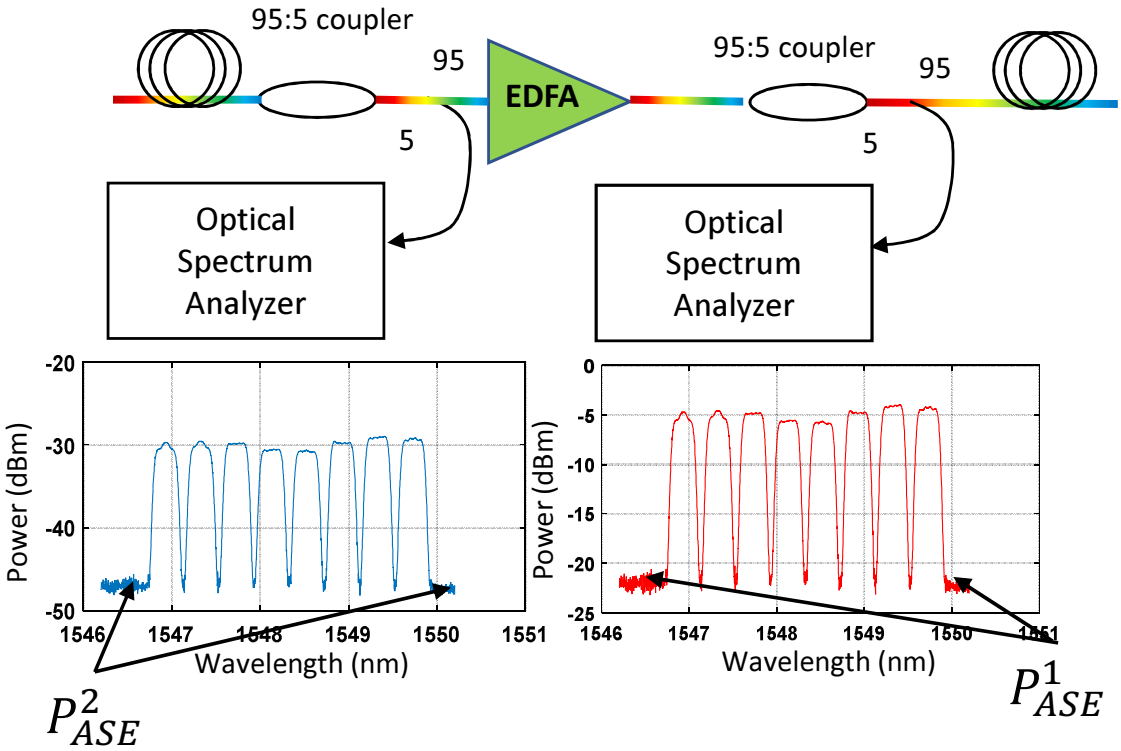

Fig. 7.4 EDFA noise figure measurement.

At each optimisation step, the per channel launch power of the corresponding span is optimised according to the algorithm described in 10, while the power of the following spans remains at 0 dBm as suggested according to benchmark solution. The pre-FEC bit error rate

of Ch51 and Ch52 against the optimisation step are shown in figure 7.5. The pre-FEC BER performance of Ch52 is associated with the left axis, the pre-FEC BER of Ch51 associated with the axis on the right. From figure 7.5, the pre-FEC BER of both channels reduces with the increasing steps of optimisation. The span power optimisation strategy can achieve around 1.1×10^{-3} pre-FEC BER reduction for both Ch52 and Ch51 when all the optimisation steps are conducted.

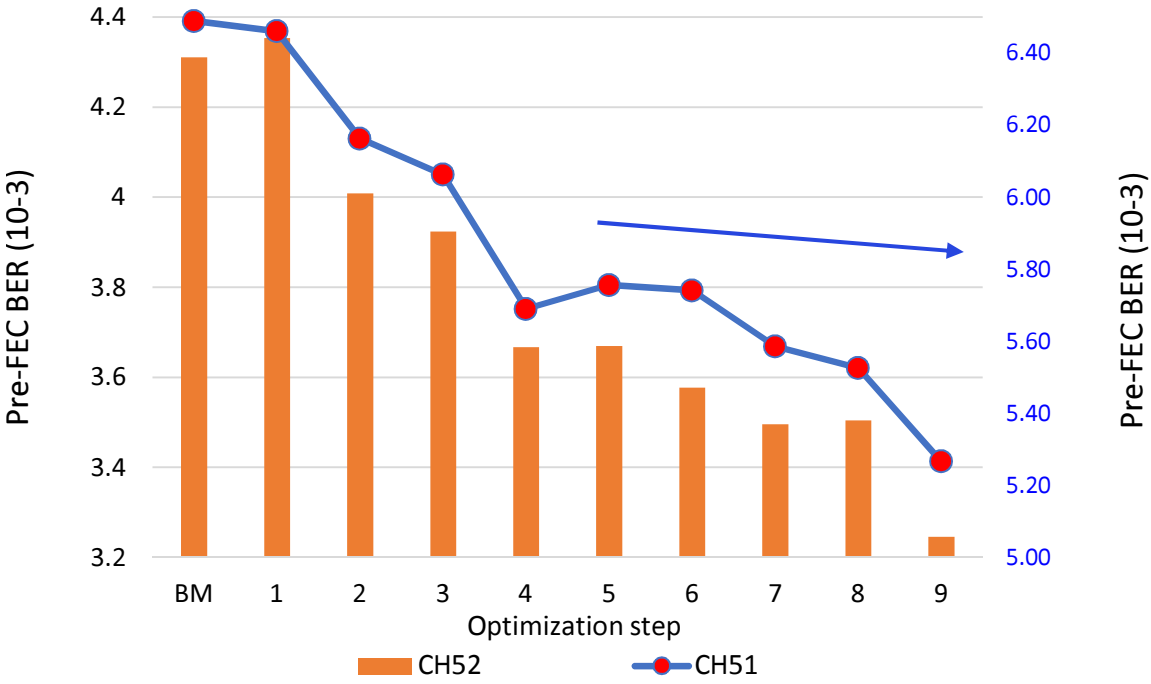

Fig. 7.5 Pre-FEC BER reduction versus fibre span level optimisation steps.

After the span level power optimisation, we further investigate the impact of the input power of the ROADM over the signal quality. As discussed in the previous section, the increasing output power of pre-amplifier (EDFA 6 in the testbed) will result in the SNR improvement. However, results in figure 7.6 indicate that the pre-FEC bit error rate of CH51 and CH52 do not reduce over the increasing per channel ROADM input power. It is because, with the increasing output power of pre-amplifier, the input power of post-amplifier also grows. This, in turn, decreases the gain of post-amplifier as post-amplifier needs to guarantee

the optimal power of the following span. The amplification gain reduction of post-amplifier leads to its noise figure increasing, as demonstrated as the red curve in figure 7.7. As a result, the benefit of optimising the ROADM input power vanishes as more ASE noise is introduced to the following span.

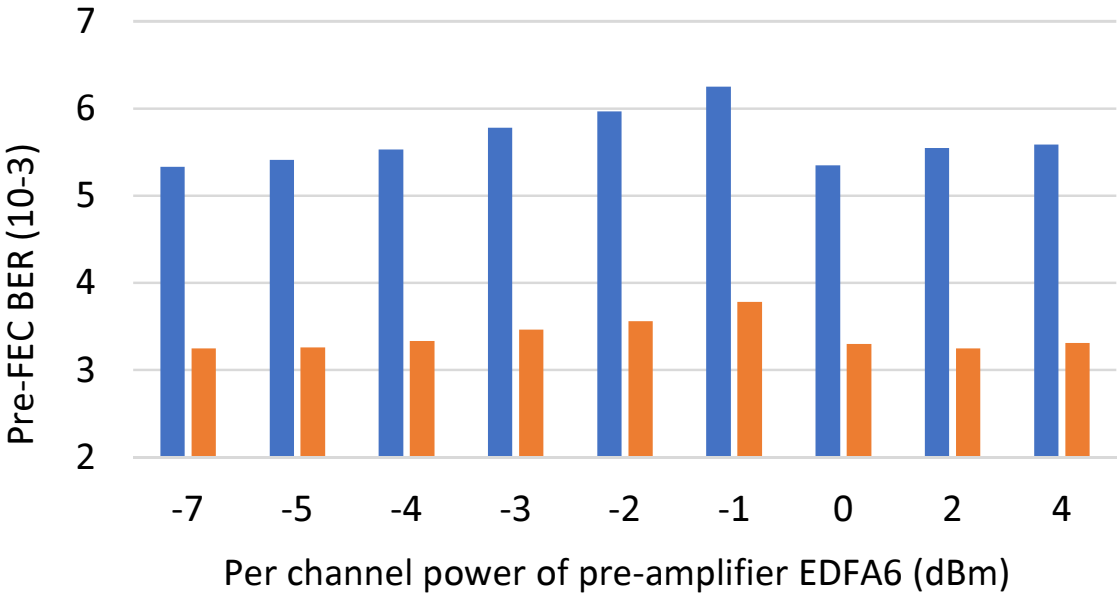

Fig. 7.6 Pre-FEC BER versus increasing per channel ROADM input power.

To overcome the noise figure increasing problem of the post-amplifier and to further improve the signal QoT, two solutions are proposed: 1) adding an attenuator at the output of the post-amplifier (EDFA 7); and 2) removing the post-amplifier by further increasing the gain of pre-amplifier.

For the first solution, the post-amplifier can operate in high gain mode with a relatively low noise figure by placing an attenuator. The attenuator is then adjusted to ensure the optimal power in the following fibre span. Therefore, the proposed benefit of decreasing ROADM SNR degradation can be achieved. The results of the first case are shown in figure 7.8. It shows the pre-FEC BER of both channels is reduced around 7% compared to the span-optimised-only network when the ROADM input power increases from 0 dBm to 5 dBm using solution 1.

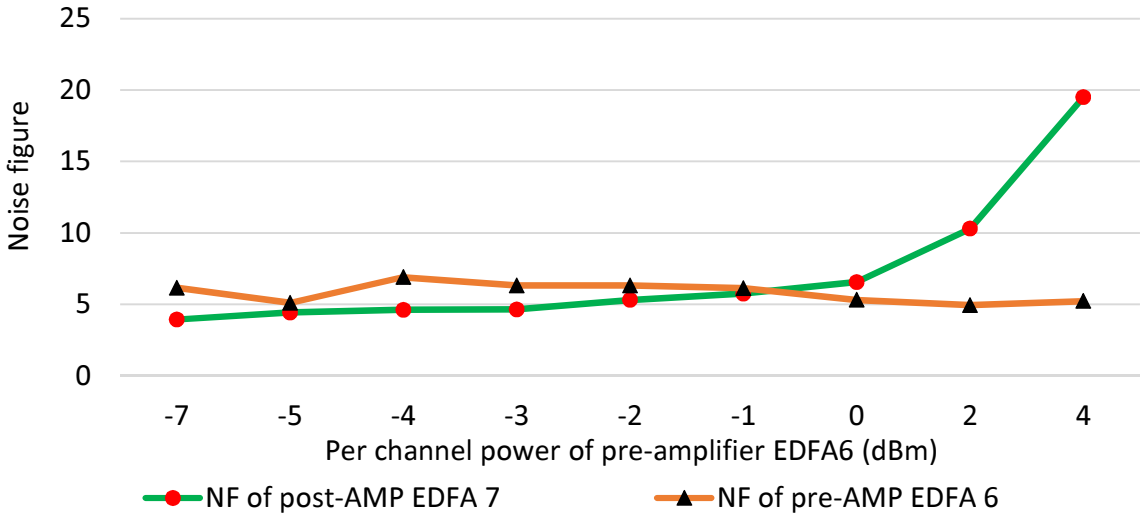

Fig. 7.7 Noise figure of post-amplifier EDFA versus the increasing pre-amplifier per channel output power (ROADM input power).

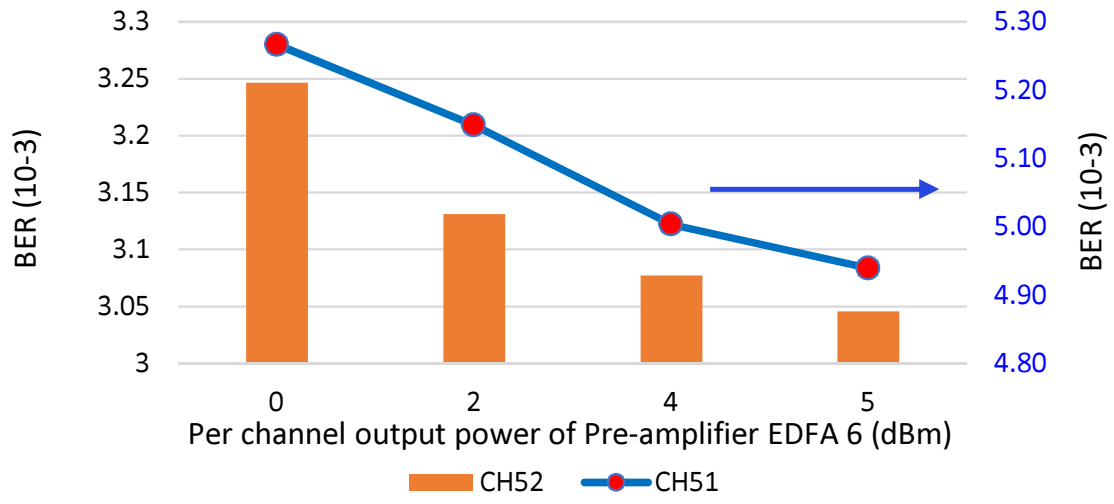

Fig. 7.8 Pre-FEC BER reduction versus the per channel output power of pre-amplifier for two tested channels.

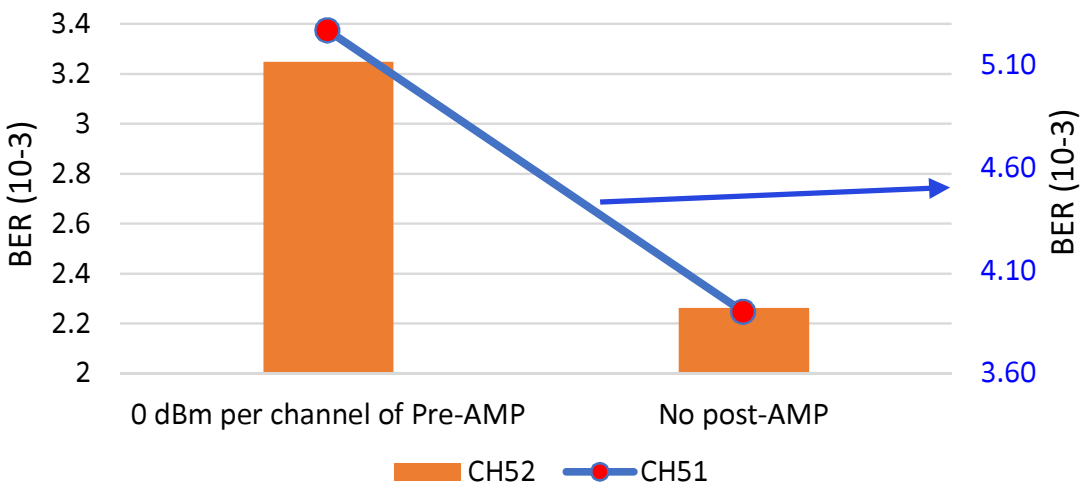

Fig. 7.9 Pre-FEC BER performance with and without post-amplifier for two tested channels.

In solution 2, the pre-amplifier needs to provide sufficiently high power to compensate both span loss and the WSS insertion loss. In this case, the WSS can directly adjust the power to be the optimum power of the following span. The pre-FEC BER is depicted in figure 7.9. Figure 7.9 shows around 1.2×10^{-3} pre-FEC BER reduction respectively for both Ch51 and Ch52 by removing the post-amplifier. Therefore, combining span power optimisation and the proper ROADM input power management solution, 50% pre-FEC BER decreasing can be achieved.

7.4 Simulation Setup and Results Analysis

To evaluate the performance of the power optimisation strategy described previously in the network, we build a simulation testbed using the BT topology. In the simulation, the fixed launch power of the fibre spans and the ROADMs is used as the benchmark (BM) solution. To make a fair comparison, the same ROADM input power is applied to the proposed strategy with the span power optimised using equation 7.2. Matlab is used as the simulation software to study the proposed coordinated power optimisation/management strategy in the EON.

We consider the network operates in 4 THz bandwidth of C-band with 12.5 GHz grid for the flex-grid elastic optical network. The ROADM insertion loss is assumed to be 14 dB and noise figure of the EDFA is set randomly between 4.5 dB and 6.5 dB. We assume spans within the same optical link are of identical length while the maximum span length does not exceed 60 km. We use The same set of fibre parameters as described in chapter 2. To evaluate the impact of two power management strategy over the network capacity, we sequentially load the traffic requests to BT network topology, which is demonstrated in figure 7.10. Each request consists of a pair of randomly selected nodes as source and destination with bit rate demand of 100 Gbps. For each connection, we calculate a least congested path using the equation 5.2 and search for available frequency slots with first-fit spectrum assignment. 5000 traffic requests are randomly generated to calculate the statistic behaviour as they are provisioned into the network sequentially. We repeat the process 100 times for both the proposed span power optimised solution and the benchmark method to obtain the averaged results.

The network blocking probability of the benchmark solution and the proposed span power optimised solution is shown in figure 7.11. From figure 7.11 (a), it can be seen that the optimum power spectral density of the benchmark solution is 12.6 mW/THz to achieve the lowest network blocking probability. As the span power is optimized in the proposed method, the one with highest ROADM input power spectral density of 79.6 mW/THz achieves the minimum network blocking probability.

The average network capacity of the benchmark (BM) solution and the proposed span power optimised (SPO) solution over the increasing input PSD ofROADM PSD shown in figure 7.12 when network blocking occurs. It can be seen that the optimal PSD of the benchmark is 12.6 mW/THz to achieve highest network throughput. Input PSD of ROADM is equivalent to the PSD in fibre span for BM. Therefore, when signal PSD is low, the signal is transmitted in the linear regime. Thus, the SNR degradation due to ASE noise and NLI

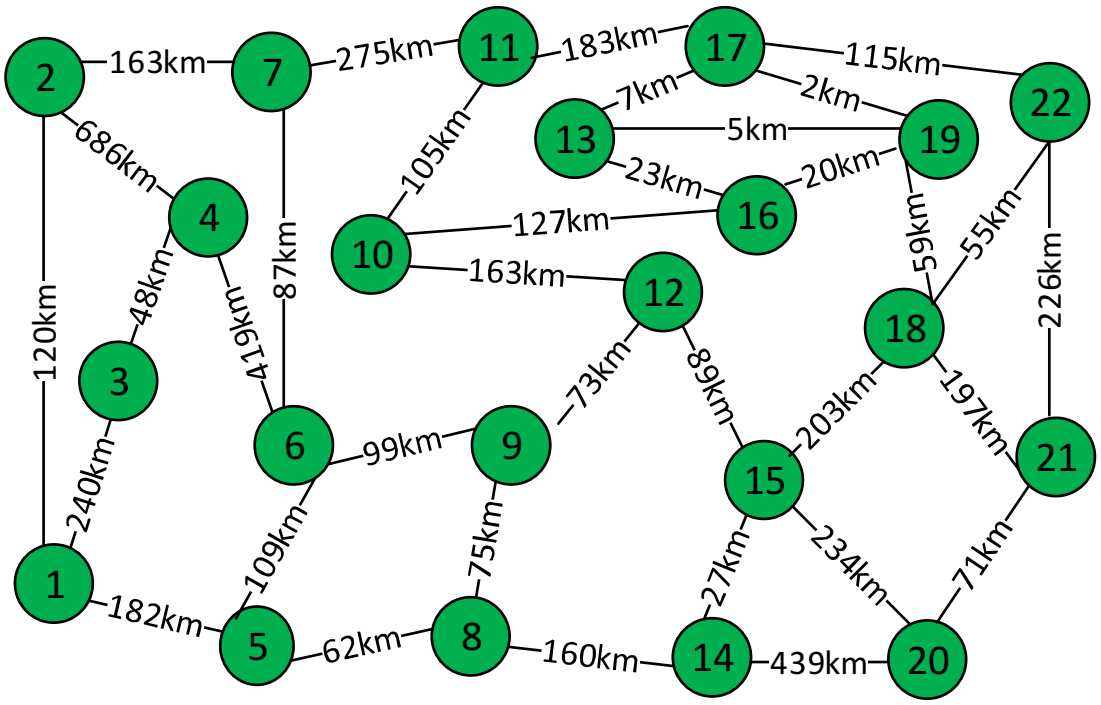

Fig. 7.10 BT network topology.

are both high. When signal PSD becomes high, the network operates towards the highly nonlinear regime. The advantage of less SNR degradation of ROADM collapses as the NLI dominates the performance. This leads to the increase of network capacity first and then decreasing against the increasing PSD.

Comparing the BM with SPO, SPO is able to provide an additional 5 Tbps more network throughput when the input PSD of ROADM is 12.6 mW/THz. When the input PSD of ROADM increases, SPO can further improve the throughput as the increasing input PSD of ROADM reduce impact from ROADM insertion loss, while the PSD of each span remains optimised. The proposed SPO method can theoretically achieve 402 Tbps network capacity before blocking occurs if the input PSD of ROADM is sufficiently high. As a result, it makes the impact of ROADM insertion less negligible. In this case, the results are equivalent to removing the post amplifiers of the ROAMDs. Comparing the performance of the benchmark power optimisation method with the proposed power optimisation solution, the proposed

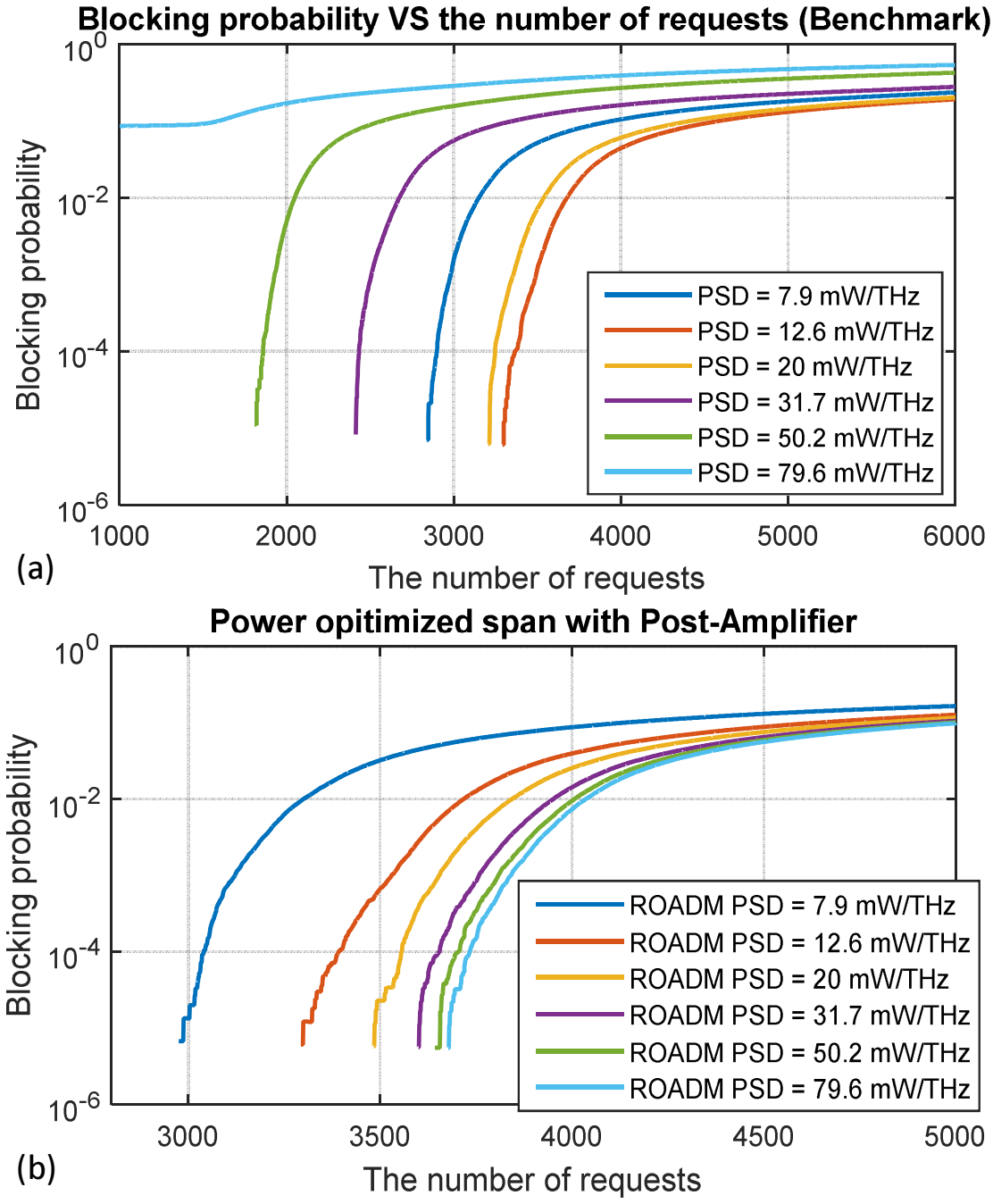

Fig. 7.11 Network traffic requests blocking probability for various PSDs. (a) Benchmark solution. (b) The proposed span power optimised solution with post-amplifier

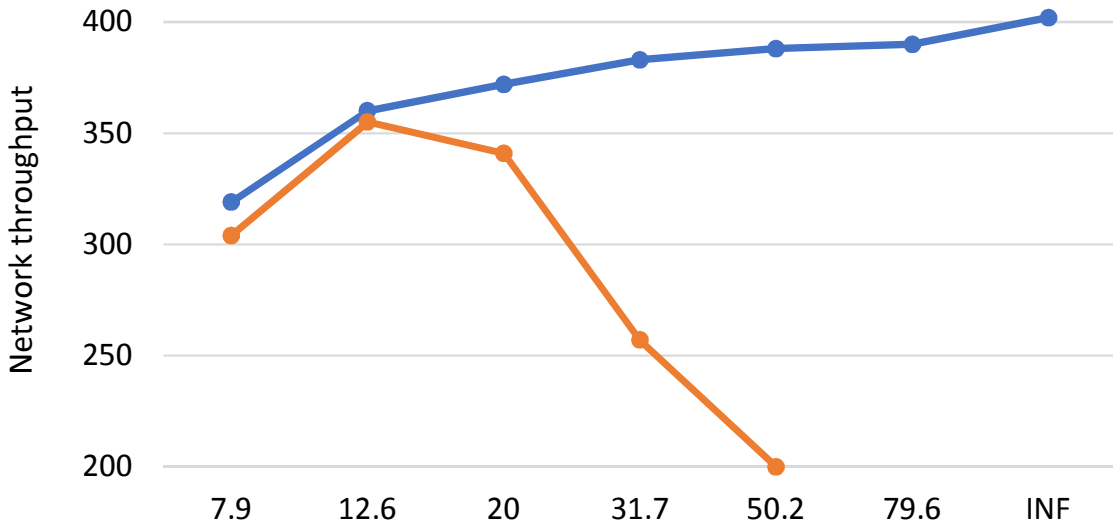

Fig. 7.12 Network capacity of benchmark solution and the proposed power optimisation solution when network blocking occurs

SPO achieves 15% more network throughput compared to BM, due to coordinated ROADM and fibre span power optimisation.

7.5 Summary

In this work, we proposed a coordinated fibre span power optimisation and ROADM input power management strategy to improve the network capacity. Through the experiment, the results show that up to 50% pre-FEC BER reduction with the coordinated fibre span power optimisation and the proposed ROADM power management strategy compared with the normal power optimisation strategy in the network. Our simulation shows that the combined optimisation method outperforms the regular optimisation strategy by providing 15% additional network capacity.

Chapter 8

Conclusion and Future Work

8.1 Review of Thesis Achievement

In this thesis, the main objective is to solve the capacity crunch issue by improving the throughput of the future dispersion uncompensated elastic optical networks with polarisation multiplexed signal and coherent transmission and detection in the nonlinear regime. In such optical networks, numerous impairments such as chromatic dispersion and polarisation mode dispersion linear can be fully compensated with the digital signal processing technique at the coherent receivers. Therefore, the stochastic noise and non-linear impairments which are unable to be compensated in real time, become the major penalties affecting the signal quality, the system reach distance and the overall network capacity. Hence, it is necessary to capture these information for service provisioning in the optical networks.

Compared to the simple model of stochastic noise, the nonlinear impairments are usually associated with solving complex mathematical equations. Hence, our first contribution in this work is to propose a simplified nonlinear impairments estimation model for the fast routing, modulation format and spectrum allocation and power optimisation in the elastic optical networks. The flexible and adaptive optical network resource assignment and optimisation based on the developed nonlinear impairments model with multiple optimisation target is

also achieved by the proposed solution. Further, the nonlinearity-aware resource allocation is proposed for provisioning dynamic traffic in the elastic optical networks. The goal of achieving higher network capacity is realized by combining traffic grooming with flexible bandwidth allocation in elastic optical networks, using the excess SNR margin between the estimated SNR from the proposed NLI framework and the SNR requirement for the modulation format. We further investigate the power optimisation strategy by carrying out extensive experiments and simulation to show the QoT improvement of the signal and the network capacity improvement.

The key achievements of this thesis are described with more detail as:

- A load-aware nonlinear impairments model are developed based on Gaussian noise nonlinear impairments model to enable fast signal QoT evaluation for the resource allocation and optimisation in elastic optical networks. The proposed approach relies on the link loading concept and thus can avoid the inter-channel blocking problem when the link remains in the same loading state, as described in chapter 4. The proposed load-aware hybrid nonlinearity model combines the features of worst-case nonlinear impairments estimation strategy and the exact nonlinear impairments according to the signal power spectral density and the propagated channels along the path. The proposed load-aware hybrid nonlinearity model is proved to be an accurate and computational simplified tool.

- Following the proposed hybrid nonlinearity model, we have proposed a complete routing, modulation format and spectrum allocation scheme using the proposed nonlinearity model. The proposed resource allocation scheme considers the inter-channel blocking problem in case the link loading states alter with the increasing number of provisioned lightpaths. Hence, three service reconfiguration schemes have been raised to reconfigure the blocked service requests known as: MILP based service reconfiguration, MILP based heuristic service reconfiguration and the complete heuristic

service reconfiguration. The first objective of MILP base service reconfiguration aims to minimize the highest allocated spectrum slot index in the network. On the basis of the minimal index, the MILP problem is solved again to achieve the minimum number of allocated slots. The MILP based heuristic service request reconfiguration solves the RMSA problem in a series of request groups, where each request group is solved as a sub-MILP problem. In the complete heuristic service reconfiguration, only the blocked requests are reconfigured. This requires the least complexity from the control plane.

- Further to the algorithm proposed in chapter 4 for static traffic scenario or the traffic sequentially provisioned to the elastic optical networks, the resource allocation algorithm is demonstrated for dynamic traffic requests. The benefit of the proposed resource algorithm for online traffic demand with the proposed load-aware nonlinearity model is verified through an extensive simulation study. To further improve network capacity, we investigate the utilisation of excess SNR margin of the elastic optical network operating in the nonlinear regime. A routing, modulation format and spectrum allocation scheme is developed combining the optical traffic grooming technique provided by the capability of modulation format adaptable and bandwidth-variable transponders. The results indicate significantly network capacity improvement and the tremendous amount of transponders saving compared to other benchmark solutions.

- The final objective of this thesis is to explore the impact of power in the network to the signal quality of transmission and the overall network throughput. The coordinated fibre span power optimisation and ROADM input power management strategy are developed in this work. The proposed solution is experimentally demonstrated and corresponding approaches have been proposed. Our simulation results indicate the proposed coordinated power management strategy can decrease the bit error rate of the lightpath and thus achieve higher spectrum efficiency. The benefit of network capacity

improvement using the proposed power optimisation solution is also verified through extensive simulation.

8.2 Future Work

The area of nonlinear impairments aware power optimisation, resource allocation and networking perspectives can be continued and improved in many aspects. In the following, the most attractive and compelling of the future research of this work are listed.

8.2.1 Nonlinearity-aware virtual network mapping in heterogeneous networks

The requirement of future network applications may vary remarkably in the future heterogeneous networks. For example, the virtual network embedding cases, especially the virtual networks across multiple network domains with different data rate, latency, bit error rate and packet loss rate requirement. In such virtual networks, the embedding algorithm should consider virtual resource aggregation, virtualisation in each network domain and should consider the orchestration between each network. In this case, the nonlinearity-aware virtual optical network mapping is essential as multiple virtual networks may share the same physical link. The different link loading conditions due to the sharing pose different quality of transmission of the virtual network. Therefore, the analysis of different virtual network mapping algorithms and their impact on the nonlinear impairments in the optical networks is important. Moreover, with the establishment and expiration of virtual networks, the nonlinear impairments along the virtual network will also change. This will also cause the physical layer inter-channel blocking, which blocked the embedded virtual networks. As a result, the virtual network remapping should also be investigated to maximize the virtual network

mapping and remapping efficiency, to maximize the number of accepted virtual networks and to reduce the impact of service inter-channel blocking.

8.2.2 Nonlinearity-aware resource allocation with BVT virtualization

The nonlinear impairments-aware resource allocation in elastic optical networks relies on the powerful transponders. The bandwidth-variable transponders provide the capability of bandwidth elastic, modulation format adaptable and forward error correction coding rate flexible. Joint optimisation of network spectrum resources and the bandwidth-variable transponders with these capabilities should be investigated, especially when the number of powerful BVT are limited. The nonlinearity-aware resource allocation of virtual BVT can be explored to increase the BVT and overall network resources utilisation.

8.2.3 Energy-aware network optimisation in nonlinear regime

Energy consumption is a big challenge to the current optical networks [160] and it is related to the number of active devices. In the optical network with dynamic traffic scenarios, the utilisation of optical links and corresponding transponders and ROADMs alter with time. To improve the energy efficiency in the optical networks, the lightpaths travelling through low utilized ROADMs and links can be migrated to highly utilised links. In this case, with no traffic in certain links, the corresponding EDFA, ROAMDs and transponders can be set to sleep mode to avoid energy waste. However, some links may be highly congested and cause the QoT of the lightpaths degrading in this case due to high nonlinear impairments. Therefore, the trade-off between the energy efficiency of the network and QoT of lightpath as well as the spectral efficiency of the network is an interesting topic to study. Corresponding network optimisation can be introduced to increase the network spectral efficiency or reduce the energy consumption according to their traffic patterns and requirement.

8.2.4 Nonlinearity-aware resource optimisation in filter-less optical networks

Recently, semi or full filter-less optical networks have drawn a lot of attention due to its low cost, low management complexity and high resilience [161]. In such a network without active optical switching elements like ROADMs. the channel is propagated in a multicast or broadcast way. The unflattened gain of EDFA along the optical spans causes different degrees of signal distortion due to both ASE noise and nonlinear impairments, while the power difference cannot be compensated by power equalisation without ROADM. Therefore, the nonlinear impairments management is essential in filter-less optical networks. The corresponding spectrum and power allocation should be designed to consider the impact of EDFA according to different traffic scenarios. Joint network and BVT power optimisation should also be studied to reduce or overcome the impact of unflattened amplification gain.

8.2.5 Signal power spectra density-aware optimisation in non-linear regime

In the optical networks, the signal power spectral density may vary with different transponders using different lasers, FEC overhead, modulation schemes and spectra shaping techniques. Especially considering the characteristics of unflattened EDFA, the power alters with different channel assigned. This results in poor management of ASE noise and nonlinear impairments, which cause network underutilised. The joint impact of multiple signal PSDs and the EDFA unflattened gain causing non-identical ASE noise, the non-identical noise figure of EDFA should be experimentally investigated. The corresponding monitoring techniques should be deployed to obtain information from intermediate optical nodes. Machine learning technique can be applied to optimise and enable signal PSD-aware network resource allocation.

References

[1] N. Golmie, T. Ndousse, and D. Su, "A differentiated optical services model for WDM networks," *IEEE Communications Magazine*, vol. 38, no. 2, pp. 68–73, Feb. 2000. [Online]. Available: http://ieeexplore.ieee.org/document/819898/

[2] J. Pan, S. Paul, and R. Jain, "A survey of the research on future internet architectures," *IEEE Communications Magazine*, vol. 49, no. 7, pp. 26–36, Jul. 2011. [Online]. Available: http://ieeexplore.ieee.org/document/5936152/

[3] A. A. M. Saleh, "Architectural Principles of Optical Regional and Metropolitan Access Networks," *Journal of Lightwave Technology*, vol. 17, no. 12, p. 18, 1999.

[4] "VNI Global Fixed and Mobile Internet Traffic Forecasts." [Online]. Available: http://www.cisco.com/c/en/us/solutions/service-provider/visual-networking-index-vni/index.html

[5] P. P. Mitra and J. B. Stark, "Nonlinear limits to the information capacity of optical fibre communications," *Nature*, vol. 411, no. 6841, p. 1027, 2001.

[6] A. Gumaste and T. Antony, *DWDM network designs and engineering solutions*. Cisco Press, 2003.

[7] Y. Pointurier, "Design of low-margin optical networks," *IEEE/OSA Journal of Optical Communications and Networking*, vol. 9, no. 1, pp. A9–A17, 2017.

[8] K. Zhu, H. Zang, and B. Mukherjee, "A comprehensive study on next-generation optical grooming switches," *IEEE Journal on Selected Areas in Communications*, vol. 21, no. 7, pp. 1173–1186, 2003.

[9] G. P. Agrawal, *Fiber-optic communication systems*. John Wiley & Sons, 2012, vol. 222.

[10] S. Iano, T. Sato, S. Sentsui, T. Kuroha, and Y. Nishimura, "Multicore optical fiber," in *Optical Fiber Communication Conference*. Optical Society of America, 1979, p. WB1.

[11] K. Takenaga, Y. Arakawa, Y. Sasaki, S. Tanigawa, S. Matsuo, K. Saitoh, and M. Koshiba, "A large effective area multi-core fiber with an optimized cladding thickness," *Optics express*, vol. 19, no. 26, pp. B543–B550, 2011.

[12] M. Koshiba, K. Saitoh, K. Takenaga, and S. Matsuo, "Multi-core fiber design and analysis: coupled-mode theory and coupled-power theory," *Optics express*, vol. 19, no. 26, pp. B102–B111, 2011.

[13] G. P. Agrawal, "Nonlinear fiber optics," in *Nonlinear Science at the Dawn of the 21st Century*. Springer, 2000, pp. 195–211.

[14] S. Azodolmolky, M. Klinkowski, E. Marin, D. Careglio, J. S. Pareta, and I. Tomkos, "A survey on physical layer impairments aware routing and wavelength assignment algorithms in optical networks," *Computer Networks*, vol. 53, no. 7, pp. 926–944, 2009.

[15] C. V. Saradhi and S. Subramaniam, "Physical layer impairment aware routing (pliar) in wdm optical networks: issues and challenges," *IEEE Communications Surveys & Tutorials*, vol. 11, no. 4, 2009.

[16] M. N. Chughtai, "Study of physical layer impairments in high speed optical networks," Ph.D. dissertation, KTH Royal Institute of Technology, 2012.

[17] C. Politi, C. Matrakidis, and A. Stavdas, "A tutorial on physical-layer impairments in optical networks," in *Cross-Layer Design in Optical Networks*. Springer, 2013, pp. 5–29.

[18] B. Mukherjee, *Optical communication networks*. McGraw-Hill New York, 1997, vol. 14.

[19] M. Kserawi, S. Shimizu, N. Wada, A. G. Reza, and J.-K. K. Rhee, "Theories and applications of chromatic dispersion penalty mitigation in all optical ofdm transmission system," *Optics Express*, vol. 21, no. 2, pp. 1669–1674, 2013.

[20] C. Laperle, B. Villeneuve, Z. Zhang, D. McGhan, H. Sun, and M. O'Sullivan, "Wavelength division multiplexing (wdm) and polarization mode dispersion (pmd) performance of a coherent 40gbit/s dual-polarization quadrature phase shift keying (dp-qpsk) transceiver," in *National Fiber Optic Engineers Conference*. Optical Society of America, 2007, p. PDP16.

[21] Z. Wang, C. Xie, and X. Ren, "Pmd and pdl impairments in polarization division multiplexing signals with direct detection," *Optics express*, vol. 17, no. 10, pp. 7993–8004, 2009.

[22] P. M. Becker, A. A. Olsson, and J. R. Simpson, *Erbium-doped fiber amplifiers: fundamentals and technology*. Elsevier, 1999.

[23] R. Olshansky, "Noise figure for erbium-doped optical fibre amplifiers," *Electronics Letters*, vol. 24, no. 22, pp. 1363–1365, 1988.

[24] D. M. Baney, P. Gallion, and R. S. Tucker, "Theory and measurement techniques for the noise figure of optical amplifiers," *Optical fiber technology*, vol. 6, no. 2, pp. 122–154, 2000.

[25] A. Yariv, "Signal-to-noise considerations in fiber links with periodic or distributed optical amplification," *Optics letters*, vol. 15, no. 19, pp. 1064–1066, 1990.

[26] H. Kogelnik and A. Yariv, "Considerations of noise and schemes for its reduction in laser amplifiers," *Proceedings of the IEEE*, vol. 52, no. 2, pp. 165–172, 1964.

[27] R. Kaler and R. Kaler, "Gain and noise figure performance of erbium doped fiber amplifiers (edfas) and compact edfas," *Optik-International Journal for Light and Electron Optics*, vol. 122, no. 5, pp. 440–443, 2011.

[28] H. Ono, M. Yamada, and M. Shimizu, "S-band erbium-doped fiber amplifiers with a multistage configuration-design, characterization, and gain tilt compensation," *Journal of Lightwave technology*, vol. 21, no. 10, p. 2240, 2003.

[29] K. Kikushima and H. Yoshinaga, "Distortion due to gain tilt of erbium-doped fiber amplifiers," *IEEE photonics technology letters*, vol. 3, no. 10, pp. 945–947, 1991.

[30] L. Tomkos, R. Hesse, N. Antoniades, and A. Boskovic, "Impact of filter concatenation on the performance of metropolitan area optical networks utilizing directly modulated lasers," in *Optical Fiber Communication Conference*. Optical Society of America, 2001, p. WBB4.

[31] J. D. Downie, I. Tomkos, N. Antoniades, and A. Boskovic, "Effects of filter concatenation for directly modulated transmission lasers at 2.5 and 10 gb/s," *Journal of Lightwave Technology*, vol. 20, no. 2, p. 218, 2002.

[32] O. Gerstel, M. Jinno, A. Lord, and S. B. Yoo, "Elastic optical networking: A new dawn for the optical layer?" *IEEE Communications Magazine*, vol. 50, no. 2, 2012.

[33] E. Ip and J. M. Kahn, "Compensation of dispersion and nonlinear impairments using digital backpropagation," *Journal of Lightwave Technology*, vol. 26, no. 20, pp. 3416–3425, 2008.

[34] E. F. Mateo, X. Zhou, and G. Li, "Improved digital backward propagation for the compensation of inter-channel nonlinear effects in polarization-multiplexed wdm systems," *Optics Express*, vol. 19, no. 2, pp. 570–583, 2011.

[35] F. Yaman and G. Li, "Nonlinear impairment compensation for polarization-division multiplexed wdm transmission using digital backward propagation," *IEEE Photonics Journal*, vol. 1, no. 2, pp. 144–152, 2009.

[36] G. P. Agrawal, "Nonlinear fiber optics: its history and recent progress," *JOSA B*, vol. 28, no. 12, pp. A1–A10, 2011.

[37] K. Torii, T. Tanaka, M. Yuki, H. Nakamoto, T. Naito, and I. Yokota, "Impact of stimulated raman scattering between wdm signals over an ultra-wide bandwidth," in *Optical Fiber Communications Conference, 2003. OFC 2003*. IEEE, 2003, pp. 332–334.

[38] C. A. Balanis, *Advanced engineering electromagnetics*. John Wiley & Sons, 1999.

[39] M. Sheik-Bahae and M. P. Hasselbeck, "Third-order optical nonlinearities," *Handbook of Optics*, vol. 4, pp. 16–1, 2000.

[40] E. Mateo, L. Zhu, and G. Li, "Impact of xpm and fwm on the digital implementation of impairment compensation for wdm transmission using backward propagation," *Optics Express*, vol. 16, no. 20, pp. 16 124–16 137, 2008.

[41] P. Poggiolini, G. Bosco, A. Carena, V. Curri, Y. Jiang, and F. Forghieri, "The gn-model of fiber non-linear propagation and its applications," *Journal of lightwave technology*, vol. 32, no. 4, pp. 694–721, 2014.

[42] P. Poggiolini, "The gn model of non-linear propagation in uncompensated coherent optical systems," *Journal of Lightwave Technology*, vol. 30, no. 24, pp. 3857–3879, 2012.

[43] A. Carena, V. Curri, G. Bosco, P. Poggiolini, and F. Forghieri, "Modeling of the impact of nonlinear propagation effects in uncompensated optical coherent transmission links," *Journal of Lightwave technology*, vol. 30, no. 10, pp. 1524–1539, 2012.

[44] P. Johannisson and E. Agrell, "Modeling of nonlinear signal distortion in fiber-optic networks," *Journal of Lightwave Technology*, vol. 32, no. 23, pp. 3942–3950, 2014.

[45] S. J. Savory, "Approximations for the nonlinear self-channel interference of channels with rectangular spectra," *IEEE Photonics Technology Letters*, vol. 25, no. 10, pp. 961–964, 2013.

[46] P. Poggiolini, G. Bosco, A. Carena, V. Curri, Y. Jiang, and F. Forghieri, "A detailed analytical derivation of the gn model of non-linear interference in coherent optical transmission systems," *arXiv preprint arXiv:1209.0394*, 2012.

[47] D. J. Ives, P. Bayvel, and S. J. Savory, "Adapting transmitter power and modulation format to improve optical network performance utilizing the gaussian noise model of nonlinear impairments," *Journal of Lightwave Technology*, vol. 32, no. 21, pp. 3485–3494, 2014.

[48] A. Bononi, O. Beucher, and P. Serena, "Single-and cross-channel nonlinear interference in the gaussian noise model with rectangular spectra," *Optics express*, vol. 21, no. 26, pp. 32 254–32 268, 2013.

[49] F. Zhang, Q. Zhuge, and D. V. Plant, "Fast analytical evaluation of fiber nonlinear noise variance in mesh optical networks," *IEEE/OSA Journal of Optical Communications and Networking*, vol. 9, no. 4, pp. C88–C97, 2017.

[50] P. Poggiolini, G. Bosco, A. Carena, R. Cigliutti, V. Curri, F. Forghieri, R. Pastorelli, and S. Piciaccia, "The logon strategy for low-complexity control plane implementation in new-generation flexible networks," in *Optical Fiber Communication Conference and Exposition and the National Fiber Optic Engineers Conference (OFC/NFOEC), 2013*. IEEE, 2013, pp. 1–3.

[51] D. J. Ives, P. Bayvel, and S. J. Savory, "Routing, modulation, spectrum and launch power assignment to maximize the traffic throughput of a nonlinear optical mesh network," *Photonic Network Communications*, vol. 29, no. 3, pp. 244–256, 2015.

[52] I. Roberts, J. M. Kahn, and D. Boertjes, "Convex channel power optimization in nonlinear wdm systems using gaussian noise model," *Journal of Lightwave Technology*, vol. 34, no. 13, pp. 3212–3222, 2016.

[53] L. Yan, E. Agrell, H. Wymeersch, and M. Brandt-Pearce, "Resource allocation for flexible-grid optical networks with nonlinear channel model," *Journal of Optical Communications and Networking*, vol. 7, no. 11, pp. B101–B108, 2015.

[54] L. Yan, E. Agrell, M. N. Dharmaweera, and H. Wymeersch, "Joint assignment of power, routing, and spectrum in static flexible-grid networks," *Journal of Lightwave Technology*, vol. 35, no. 10, pp. 1766–1774, 2017.

[55] L. Yan, J. Zhao, E. Agrell, and H. Wymeersch, "Power optimization in nonlinear flexible-grid optical networks," in *Optical Communication (ECOC), 2015 European Conference on*. IEEE, 2015, pp. 1–3.

[56] D. R. Zimmerman and L. H. Spiekman, "Amplifiers for the masses: Edfa, edwa, and soa amplets for metro and access applications," *Journal of lightwave technology*, vol. 22, no. 1, p. 63, 2004.

[57] A. E. Willner and S.-M. Hwan, "Transmission of many wdm channels through a cascade of edfa's in long-distance links and ring networks," *Journal of lightwave technology*, vol. 13, no. 5, pp. 802–816, 1995.

[58] E. V. Vanin, U. Persson, and G. Jacobsen, "Spectral functional forms for gain and noise characterization of erbium-doped fiber amplifiers," *Journal of lightwave technology*, vol. 20, no. 2, p. 243, 2002.

[59] M. Pal, M. C. Paul, A. Dhar, A. Pal, R. Sen, K. Dasgupta, and S. K. Bhadra, "Investigation of the optical gain and noise figure for multi-channel amplification in edfa under optimized pump condition," *Optics Communications*, vol. 273, no. 2, pp. 407–412, 2007.

[60] J. Gujral and V. Goel, "Analysis of augmented gain edfa systems using single and multi-wavelength sources," *International Journal of Computer Applications (0975-888)*, vol. 47, no. 4, 2012.

[61] C. J. Bastos-Filho, E. d. A. Barboza, J. F. Martins-Filho, U. C. de Moura, and J. R. de Oliveira, "Mapping edfa noise figure and gain flatness over the power mask using neural networks," *Journal of Microwaves, Optoelectronics and Electromagnetic Applications (JMOe)*, vol. 12, pp. 128–139, 2013.

[62] E. d. A. Barboza, C. J. Bastos-Filho, J. F. Martins-Filho, U. C. de Moura, and J. R. de Oliveira, "Self-adaptive erbium-doped fiber amplifiers using machine learning," in *Microwave & Optoelectronics Conference (IMOC), 2013 SBMO/IEEE MTT-S International*. IEEE, 2013, pp. 1–5.

[63] S. Tibuleac and M. Filer, "Transmission impairments in dwdm networks with reconfigurable optical add-drop multiplexers," *Journal of Lightwave Technology*, vol. 28, no. 4, pp. 557–568, 2010.

[64] S. Gringeri, B. Basch, V. Shukla, R. Egorov, and T. Xia, "Flexible architectures for optical transport nodes and networks," *IEEE Communications Magazine*, vol. 48, no. 7, pp. 40–50, Jul. 2010.

[65] N. Amaya, M. Irfan, G. Zervas, R. Nejabati, D. Simeonidou, J. Sakaguchi, W. Klaus, B. J. Puttnam, T. Miyazawa, Y. Awaji *et al.*, "Fully-elastic multi-granular network with space/frequency/time switching using multi-core fibres and programmable optical nodes," *Optics Express*, vol. 21, no. 7, pp. 8865–8872, 2013.

[66] N. Amaya, G. S. Zervas, and D. Simeonidou, "Architecture on demand for transparent optical networks," in *Transparent Optical Networks (ICTON), 2011 13th International Conference on*. IEEE, 2011, pp. 1–4.

[67] R. Koetter and A. Vardy, "Algebraic soft-decision decoding of reed-solomon codes," *IEEE Transactions on Information Theory*, vol. 49, no. 11, pp. 2809–2825, 2003.

[68] R. A. Shafik, M. S. Rahman, and A. R. Islam, "On the extended relationships among evm, ber and snr as performance metrics," in *Electrical and Computer Engineering, 2006. ICECE'06. International Conference on*. IEEE, 2006, pp. 408–411.

[69] W. Webb and T. Keller, *Single-and multi-carrier quadrature amplitude modulation: principles and applications for personal communications, WLANs and broadcasting*. John Wiley & Sons, 2000.

[70] A. Goldsmith, *Wireless communications*. Cambridge university press, 2005.

[71] K. Cho and D. Yoon, "On the general ber expression of one-and two-dimensional amplitude modulations," *IEEE Transactions on Communications*, vol. 50, no. 7, pp. 1074–1080, 2002.

[72] F. Chang, K. Onohara, and T. Mizuochi, "Forward error correction for 100 g transport networks," *IEEE Communications Magazine*, vol. 48, no. 3, 2010.

[73] C. E. Shannon, "A mathematical theory of communication," *ACM SIGMOBILE mobile computing and communications review*, vol. 5, no. 1, pp. 3–55, 2001.

[74] O. I. Forum, "100G Forward Error Correction White Paper ," Optical Internetworking Forum, Tech. Rep., 05 2010.

[75] G. Tzimpragos, C. Kachris, I. B. Djordjevic, M. Cvijetic, D. Soudris, and I. Tomkos, "A survey on fec codes for 100 g and beyond optical networks," *IEEE Communications Surveys & Tutorials*, vol. 18, no. 1, pp. 209–221, 2016.

[76] J. Berthold, A. A. M. Saleh, L. Blair, and J. M. Simmons, "Optical Networking: Past, Present, and Future," *Journal of Lightwave Technology*, vol. 26, no. 9, pp. 1104–1118, May 2008. [Online]. Available: http://ieeexplore.ieee.org/document/4542876/

[77] R. Ramaswami, K. Sivarajan, and G. Sasaki, *Optical Networks: A Practical Perspective, 3rd Edition*, 3rd ed. San Francisco, CA, USA: Morgan Kaufmann Publishers Inc., 2009.

[78] D. Banerjee and B. Mukherjee, "Wavelength-routed optical networks: linear formulation, resource budgeting tradeoffs, and a reconfiguration study," *IEEE/ACM Transactions on Networking*, vol. 8, no. 5, pp. 598–607, Oct. 2000. [Online]. Available: https://ieeexplore.ieee.org/document/879346/

[79] I. T. S. Sector, "ITU-T: Spectral grids for WDM applications: DWDM frequency grid," *TELECOMMUNICATION STANDARDIZATION SECTOR OF ITU*, Feb. 2012.

[80] B. Ramamurthy, S. Yaragorla, and X. Yang, "Translucent optical wdm networks for the next-generation backbone networks," in *Global Telecommunications Conference, 2001. GLOBECOM'01. IEEE*, vol. 1. IEEE, 2001, pp. 60–64.

[81] B. Ramamurthy, H. Feng, D. Datta, J. P. Heritage, and B. Mukherjee, "Transparent vs. opaque vs. translucent wavelength-routed optical networks," in *Optical Fiber Communication Conference, 1999, and the International Conference on Integrated Optics and Optical Fiber Communication. OFC/IOOC'99. Technical Digest*, vol. 1. IEEE, 1999, pp. 59–61.

[82] B. Sartorius, "3r regeneration for all-optical networks," in *Transparent Optical Networks, 2001. Proceedings of 2001 3rd International Conference on*. IEEE, 2001, pp. 333–337.

[83] M. Rochette, J. L. Blows, and B. J. Eggleton, "3r optical regeneration: An all-optical solution with ber improvement," *Optics Express*, vol. 14, no. 14, pp. 6414–6427, 2006.

[84] C. A. Brackett, "Dense wavelength division multiplexing networks: Principles and applications," *IEEE Journal on Selected Areas in Communications*, vol. 8, no. 6, pp. 948–964, 1990.

[85] M. Jinno, H. Takara, B. Kozicki, Y. Tsukishima, Y. Sone, and S. Matsuoka, "Spectrum-efficient and scalable elastic optical path network: architecture, benefits, and enabling technologies," *IEEE communications magazine*, vol. 47, no. 11, 2009.

[86] M. Jinno, B. Kozicki, H. Takara, A. Watanabe, Y. Sone, T. Tanaka, and A. Hirano, "Distance-adaptive spectrum resource allocation in spectrum-sliced elastic optical path network [topics in optical communications]," *IEEE Communications Magazine*, vol. 48, no. 8, 2010.

[87] G. Zhang, M. De Leenheer, A. Morea, and B. Mukherjee, "A survey on ofdm-based elastic core optical networking," *IEEE Communications Surveys & Tutorials*, vol. 15, no. 1, pp. 65–87, 2013.

[88] N. Sambo, P. Castoldi, A. D'Errico, E. Riccardi, A. Pagano, M. S. Moreolo, J. M. Fabrega, D. Rafique, A. Napoli, S. Frigerio *et al.*, "Next generation sliceable bandwidth variable transponders," *IEEE Communications Magazine*, vol. 53, no. 2, pp. 163–171, 2015.

[89] Y. Ou, S. Yan, A. Hammad, B. Guo, S. Peng, R. Nejabati, and D. Simeonidou, "Demonstration of virtualizeable and software-defined optical transceiver," *Journal of Lightwave Technology*, vol. 34, no. 8, pp. 1916–1924, 2016.

[90] Y. Ou, A. Hammad, S. Peng, R. Nejabati, and D. Simeonidou, "Online and offline virtualization of optical transceiver," *Journal of Optical Communications and Networking*, vol. 7, no. 8, pp. 748–760, 2015.

[91] M. Jinno, H. Takara, Y. Sone, K. Yonenaga, and A. Hirano, "Multiflow optical transponder for efficient multilayer optical networking," *IEEE Communications Magazine*, vol. 50, no. 5, 2012.

[92] V. López and L. Velasco, *Elastic Optical Networks: Architectures, Technologies, and Control*. Springer, 2016.

[93] T. Rahman, A. Napoli, D. Rafique, B. Spinnler, M. Kuschnerov, I. Lobato, B. Clouet, M. Bohn, C. Okonkwo, and H. de Waardt, "On the mitigation of optical filtering penalties originating from roadm cascade," *IEEE Photonics Technology Letters*, vol. 26, no. 2, pp. 154–157, 2014.

[94] S. Perrin, "Next-Generation ROADM Architectures and Benefit," Whilte paper, FUJITSU, Tech. Rep., Mar. 2015. [Online]. Available: https://www.fujitsu.com/us/Images/Fujitsu-NG-ROADM.pdf

[95] J. M. Simmons, "A closer look at roadm contention," *IEEE Communications Magazine*, vol. 55, no. 2, pp. 160–166, 2017.

[96] H. Yang, B. Robertson, P. Wilkinson, and D. Chu, "Low-cost cdc roadm architecture based on stacked wavelength selective switches," *IEEE/OSA Journal of Optical Communications and Networking*, vol. 9, no. 5, pp. 375–384, 2017.

[97] B. C. Chatterjee, N. Sarma, and E. Oki, "Routing and spectrum allocation in elastic optical networks: A tutorial," *IEEE Communications Surveys & Tutorials*, vol. 17, no. 3, pp. 1776–1800, 2015.

[98] K. Christodoulopoulos, I. Tomkos, and E. Varvarigos, "Elastic bandwidth allocation in flexible ofdm-based optical networks," *Journal of Lightwave Technology*, vol. 29, no. 9, pp. 1354–1366, 2011.

[99] H. Zang, J. P. Jue, B. Mukherjee *et al.*, "A review of routing and wavelength assignment approaches for wavelength-routed optical wdm networks," *Optical networks magazine*, vol. 1, no. 1, pp. 47–60, 2000.

[100] R. Ramaswami and K. N. Sivarajan, "Routing and wavelength assignment in all-optical networks," *IEEE/ACM Transactions on Networking (TON)*, vol. 3, no. 5, pp. 489–500, 1995.

[101] D. Banerjee and B. Mukherjee, "A practical approach for routing and wavelength assignment in large wavelength-routed optical networks," *IEEE Journal on selected areas in communications*, vol. 14, no. 5, pp. 903–908, 1996.

[102] Y. Wang, X. Cao, and Y. Pan, "A study of the routing and spectrum allocation in spectrum-sliced elastic optical path networks," in *INFOCOM, 2011 Proceedings IEEE*. IEEE, 2011, pp. 1503–1511.

[103] R. Ramamurthy and B. Mukherjee, "Fixed-alternate routing and wavelength conversion in wavelength-routed optical networks," *IEEE/ACM Transactions on networking*, vol. 10, no. 3, pp. 351–367, 2002.

[104] B. Mukherjee, *Optical WDM networks*. Springer Science & Business Media, 2006.

[105] U. Brandes, "A faster algorithm for betweenness centrality," *Journal of mathematical sociology*, vol. 25, no. 2, pp. 163–177, 2001.

[106] D. B. West *et al.*, *Introduction to graph theory*. Prentice hall Upper Saddle River, 2001, vol. 2.

[107] S. J. Savory, "Congestion aware routing in nonlinear elastic optical networks," *IEEE Photonics Technology Letters*, vol. 26, no. 10, pp. 1057–1060, 2014.

[108] J. P. Jue and G. Xiao, "An adaptive routing algorithm for wavelength-routed optical networks with a distributed control scheme," in *Computer Communications and Networks, 2000. Proceedings. Ninth International Conference on*. IEEE, 2000, pp. 192–197.

[109] A. Rosa, C. Cavdar, S. Carvalho, J. Costa, and L. Wosinska, "Spectrum allocation policy modeling for elastic optical networks," in *High Capacity Optical Networks and Enabling Technologies (HONET), 2012 9th International Conference on*. IEEE, 2012, pp. 242–246.

[110] R. Wang and B. Mukherjee, "Spectrum management in heterogeneous bandwidth optical networks," *Optical Switching and Networking*, vol. 11, pp. 83–91, 2014.

[111] Y. Yin, Z. Zhu, S. B. Yoo *et al.*, "Fragmentation-aware routing, modulation and spectrum assignment algorithms in elastic optical networks," in *Optical Fiber Communication Conference*. Optical Society of America, 2013, pp. OW3A–5.

[112] E. A. Varvarigos and K. Christodoulopoulos, "Algorithmic aspects in planning fixed and flexible optical networks with emphasis on linear optimization and heuristic techniques," *Journal of Lightwave Technology*, vol. 32, no. 4, pp. 681–693, 2014.

[113] Z. Fan, Y. Li, G. Shen, and C.-K. C. Chan, "Distance-adaptive spectrum resource allocation using subtree scheme for all-optical multicasting in elastic optical networks," *Journal of Lightwave Technology*, vol. 35, no. 9, pp. 1460–1468, 2017.

[114] M. Klinkowski, M. Ruiz, L. Velasco, D. Careglio, V. Lopez, and J. Comellas, "Elastic spectrum allocation for time-varying traffic in flexgrid optical networks," *IEEE journal on selected areas in communications*, vol. 31, no. 1, pp. 26–38, 2013.

[115] M. Klinkowski and K. Walkowiak, "Routing and spectrum assignment in spectrum sliced elastic optical path network," *IEEE Communications Letters*, vol. 15, no. 8, pp. 884–886, 2011.

[116] K. Assis, A. Hammad, R. Almeida, and D. Simeonidou, "Approaches to maximize the open capacity of elastic optical networks," in *Communications (ICC), 2016 IEEE International Conference on*. IEEE, 2016, pp. 1–6.

[117] H. Liu, B. Zhou, and Y. Chen, "Spectrum allocation based on spectrum integration and re-routing for elastic optical networks," *IET Optoelectronics*, vol. 10, no. 5, pp. 179–183, 2016.

[118] W. Lu and Z. Zhu, "Dynamic service provisioning of advance reservation requests in elastic optical networks," *Journal of Lightwave Technology*, vol. 31, no. 10, pp. 1621–1627, 2013.

[119] T. Ohba, S. Arakawa, and M. Murata, "Virtual network reconfiguration in elastic optical path networks for future bandwidth allocation," *IEEE/OSA Journal of Optical Communications and Networking*, vol. 8, no. 9, pp. 633–644, 2016.

[120] A. Pagès, J. Perelló, S. Spadaro, and J. Comellas, "Optimal route, spectrum, and modulation level assignment in split-spectrum-enabled dynamic elastic optical networks," *IEEE/OSA Journal of Optical Communications and Networking*, vol. 6, no. 2, pp. 114–126, 2014.

[121] Z. Zhu, W. Lu, L. Zhang, and N. Ansari, "Dynamic service provisioning in elastic optical networks with hybrid single-/multi-path routing," *Journal of Lightwave Technology*, vol. 31, no. 1, pp. 15–22, 2013.

[122] B. Kozicki, H. Takara, and M. Jinno, "Enabling technologies for adaptive resource allocation in elastic optical path network (slice)," in *Communications and Photonics Conference and Exhibition (ACP), 2010 Asia*. IEEE, 2010, pp. 23–24.

[123] G. Zhang, M. De Leenheer, and B. Mukherjee, "Optical traffic grooming in ofdm-based elastic optical networks," *Journal of Optical Communications and Networking*, vol. 4, no. 11, pp. B17–B25, 2012.

[124] J. Zhang, Y. Ji, M. Song, Y. Zhao, X. Yu, J. Zhang, and B. Mukherjee, "Dynamic traffic grooming in sliceable bandwidth-variable transponder-enabled elastic optical networks," *Journal of Lightwave Technology*, vol. 33, no. 1, pp. 183–191, 2015.

[125] M. N. Dharmaweera, J. Zhao, L. Yan, M. Karlsson, and E. Agrell, "Traffic-grooming- and multipath-routing-enabled impairment-aware elastic optical networks," *IEEE/OSA Journal of Optical Communications and Networking*, vol. 8, no. 2, pp. 58–70, 2016.

[126] P. S. Khodashenas, J. Comellas, S. Spadaro, J. Perelló, and G. Junyent, "Using spectrum fragmentation to better allocate time-varying connections in elastic optical networks," *Journal of Optical Communications and Networking*, vol. 6, no. 5, pp. 433–440, 2014.

[127] M. Zhang, C. You, H. Jiang, and Z. Zhu, "Dynamic and adaptive bandwidth defragmentation in spectrum-sliced elastic optical networks with time-varying traffic," *Journal of Lightwave Technology*, vol. 32, no. 5, pp. 1014–1023, 2014.

[128] M. Zhang, C. You, and Z. Zhu, "On the parallelization of spectrum defragmentation reconfigurations in elastic optical networks," *IEEE/ACM Transactions on Networking*, vol. 24, no. 5, pp. 2819–2833, 2016.

[129] P. Wright, M. C. Parker, and A. Lord, "Minimum-and maximum-entropy routing and spectrum assignment for flexgrid elastic optical networking," *IEEE/OSA Journal of Optical Communications and Networking*, vol. 7, no. 1, pp. A66–A72, 2015.

[130] F. Cugini, F. Paolucci, G. Meloni, G. Berrettini, M. Secondini, F. Fresi, N. Sambo, L. Poti, and P. Castoldi, "Push-pull defragmentation without traffic disruption in flexible grid optical networks," *Journal of Lightwave Technology*, vol. 31, no. 1, pp. 125–133, 2013.

[131] S. Peng, R. Nejabati, and D. Simeonidou, "Impairment-aware optical network virtualization in single-line-rate and mixed-line-rate wdm networks," *IEEE/OSA Journal of Optical Communications and Networking*, vol. 5, no. 4, pp. 283–293, 2013.

[132] H. Beyranvand and J. A. Salehi, "A quality-of-transmission aware dynamic routing and spectrum assignment scheme for future elastic optical networks," *Journal of Lightwave Technology*, vol. 31, no. 18, pp. 3043–3054, 2013.

[133] D. B. Chua, E. D. Kolaczyk, and M. Crovella, "Network kriging," *IEEE Journal on Selected Areas in Communications*, vol. 24, no. 12, pp. 2263–2272, 2006.

[134] I. Sartzetakis, K. Christodoulopoulos, C. Tsekrekos, D. Syvridis, and E. Varvarigos, "Quality of transmission estimation in wdm and elastic optical networks accounting for space–spectrum dependencies," *IEEE/OSA Journal of Optical Communications and Networking*, vol. 8, no. 9, pp. 676–688, 2016.

[135] I. Sartzetakis, K. Christodoulopoulos, C. P. Tsekrekos, D. Syvridis, and E. M. Varvarigos, "Estimating qot of unestablished lightpaths," in *Optical Fiber Communication Conference*. Optical Society of America, 2016, pp. Tu3F–2.

[136] S. J. Savory, "Digital filters for coherent optical receivers," *Optics express*, vol. 16, no. 2, pp. 804–817, 2008.

[137] ——, "Digital coherent optical receivers: algorithms and subsystems," *IEEE Journal of Selected Topics in Quantum Electronics*, vol. 16, no. 5, pp. 1164–1179, 2010.

[138] I. Sartzetakis, K. Christodoulopoulos, and E. Varvarigos, "Qot aware adaptive elastic optical networks," in *Optical Fiber Communications Conference and Exhibition (OFC), 2017*. IEEE, 2017, pp. 1–3.

[139] J. Zhao, H. Wymeersch, and E. Agrell, "Nonlinear impairment aware resource allocation in elastic optical networks," in *Optical Fiber Communication Conference*. Optical Society of America, 2015, pp. M2I–1.

[140] ——, "Nonlinear impairment-aware static resource allocation in elastic optical networks," *Journal of Lightwave Technology*, vol. 33, no. 22, pp. 4554–4564, 2015.

[141] A. Alvarado, D. J. Ives, S. J. Savory, and P. Bayvel, "On the impact of optimal modulation and fec overhead on future optical networks," *Journal of Lightwave Technology*, vol. 34, no. 9, pp. 2339–2352, 2016.

[142] D. Rafique, M. Mussolin, M. Forzati, J. Mårtensson, M. N. Chugtai, and A. D. Ellis, "Compensation of intra-channel nonlinear fibre impairments using simplified digital back-propagation algorithm," *Optics express*, vol. 19, no. 10, pp. 9453–9460, 2011.

[143] A. Bononi, P. Serena, A. Morea, and G. Picchi, "Regeneration savings in flexible optical networks with a new load-aware reach maximization," *Optical Switching and Networking*, vol. 19, pp. 123–134, 2016.

[144] L. Yan, Y. Xu, M. Brandt-Pearce, N. Dharmaweera, and E. Agrell, "Regenerator allocation in nonlinear elastic optical networks with random data rates," in *2018*

Optical Fiber Communications Conference and Exposition (OFC). IEEE, 2018, pp. 1–3.

[145] ——, "Regenerator site predeployment in nonlinear dynamic flexible-grid networks," in *Optical Communication (ECOC), 2017 European Conference on*. IEEE, 2017, pp. 1–3.

[146] R. Wang, S. Bidkar, R. Nejabati, and D. Simeonidou, "Load and nonlinearity aware resource allocation in elastic optical networks," in *Optical Fiber Communication Conference*. Optical Society of America, 2017, pp. W1H–5.

[147] E. Torrengo, R. Cigliutti, G. Bosco, A. Carena, V. Curri, P. Poggiolini, A. Nespola, D. Zeolla, and F. Forghieri, "Experimental validation of an analytical model for nonlinear propagation in uncompensated optical links," *Optics express*, vol. 19, no. 26, pp. B790–B798, 2011.

[148] L. Galdino, G. Liga, G. Saavedra, D. Ives, R. Maher, A. Alvarado, S. Savory, R. Killey, and P. Bayvel, "Experimental demonstration of modulation-dependent nonlinear interference in optical fibre communication," in *ECOC 2016; 42nd European Conference on Optical Communication; Proceedings of*. VDE, 2016, pp. 1–3.

[149] G. Saavedra, M. Tan, D. J. Elson, L. Galdino, D. Semrau, M. A. Iqbal, I. D. Phillips, P. Harper, A. Ellis, B. C. Thomsen *et al.*, "Experimental analysis of nonlinear impairments in fibre optic transmission systems up to 7.3 thz," *Journal of Lightwave Technology*, vol. 35, no. 21, pp. 4809–4816, 2017.

[150] A. J. Stark, Y.-T. Hsueh, T. F. Detwiler, M. M. Filer, S. Tibuleac, and S. E. Ralph, "System performance prediction with the gaussian noise model in 100g pdm-qpsk coherent optical networks," *Journal of Lightwave Technology*, vol. 31, no. 21, pp. 3352–3360, 2013.

[151] O. Vassilieva, T. Yamauchi, S. Oda, I. Kim, T. Hoshida, Y. Aoki, J. C. Rasmussen, and M. Sekiya, "Systematic analysis of intra-superchannel nonlinear crosstalk in flexible grid networks," in *Optical Communication (ECOC), 2014 European Conference on*. IEEE, 2014, pp. 1–3.

[152] D. J. Ives, A. Lord, P. Wright, and S. J. Savory, "Quantifying the impact of nonlinear impairments on blocking load in elastic optical networks," in *Optical Fiber Communication Conference*. Optical Society of America, 2014, pp. W2A–55.

[153] R. Wang, S. Bidkar, R. Nejabati, and D. Simeonidou, "Load-aware nonlinearity estimation for efficient resource allocation in elastic optical networks," in *2017 International Conference on Optical Network Design and Modeling (ONDM)*, May 2017, pp. 1–6.

[154] R. Schmogrow, M. Winter, M. Meyer, D. Hillerkuss, S. Wolf, B. Baeuerle, A. Ludwig, B. Nebendahl, S. Ben-Ezra, J. Meyer *et al.*, "Real-time nyquist pulse generation beyond 100 gbit/s and its relation to ofdm," *Optics Express*, vol. 20, no. 1, pp. 317–337, 2012.

[155] D. Hillerkuss, R. Schmogrow, M. Meyer, S. Wolf, M. Jordan, P. Kleinow, N. Lindenmann, P. C. Schindler, A. Melikyan, X. Yang *et al.*, "Single-laser 32.5 tbit/s nyquist wdm transmission," *Journal of Optical Communications and Networking*, vol. 4, no. 10, pp. 715–723, 2012.

[156] J. Y. Yen, "Finding the k shortest loopless paths in a network," *management Science*, vol. 17, no. 11, pp. 712–716, 1971.

[157] I. Chlamtac, A. Ganz, and G. Karmi, "Lightpath communications: An approach to high bandwidth optical wan's," *IEEE transactions on communications*, vol. 40, no. 7, pp. 1171–1182, 1992.

[158] R. Wang, F. Meng, R. Nejabati, and D. Simeonidou, "A novel traffic grooming scheme for nonlinear elastic optical network," in *2017 European Conference on Optical Communication (ECOC)*. IEEE, 2017, pp. 1–3.

[159] R. Wang, Y. Bi, Y. Ou, E. Hugues-Salas, F. Meng, S. Yan, R. Nejabati, and D. Simeonidou, "Coordinated fibre span power optimisation and roadm input power management strategy for optical networks," in *2018 European Conference on Optical Communication (ECOC)*. IEEE, 2018, pp. 1–3.

[160] Z. Zhang, S. Su, K. Shuang, W. Li, and M. A. Zia, "Energy aware virtual network migration," in *Global Communications Conference (GLOBECOM), 2016 IEEE*. IEEE, 2016, pp. 1–6.

[161] É. Archambault, D. O'Brien, C. Tremblay, F. Gagnon, M. P. Bélanger, and É. Bernier, "Design and simulation of filterless optical networks: Problem definition and performance evaluation," *Journal of Optical Communications and Networking*, vol. 2, no. 8, pp. 496–501, 2010.